BUCKLING BEHAVIOR OF REINFORCED CONCRETE WALL PANEL MODELS

by

Arturo C. Muñoz

B.S., Kansas State University, 1977

A MASTER'S THESIS

submitted in partial fulfillment of the

requirements for the degree

MASTER OF SCIENCE

Department of Civil Engineering

KANSAS STATE UNIVERSITY

Manhattan, Kansas

1981

Approved:

Major Professor

SPEC
COLL
LD
2668
T4
1981
M86
c.2

TABLE OF CONTENTS

TABLE OF CONTENTS (continued)

LIST OF FIGURES

LIST OF FIGURES (continued)

LIST OF FIGURES (continued)

LIST OF TABLES

THIS BOOK
CONTAINS
NUMEROUS PAGES
WITH ILLEGIBLE
PAGE NUMBERS
THAT ARE CUT OFF,
MISSING OR OF POOR
QUALITY TEXT.

THIS IS AS RECEIVED
FROM THE
CUSTOMER.

ACKNOWLEDGMENTS

Sincere appreciation is extended to Dr. Stuart E. Swartz for his guidance and assistance throughout my graduate program. Special thanks are extended to Dr. Robert R. Snell for his guidance and for extending me the financial assistance through the Civil Engineering Department.

Sincerest gratitude is extended to Mr. Russell Gillespie for his assistance in the Civil Engineering Design Shop and to Mr. Tom Gates for his helpful suggestions for solving design problems. Deepest appreciation is extended to my fiancée, Miss Soledad N. Luna, for her moral and understanding support. A special thank you is extended to Peggy Selvidge for deciphering my writing and preparing the final manuscript.

Chapter 1

INTRODUCTION

Rectangular reinforced concrete panels are commonly used as components of box girder bridges, folded plate roofs and as wall panels. The latter are used extensively in high-rise building construction. These plates may be cast in place or may be tilt-up, precast panels. They are utilized as shear walls, bearing walls or as shear and bearing walls. These panels are generally supported monolithically along all sides, as in folded plates or box girders, or may be supported with small restraint against rotation, as in precast panels for walls. These wall panels may or may not have continuous supports along all edges with respect to displacements normal to the panel surface (13).* Concrete panels utilized in this manner may be subjected to in-plane, relatively uniform, compressive stresses of considerable magnitude.

It is becoming more feasible and economical to fabricate thinner panel sections by precasting methods with greater quality control on mix design and workmanship. An important element in obtaining thinner panels is the availability of higher strength concretes. The thinner panels will also help reduce the dead load of a structure substantially.

There are, however, some factors that forestall the acceptance of the use of thin panels. First, there is a lack of knowledge of the ultimate strength of wall panels when subjected to combinations of shearing and bearing loads with different practical connections.

---

*numbers in parentheses refer to items listed in Bibliography.

Second, there is a lack of knowledge of the buckling capacity of the panels when subjected to bearing, shear, or a combination of shear and bearing with different practical connections.

Hence, it is becoming increasingly important to acquire information concerning the buckling characteristics of concrete panels with different types of supports and loadings.

It is the purpose of this report to present results from direct model tests of rectangular reinforced concrete panels which were proportioned to fail by buckling.

Some of the model panels were simply-supported along all edges while other panels were supported by systems which may be encountered in practice. The model panels were subjected to in-plane uniaxial compression with a minimum amount of eccentricity.

This report contains background information on modelling in concrete and a discussion of available information on buckling of concrete plates in Chapter 2.

The test program, design of fixtures and construction of test specimens are described in Chapter 3.

Test results are given in Chapter 4.

Chapter 2

LITERATURE REVIEW

2.1 Model Studies

A model structure may be defined as a physical replica of some prototype structure which is normally smaller in size and which can be used experimentally to predict the behavior of the prototype (14). Basic dimensional analysis can be used to correlate the behavior of both structures where the properties of the materials allow. Complications may occur when variance exists in fundamental dimensionless quantities such as Poisson's Ratio or maximum strain. This is particularly true when the structural behavior is not linear. The direct model method employs a true to scale model which reproduces the prototype to a constant linear scale with only minor details (that have no affect on the structural behavior of the prototype) occasionally omitted. This method may be used to study the response of structures loaded to collapse if high material compatibility is obtainable.

Generally, both stress-strain diagrams and failure criteria for the prototype and model materials must be compatible. The required compatibility of material failure criteria is a function of the particular overall structural failure criterion appropriate to the study. The present state of knowledge with regard to failure criteria for reinforced concrete is unsatisfactory (1). Consequently, no firm conclusions can now be developed concerning the exact required criteria for the model materials. However, it seems reasonable to strive to use materials in the model as similar as possible to prototype materials to minimize uncertainty.

After completing the feasibility and similitude studies the general outline of the model test program is established. It then remains to fill the outline with the detailed design of the model, the test apparatus, instrumentation, and loading sequence necessary to fulfill the objectives of the test. These latter detailed operations may not be entirely independent in the earlier studies. For example, it may be found that the available materials will not fulfill some of the specifications, and adjustments must be made in the plans to either relax the specifications, develop new materials or to find another solution.

The interrelationship of all phases of the model test program is illustrated by the detailed design of the model. Restricting the discussion to direct models, the objective may be a design study or a research study. For a design study the model design must predict the behavior of the prototype as closely as possible. In order to design a valid model the reliability of every element going into the model must be considered. This reliability may be related to similitude and cost. For a research study the model design must cause the desired behavior to predominate. In the present case it was desired to obtain information on concrete plate buckling. A physical model rests particularly on assumptions regarding the similarity with which the model material properties, support conditions, and loading patterns are representative of the prototype. Although the arithmetic or analytical model may be performed without error to eight places, the resulting accuracy may well be worse than that for the physical model. Time and cost factors are usually weighed heavily in favor of the

analytical models. However, it is possible to construct and test physical models very quickly but usually at the expense of accuracy. Usually there is not sufficient time available to take all the precautions in fabricating, loading and testing. To study the behavior of structures in detail or to establish the mode of failure and the magnitude of the collapse load, the testing of structural models must be conducted. It is in the building and testing of realistic models that the future of structural modeling lies.

2.2 Model Concrete

Model concrete is usually designed to meet as closely as possible the known requirements of any prototype concrete such as compressive strength, tensile strength and shrinkage characteristics. In the paper presented by Sabnis (11), the question of similitude of the model concrete is answered. Modeling concrete by merely scaling the individual components is not possible. Of importance are the overall physical properties of the model material such that the stress-strain curve and failure envelope are similar to those of the prototype concrete. Therefore the model concrete may be designed in the same manner as concrete in any prototype structure, i.e., a combination of Portland cement, water, aggregate and additives which will display the desired properties at the desired time after casting. In practice, this means Type I or Type III cement, a water-cement ratio of 0.3-0.6 and a maximum aggregate size determined by similitude and by the thickness and reinforcement spacing of the model. From this point of view the model concrete or microconcrete mixes discussed in Chapter 3 were designed. Work done by others (1,5,8,10,14) also complement the paper by Sabnis (11), op. cit.

2.3 Micro-reinforcement

Properties to consider for reinforcement include (8):

1. Yield and ultimate strength in tension, plus yield strength in compression;
2. Shape of stress strain curve;
3. Ductility;
4. Bonding characteristics of surface.

Model reinforcing steel should have the physical properties identical to the prototype reinforcing. These requirements dictate the choice of steel as the model reinforcing.

A number of choices for model reinforcement exist:

1. Round steel wire and rod,
2. Square steel rod,
3. Cold rolled threaded steel rods,
4. Commercially available deformed wires,
5. Custom deformed wire.

The last four of the above list were not economically feasible in this geographical region, therefore the first item was selected as reinforcement. Tests were conducted on the reinforcement used to determine its strength characteristics. Results of these are shown in Chapter 3. In a paper presented by Harris (8) and others (14,5,1) a method of annealing and deforming model reinforcement to meet the properties of any prototype reinforcement is discussed.

2.4 Pumpability of Concrete

There are a wide variety and number of tests which may be conducted on concrete mixes to determine its pumpability. Plug flow is discussed

in the paper by Anderson (2). Plug flow is when the concrete slides on a thin film of mortar along the pipe wall. He then lists ten characteristics of the mix to determine its pumpability. Other authors (3,4,9) describe special tests to conduct on concrete mixtures to determine its pumpability. These papers dealt in the realm of normal weight concrete or macro-concrete and not model or micro-concrete.

2.5 Critical Load

The critical load can be determined by using Euler's Formula for buckling if the panel buckles as a column. From Figure 2.1 the critical load P_{cr} is

$$P_{cr} = \frac{n \pi^2 E_T I}{(L)^2} \quad \text{---------- Eq. (2.1)}$$

where

E_T = Tangent Modulus for concrete,

I = Moment of Inertia about bending axis,

L = unsupported length of panel,

n = number of waves panel deflects.

The critical load P_{cr} is also

$$P_{cr} = [A_c f_{cr} + A_s E_s \varepsilon_{cr}] \quad \text{---------- Eq. (2.2)}$$

where

A_c, A_s = area of concrete, steel, respectively,

E_s = Modulus of Elasticity for steel,

f_{cr} = critical concrete stress,

ε_{cr} = critical strain.

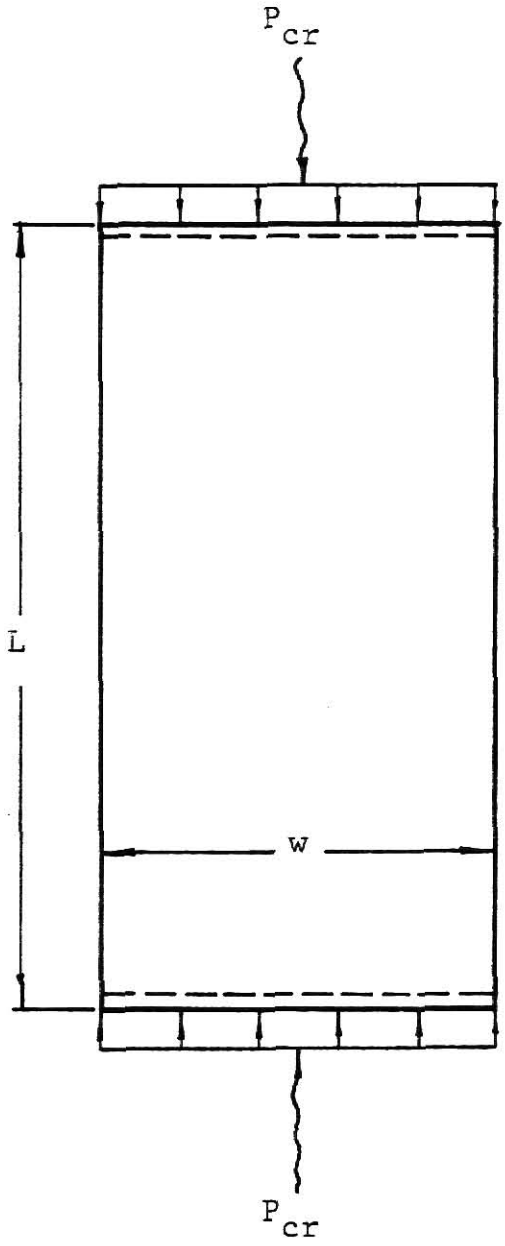

All edges parallel to applied load have various supports.

Figure 2.1 Applied Load on Test Panel

It may be assumed that the stress-strain curve for the micro-concrete is a second order parabolic equation, of the form,

$$f_c = A_1\varepsilon + B_1\varepsilon^2 + C_1 \quad \text{---------- Eq. (2.3)}$$

with the boundary conditions

$$\varepsilon = 0 \text{ when } f_c = 0.$$

Therefore,

$$C_1 = 0.$$

At the peak of the stress-strain curve is the maximum concrete stress; i.e.,

$$f_c = f'_c \text{ at } \varepsilon_c = \varepsilon_o.$$

Hence,

$$f'_c = A_1\varepsilon_o + B_1\varepsilon_o^2. \quad \text{---------- Eq. (2.4)}$$

Also the slope at $f_c = f'_c$ is a horizontal line. Therefore,

$$\frac{df_c}{d\varepsilon_o} = 0, \text{ at } f_c = f'_c,\ \varepsilon_c = \varepsilon_o$$

or,

$$\frac{df_c}{d\varepsilon_o} = A_1 + 2B_1\varepsilon_o = 0.$$

Hence,

$$A_1 = -2B_1\varepsilon_o.$$

By substitution,

$$f'_c = -2B_1\varepsilon_o^2 + B_1\varepsilon_o^2,$$

or,

$$f'_c = -B_1\varepsilon_o^2,$$

whereby

$$B_1 = \frac{-f'_c}{\varepsilon_o^2} \text{ , and } A_1 = \frac{2f'_c}{\varepsilon_o} .$$

Substituting all known parameters A_1, B_1, C_1 into Eq. (2.3) yields,

$$f_c = 2f'_c \frac{\varepsilon_c}{\varepsilon_o} - f'_c \left(\frac{\varepsilon_c}{\varepsilon_o}\right)^2$$

By collecting terms,

$$f_c = f'_c \left[2 \frac{\varepsilon_c}{\varepsilon_o} - \left(\frac{\varepsilon_c}{\varepsilon_o}\right)^2\right]. \text{ ---------- Eq. (2.3a)}$$

By defining $e = \frac{\varepsilon_c}{\varepsilon_o}$, then

$$f_c = f'_c (2e-e^2). \text{ ---------- Eq. (2.3b)}$$

Defining the Tangent Modulus for concrete as the derivative of the Modulus of Elasticity for concrete,

$$E_T = \frac{df_c}{d\varepsilon_o}$$

$$= \frac{2f'_c}{\varepsilon_o} \left[1 - \frac{\varepsilon_c}{\varepsilon_o}\right] . \text{ ---------- Eq. (2.5)}$$

By definition the critical stress for concrete also is

$$f_{cr} = f'_c \left[2 \frac{\varepsilon_{cr}}{\varepsilon_o} - \left(\frac{\varepsilon_{cr}}{\varepsilon_o}\right)^2\right] . \text{ ---------- Eq. (2.3c)}$$

By substitution of Eq. (2.5) into Eq. (2.1), then equating with Eq. (2.2) and collecting terms, one obtains,

$$\frac{n\pi^2 I}{L^2} \cdot \frac{2f'_c}{\varepsilon_o} \left[1 - \frac{\varepsilon_{cr}}{\varepsilon_o}\right] = A_c \left[f'_c \left(2 \frac{\varepsilon_{cr}}{\varepsilon_o} - \left(\frac{\varepsilon_{cr}}{\varepsilon_o}\right)^2\right] + A_s E_s \varepsilon_{cr}$$

---------- Eq. (2.6)

Equation (2.6) is now solved to determine ε_{cr}. This value is entered into Equation (2.3c) to determine the critical stress f_{cr}. With these values the buckling load of the panel can be determined by Eq. (2.2). This is the critical load of the panel due to column action.

Several panels are expected to perform as plates. The formulas presented here were derived by Swartz, et al. (12). Their formulation is discussed vividly and it is not necessary to repeat it at this time. The buckling strain is defined as

$$\varepsilon_{cr} = e_{cr}\, \varepsilon_o \qquad \text{Eq. (2.7)}$$

where

$$e_{cr} = 1 + \frac{1}{2}\,(B - \sqrt{4 + B^2}). \qquad \text{Eq. (2.8)}$$

For laboratory work the concrete buckling stress is defined as

$$f_{cr} = 0.5\, f'_c\, B\, (-B + \sqrt{4 + B^2}) \qquad \text{Eq. (2.9)}$$

and B is defined as

$$B = \frac{\pi^2}{6\varepsilon_o(1-\rho)}\,[\frac{1}{\ell} + \ell]^2(\frac{t}{w})^2; \qquad \text{Eq. (2.10)}$$

$$\ell = \frac{L}{w} \text{ if } \frac{L}{w} < 1;$$

$$\ell = 1 \text{ if } \frac{L}{w} \geq 1.$$

The plate buckling load is then defined as

$$P_{cr} = C_s w(t)[f_{cr}(1-\rho) + E_s\, \varepsilon_{cr}\, \rho]; \qquad \text{Eq. (2.11)}$$

for $\varepsilon_{cr} \leq \varepsilon_y$, or

$$P_{cr} = C_s w(t)[f_{cr}(1-\rho) + f_y \rho]; \qquad \text{Eq. (2.11a)}$$

for $\varepsilon_{cr} > \varepsilon_y$.

In the above,

C_s = factor of safety coefficient taken as 1 for laboratory experiments,

t = thickness of panel,

w = width of panel,

ρ = steel ratio.

To utilize these equations the parameter B should first be determined. Then solving Eq. (2.8) and Eq. (2.9) these values are substituted into Eq. (2.11) or (2.11a) to satisfy the given restrictions.

From ACI Code Specifications (6) for wall buckling according to Section 14.2.3, the nominal axial load strength (P_{nw}) of a wall is,

$$\phi P_{nw} = 0.55\ \phi f'_c\ A_g\ [1 - (\frac{L}{40t})^2] \quad \text{---------- Eq. (14.1)}$$

Modifying this formula for experimental analysis

$$P_{nw} = f'_c\ A_g\ [1 - (\frac{L}{40t})^2] \quad \text{---------- Eq. (14.1a)}$$

However, according to Specification 14.2.5 which limits the thickness to height or width ratio to not less than 1:25,

$$\frac{t}{L} \text{ or } \frac{t}{w} \geq \frac{1}{25} .$$

This ratio for the panels tested is

$$\frac{1}{4x12} = \frac{1}{48} \text{ which is less than } \frac{1}{25} .$$

Therefore, according to ACI Specification 14.2.5, the model panels cannot carry any load. From Euler's Formula,

$$P_{cr} = n\ \frac{\pi^2 EI}{L^2} \quad \text{---------- Eq. (2.1)}$$

and from ACI Specification 8.5.1,

$$E = 33w_c^{1.5}\sqrt{f'_c} \quad \text{---------- Eq. (2.12)}$$

in which w_c = unit weight of concrete,

$$I = \frac{1}{12}(w)(t)^3 \quad \text{---------- Eq. (2.13)}$$

By substitution,

$$P_{cr} = \frac{n\pi^2}{L^2}[33w_c^{1.5}\sqrt{f'_c}][\frac{1}{12}w(t)^3].$$

By defining the stress

$$F_a = \frac{P_{cr}}{A_g}, \text{ where } A_g = (w)(t), \text{ one obtains}$$

$$F_a = \frac{\pi^2}{L^2}[33w_c^{1.5}\sqrt{f'_c}][\frac{1}{12}(w)t^3]\frac{1}{w(t)} \quad \text{---------- Eq. (2.14)}$$

or, by collecting common terms,

$$F_a = \frac{\pi^2 \cdot 33}{12} \cdot w_c^{1.5}\sqrt{f'_c}\,[\frac{t}{L}]^2$$

$$= 27.14 \cdot w_c^{1.5}\sqrt{f'_c}\,[\frac{t}{L}]^2. \quad \text{---------- Eq. (2.15)}$$

From the ACI Journal July 1971 (7),

$$F_a = 22.22\, w_c^{1.5}\sqrt{f'_c}\,[\frac{t}{L}]^2. \quad \text{---------- Eq. (2.15a)}$$

Chapter 3

EXPERIMENTAL PROGRAM

3.1 Design and Construction of Formwork

Several factors governed the design of the formwork for the microconcrete plates. The material utilized must withstand repetitive use, provide a mar-free surface, allow monitoring of the pumping phase of the microconcrete, and facilitate in the handling and transportation of the pumped form. Plexiglass was used for the microconcrete panel form.

The plexiglass was rough cut to the approximate size then milled to the correct size to provide clean, smooth edges. Two plexiglass plates of 13 in. x 24.5 in. (33.0 cm x 62.2 cm) were used for each form. Situated between the two plates were 1/2 in. x 1/4 in. (12.7 mm x 6.4 mm) strips of plexiglass. These strips had holes drilled offset from the center of the short dimension to allow for the reinforcement of the microconcrete panel. The plexiglass strips extended down the long sides and the bottom edge of the plexiglass form. The top edge of the form remained open to allow trapped air and excess microconcrete to escape. A photograph of the completed form is shown in Figure 3.1.

A 3/4 in. double male brass fitting was tapped to the front plexiglass plate. The fitting was located near the center of the plate approximately 3/4 in. (19.0 mm) from the bottom edge, as shown in Figure 3.2, making a perpendicular angle with the surface at the plate. The microconcrete would be pumped into the mold through this fitting.

ILLEGIBLE DOCUMENT

THE FOLLOWING DOCUMENT(S) IS OF POOR LEGIBILITY IN THE ORIGINAL

THIS IS THE BEST COPY AVAILABLE

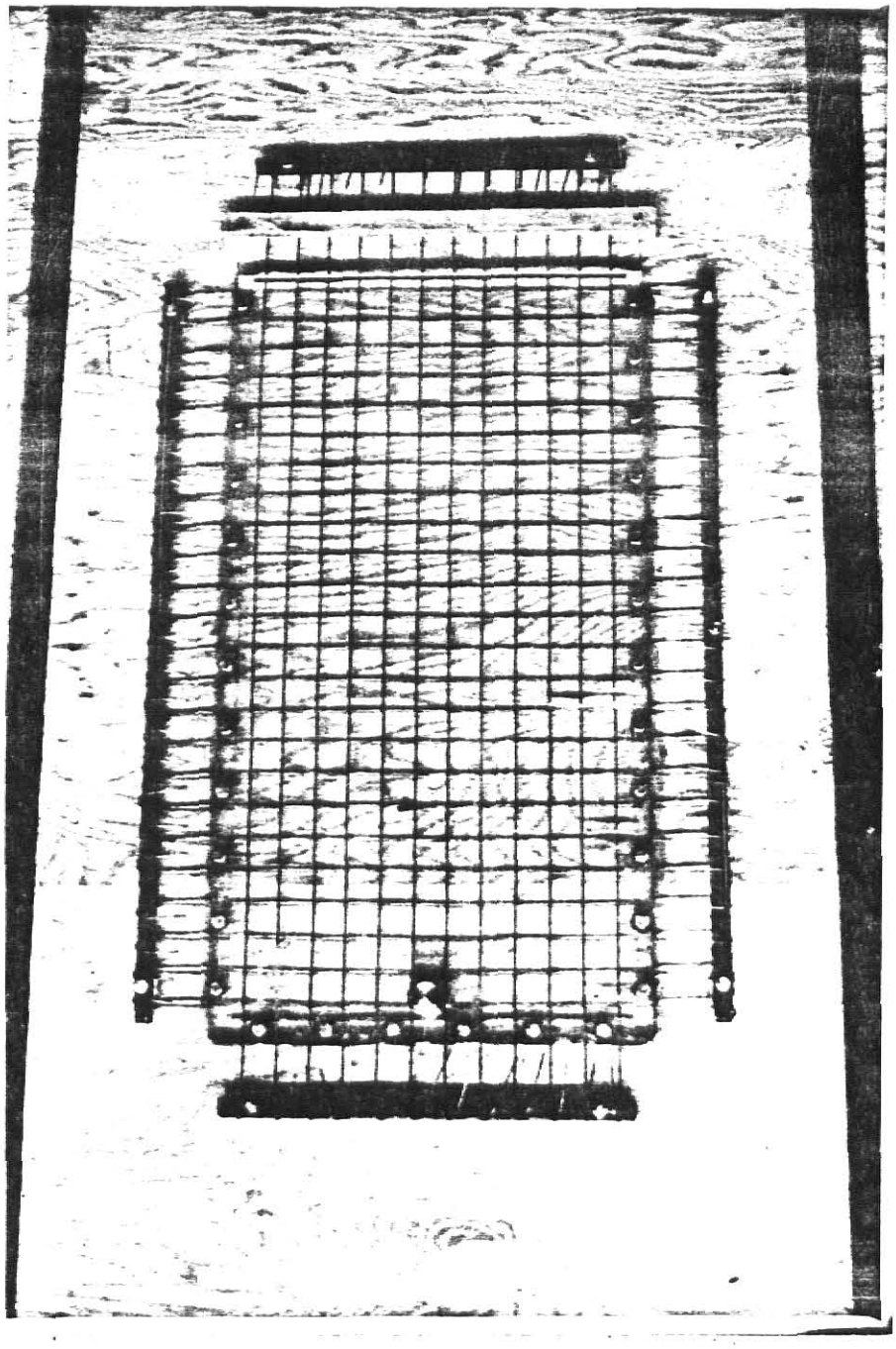

Figure 3.1 Completed Form

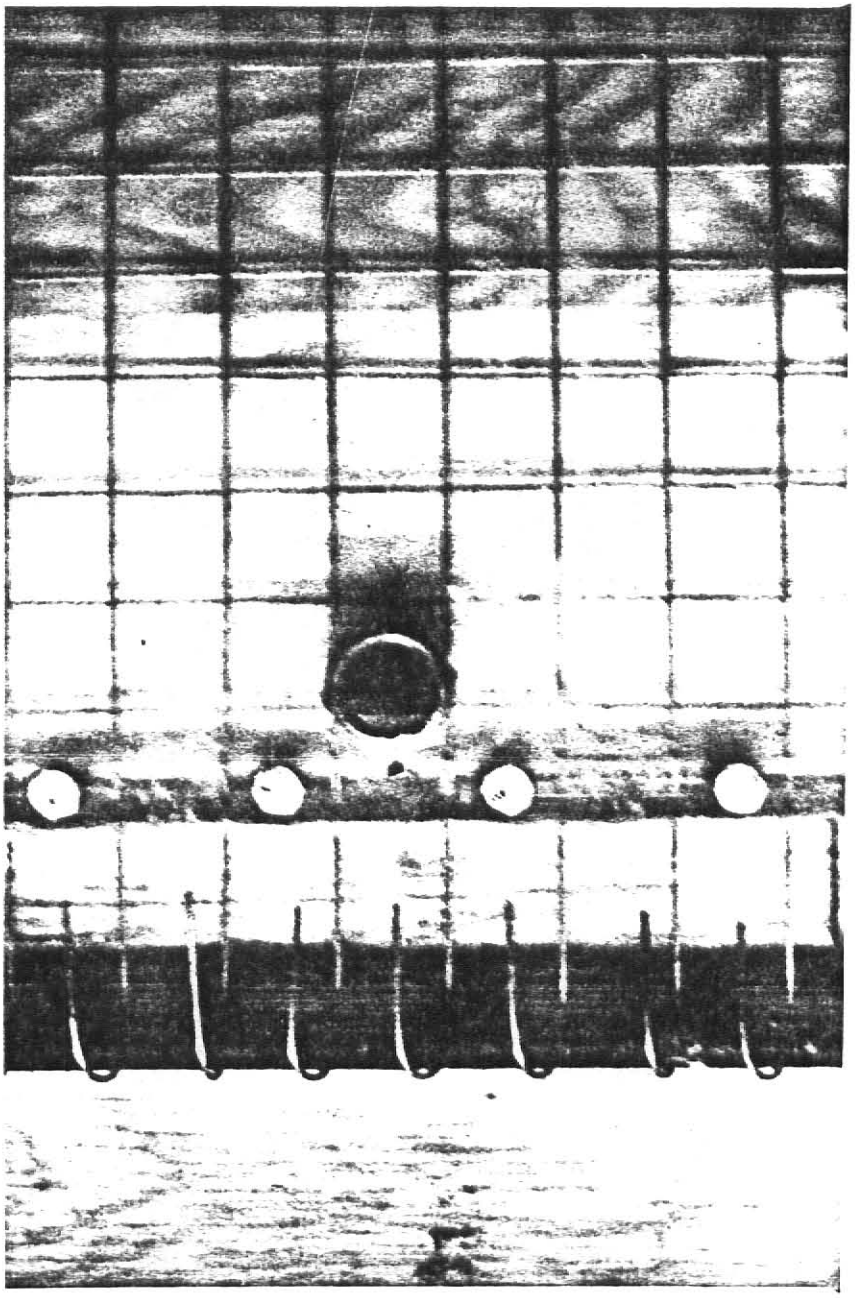

Figure 3.2 Brass Fitting

The plexiglass plates were bolted to a sheet of plywood, which served as a stiffener for the mold, supported the reinforcement for the panel and acted as a brace during the pumping phase. Assembly or disassembly was an effortless task of connecting or removing the bolts.

3.2 Microconcrete Pump

A Moyno Open Throat Pump Model 2J4 was used to pump the microconcrete into the form. The pump's performance characteristics and utilization for other research projects governed its selection. See Table 3-1 for pump specifications. One unique characteristic of the microconcrete pump is the progressing cavity principle using an auger, illustrated in Figure 3.3. This principle provides uniform discharge without pulsation, turbulence or agitation. It also allows the pump to handle relatively large particles in suspension. The pump model 2J4 can handle suspended particles less than 0.3 in. (8 mm) in diameter. The maximum size particle of the microconcrete mix is 0.049 in. (1.2 mm) in diameter. Attached to the throat of the pump is a hopper which was designed in the civil engineering shop and intended for future use when large quantities of microconcrete are required.

A manifold designed for use by other research projects is mounted to the pump shaft end. The manifold was originally designed in the T-shape configuration shown in Figure 3.4. This manifold has the capability of connecting one to six hoses. Ordinary 5/8 in. (16 mm) diameter rubber garden hoses with an advertized burst strength of 400 psi (2.8 MPa) were used. Attached to the male end of the hose was a double female couple. This allowed either hose end to be connected to the manifold or form.

Table 3-1 Concrete Pump Specifications

Item	Moyno Pump Model 2J4 Specification
Output per 100 Revolutions	2.02 Gallons (7.7 liters)
Max. Particle Size	0.3 in. (7.6 mm)

Diff. Pressure, psi.	Pump Speed, rpm.							
	150		300		450		600	
	GPM	HP	GPM	HP	GPM	HP	GPM	HP
0	3.0	1/4	6.0	1/3	9.0	1/2	12	3/4
80	1.0	1/4	4.0	1/2	6.7	3/4	9.5	1
150					2.7	1	5.5	1 1/2

1 GPM = 3.79 liters/min.

1 HP = 754 N-m/sec.

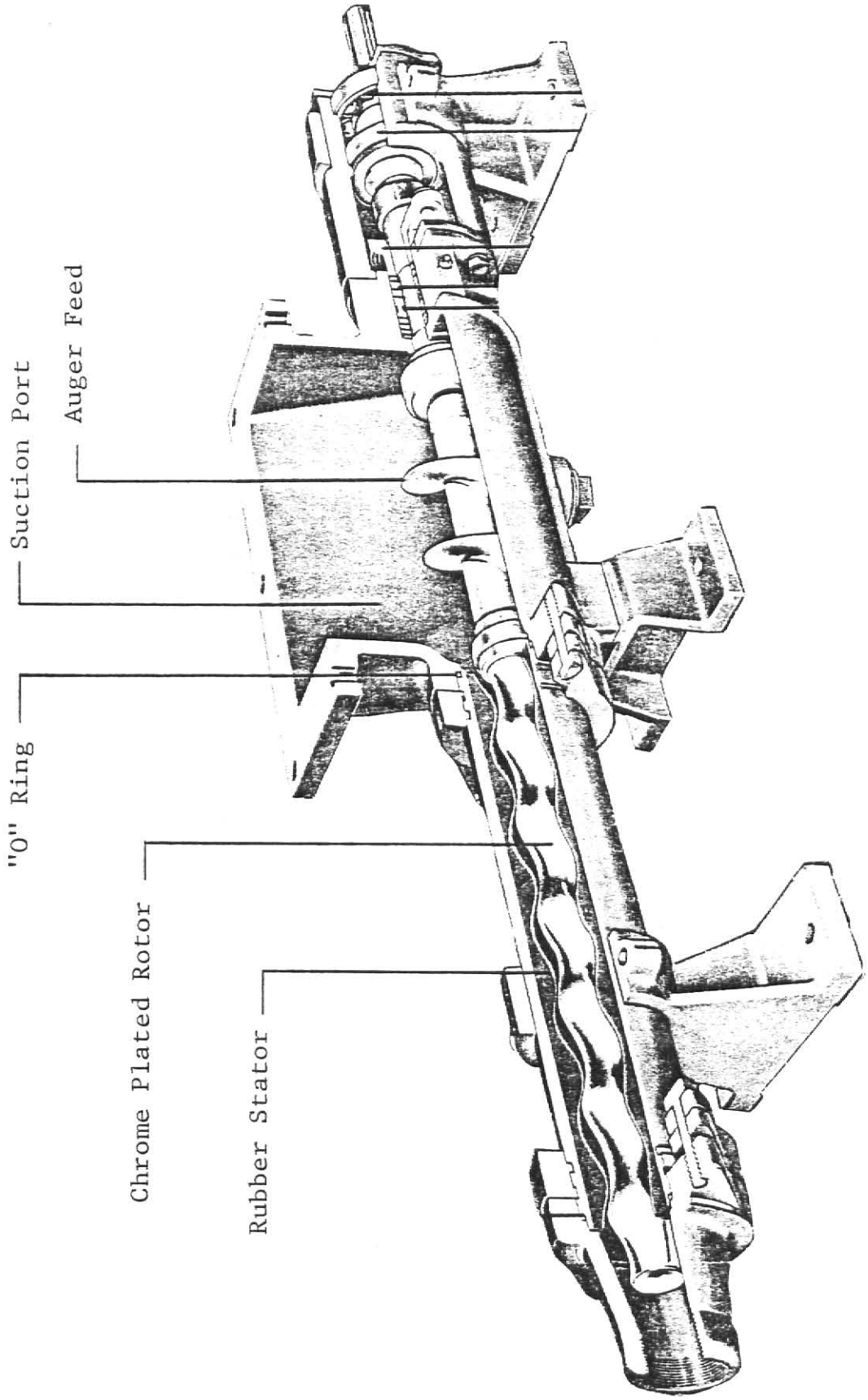

Figure 3.3 Moyno Open Throat Pump

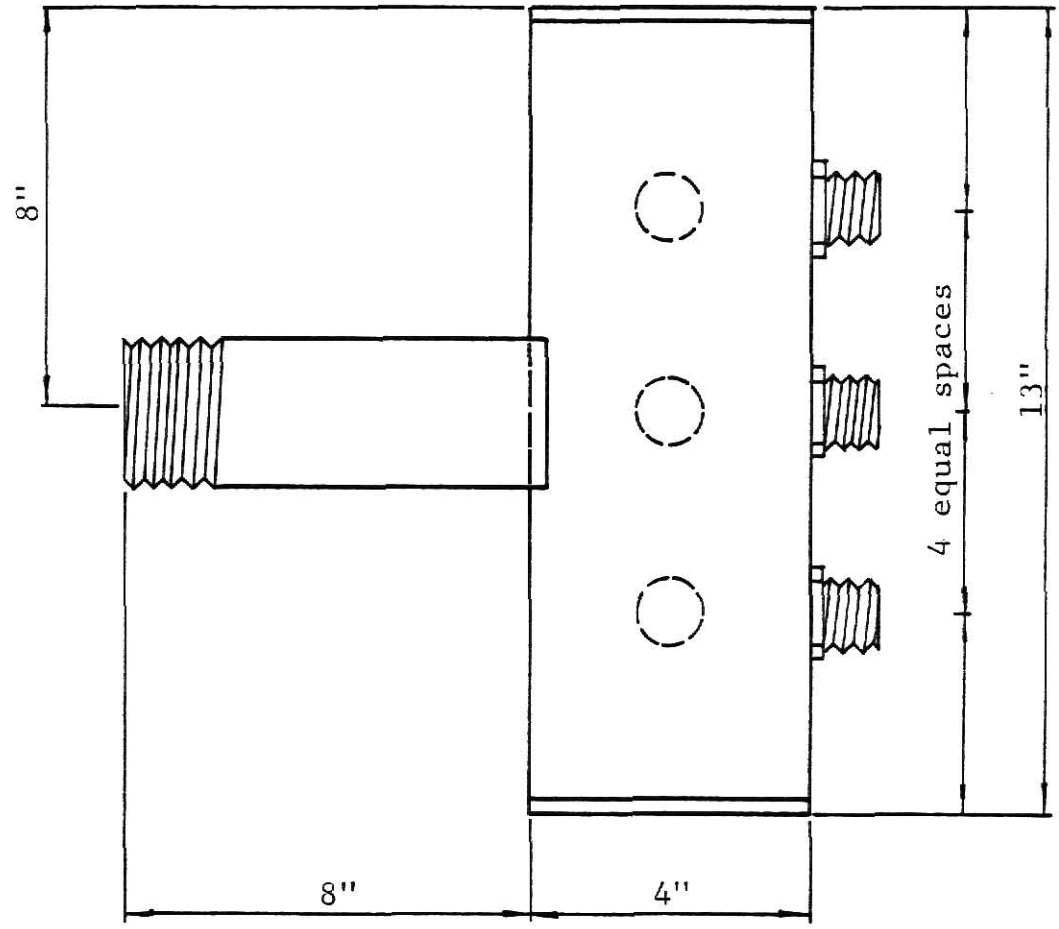

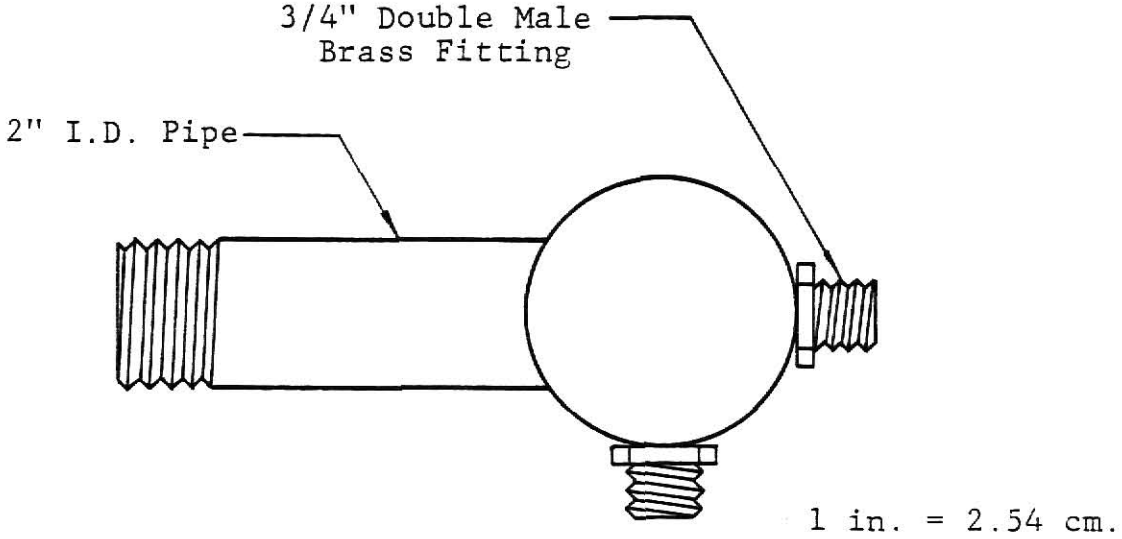

Figure 3.4 T-Shaped Manifold

3.3 Formwork Preparation

One size panel was constructed with the following dimensions:

length, L = 24 in. (610 mm),

width, w = 12 in. (305 mm),

thickness, t = 0.25 in. (6.4 mm).

Two mix designs were employed as given in Table 3-2. The area of steel selected for the microconcrete panel met ACI Code Specifications 14.2.10 and 14.2.11 (6) for minimum percentage.

A deformed ductile wire was called for in the design of the panel. To satisfy the minimum steel ratio, and concrete cover requirements, steel reinforcement with a diameter of 0.0625 in. (1.6 mm) was selected. Using this diameter steel would require a spacing of 1 in. (2.6 cm) intervals. Commercial production of a deformed wire with this diameter is not available. An undeformed stainless steel piano wire was the most feasible type of reinforcement available and thus was utilized. Tests were conducted to determine the strength of the wire. Uniaxial stress-strain properties are displayed in Figure 3.5a,b,c and Table 3-3.

Preparation of the form for fabrication of the microconcrete panel consisted of several steps. The inner surface of the plexiglass form was lightly coated with a mineral oil to prevent adhesion of the microconcrete to the plexiglass. Prior to positioning the reinforcement, a sheet of wax paper was placed over the surface of the bottom plexiglass plate to prevent the reinforcement from contacting the oil. The wax paper was removed prior to securing the reinforcement to the support system. After the reinforcement was placed in the mold it was secured to the form as shown in Figure 3.1. The upper plexiglass plate was then

Table 3-2 Microconcrete Mix Design

	Mix Design 1	Mix Design 2
Water-Cement Ratio	0.8	0.5
Aggregate Cement Ratio	3.6	2.2
Largest Particle Size	0.049 in. (1.2 mm)	0.049 in. (1.2 mm)
Type of Aggregate	Kansas River Sand	Kansas River Sand
Type of Cement	Portland Type I	Portland Type I
Specific Gravity of Aggregate	1.672	1.672
Specific Gravity of Cement	3.12	3.12
Aggregate Dry Rodded Unit Wt.	104.35 pcf (1670 kg/m^3)	104.35 pcf (1670 kg/m^3)
Aggregate Moisture Content	0%	0%
Volume of Set Retarder per Cubic Ft. of Mix per Hour Retardation		12.32 ml

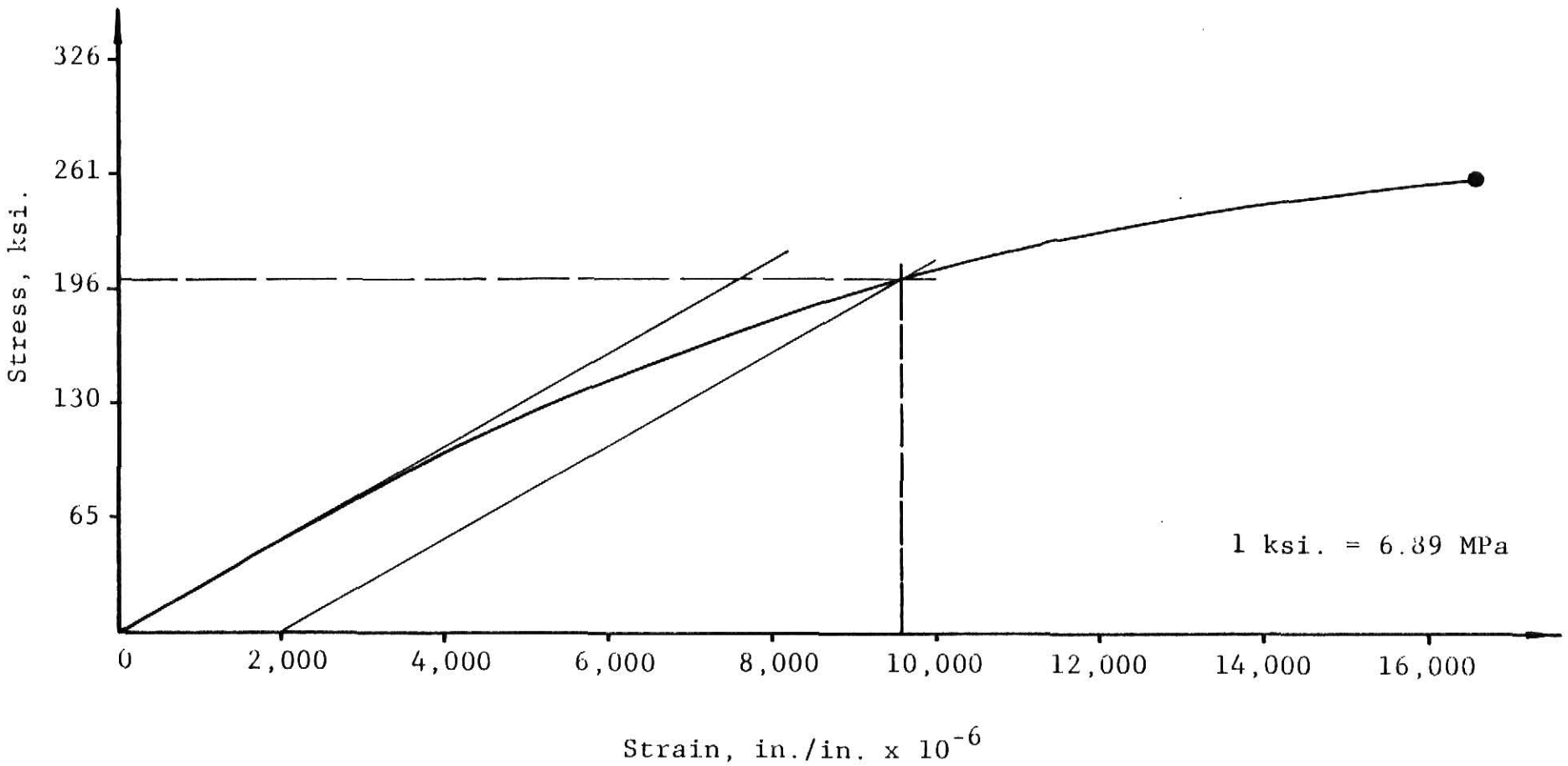

Figure 3.5a Stress-Strain Curve for Reinforcement

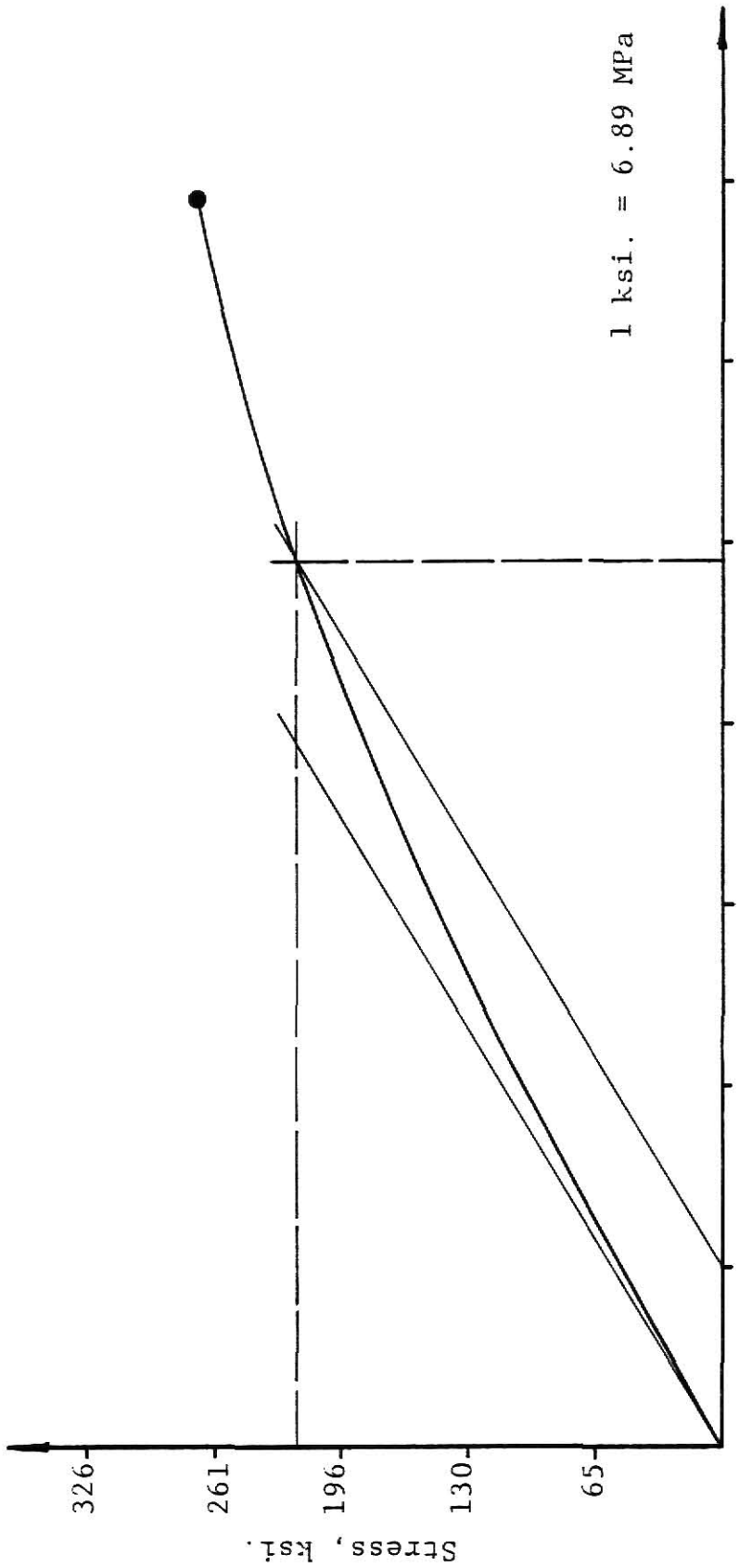

Figure 3.5b Stress-Strain Curve for Reinforcement

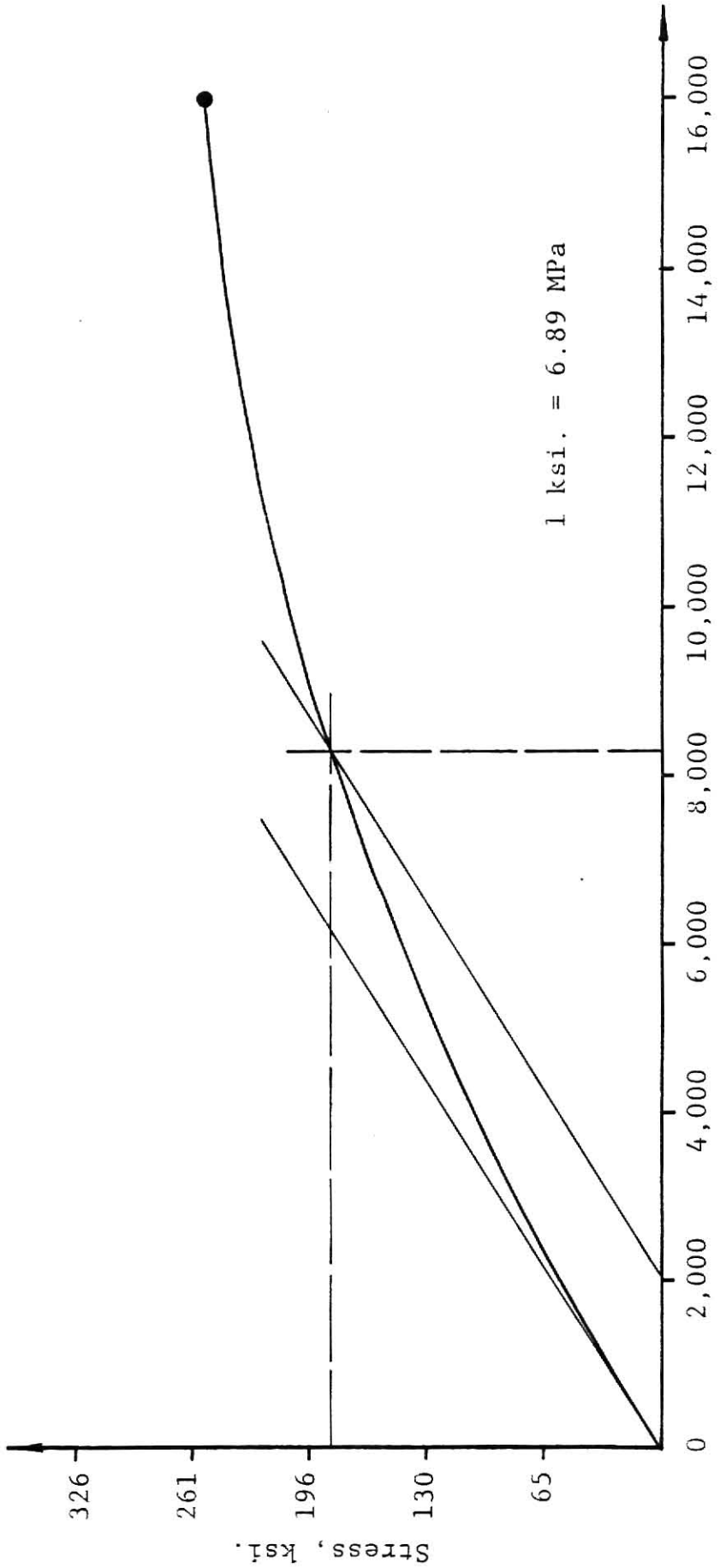

Figure 3.5c Stress-Strain Curve for Reinforcement

Table 3-3 Strength of Reinforcement

Figure	f_{ys} psi.	ε_{ys} in./in.	E psi. x 10^6
3.5a	202,000	0.0096	26.6
3.5b	215,000	0.0096	28.3
3.5c	189,000	0.0086	28.6
Mean	202,000	0.0092	27.8
Std. Devi.	13,000	0.006	1.1

1 psi. = 6.9 kPa

fastened to the system by bolts. The bolts were tightened one quarter turn beyond hand tightening to prevent the inner plexiglass strips from cracking. Before each bolt was put into place it was dipped into grease. The closed plexiglass edges were sealed with parafin. These two steps prevented the loss of water through the bolt holes or through the junction of the plexiglass plates.

3.4 Site Preparation

At the pumping site the large equipment utilized to pump the forms was coordinated to prevent a chaotic atmosphere. The concrete mixer and pump were located next to each other. This reduced any transportation time for the concrete mix. Within the vicinity the miscellaneous tools such as pans, trowels, buckets, shovels, etc., were located for their immediate use. One important item was a continual supply of running water, which could be used to prevent a possible jam within the microconcrete pump. Also located in the distant vicinity was a weigh scale and the necessary equipment utilized when weighing the materials.

3.5 Mixing Microconcrete and Pumping Forms

Mix Design #1, as given in Table 3-2, was the first design mix utilized. The proper quantities of each material were weighed then set aside. With the concrete mixer drum at rest the aggregate and cement were placed into it. The mixer was then activated for thirty seconds. A check was made to insure the cement and aggregate were well mixed. With the mixer activated the water was added in a span of thirty seconds. The mixer continued to run for five minutes with

intermittent spot checks to monitor the proper mixing of the three materials. The entire microconcrete mix was then dumped into a large flat pan which was used as a holding bin and used to transport the mix from the mixer to the pump.

For the first pumping attempt the entire volume of microconcrete mix was dumped into the dry hopper of the pump. Prior to mixing the concrete the pump was thoroughly inspected to assure its proper operation. With the microconcrete in the hopper the pump was activated. However, the mix had segregated in the hopper and the wet aggregate had settled and consolidated around the auger feed of the pump. This prevented the proper operation of the pump. The immediate solution to remedy the problem was to pump water through the pumping system prior to the introduction of the concrete mix into the hopper. The purpose of the water was to act as a lubricant. Small amounts of mix were then added to the water until a continuous flow of mix was obtained through the hopper. A continuous flow was obtained through the hopper by connecting only one hose to the manifold and placing the free end of the hose inside the hopper.

The pumping system was shut off and the hose connected to the plexiglass form. The pump was then turned on, however the mix had segregated and settled around the auger feed of the pump. Thus the mix was not pumpable. Also the design of the manifold reduced the energy of the mix due to head loss.

An innovative approach was utilized in this research to determine the pumpability of the model concrete. The simple task of placing the mixture into the pump was all that was required. It became evident

that the first design mix had to be altered. This was due to the lack of fine particles required as a lubricating agent. Therefore the water-cement and aggregate-cement ratios were decreased to provide the extra fines, as depicted in Table 3-2 for Mix Design 2. The modified mix was then tested and determined to be pumpable. The manifold design was changed in order to eliminate as much energy loss as possible. The cross-section of the modified manifold is shown in Figure 3.6. The modified manifold had the capability of connecting one hose or an adapter could be added to connect two or more hoses.

A third improvement to the pumping phase was to introduce a slurry mix of water-cement with the same ratio as the design mix. The slurry mix replaced the water as a lubricant. This tended to maintain the required water-cement ratio in the mix when added to the hopper.

With the above given improvements a third attempt was made to pump the forms. A double hose connection was fastened to the new manifold. The two hoses were connected to two molds. This connection is shown in Figure 3.7. The molds did not have any reinforcement because this trial was a test to determine if the previous modification to the pumping phase would be successful. The two molds were successfully pumped with microconcrete, however several air voids were viewed throughout both pumped molds. It was concluded that Design Mix 2 was pumpable and that one hose would be used to fill the molds.

For the fourth attempt, four molds were prepared for pumping as previously mentioned in Section 3.3. Design Mix #2 was weighed out,

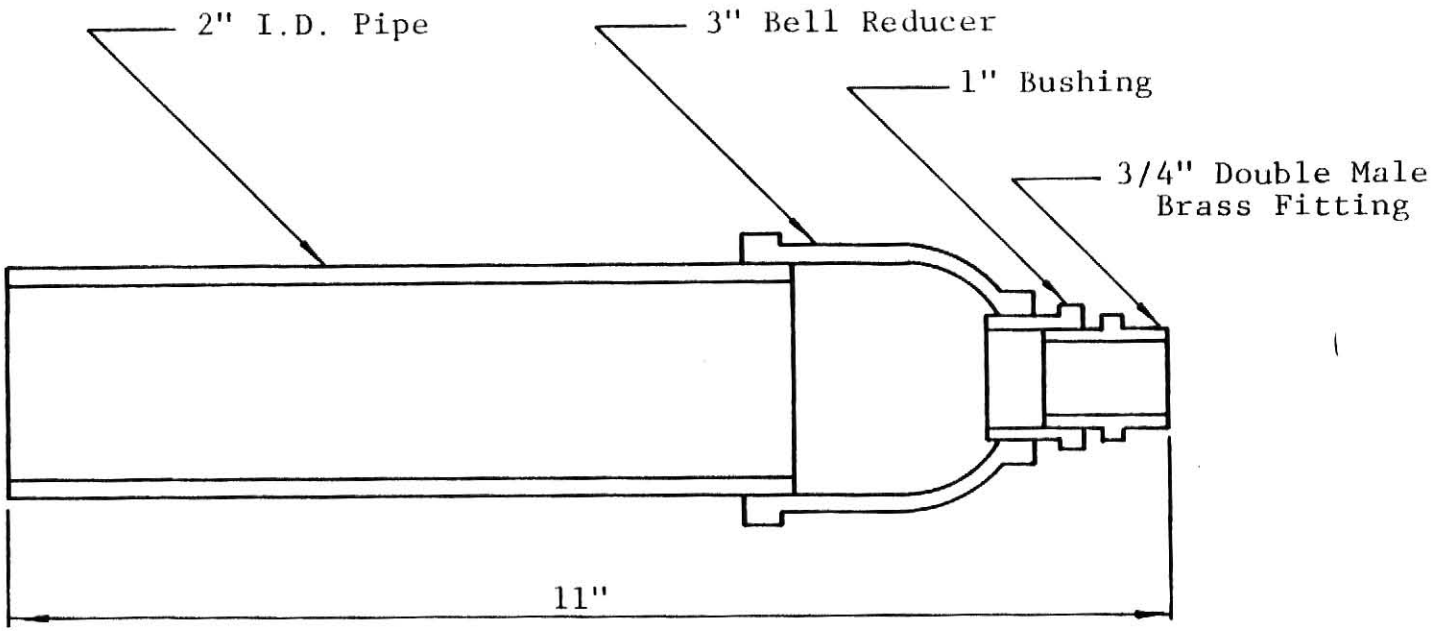

1 in. = 2.54 cm.

Section of Modified Manifold

Figure 3.6 Cross-Section of Modified Manifold

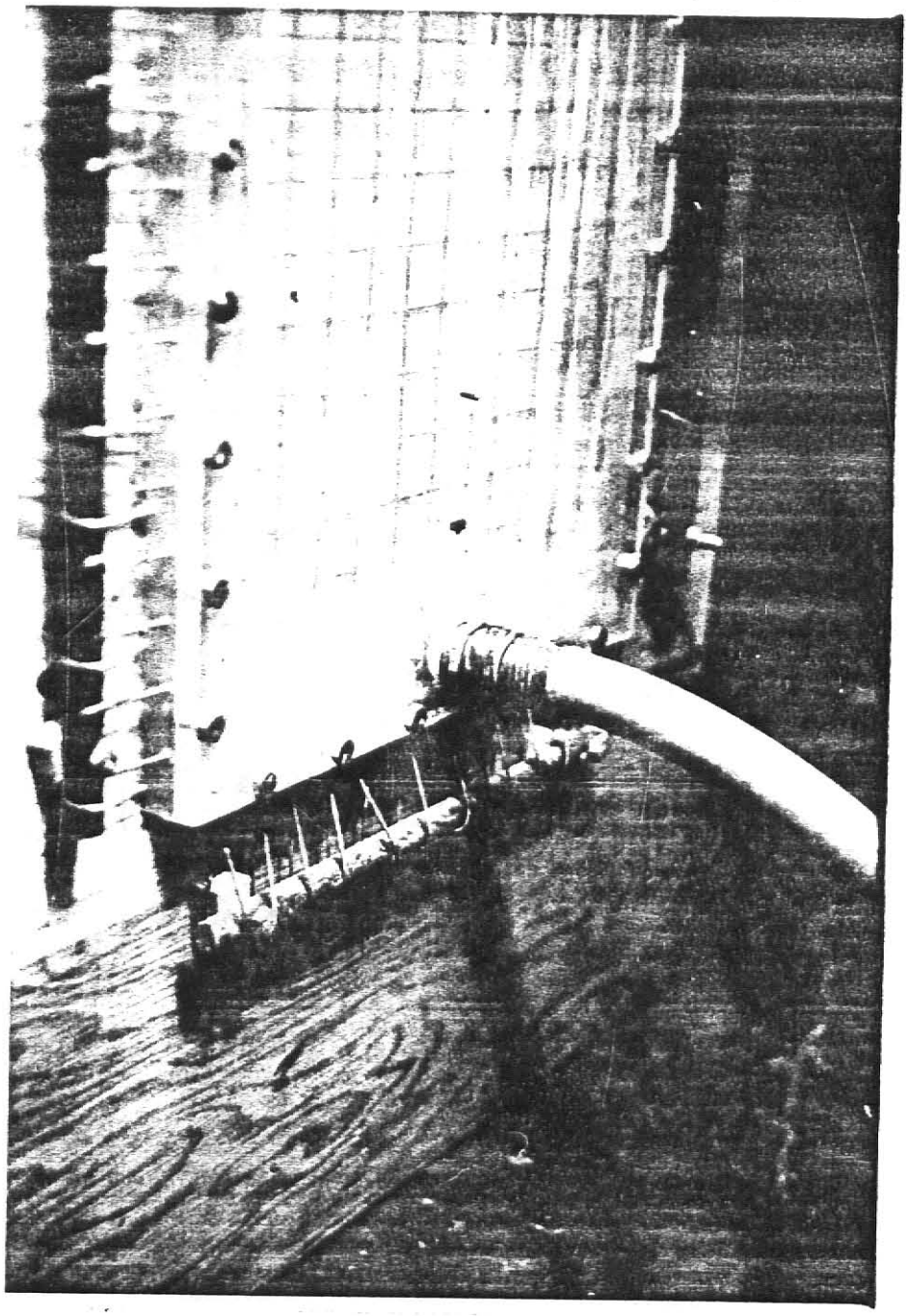

Figure 3.7 Positive Hose Connection

mixed, then placed into the hopper in small quantities until a continuous flow was achieved. One at a time the molds were successfully filled with microconcrete. After filling a single mold the pump was shut off and the mold was capped to prevent the microconcrete from escaping through the brass fitting.

It became difficult to connect the hose to each mold after pumping a previous mold due to aggregate particles adhering to the threads of the hose connection. By the time the fourth mold was pumped the microconcrete had begun its initial set. Thus the fourth mold was not filled because the hose plugged at the mold connection.

It was evident that three factors prohibited the pumping of the molds. First, the opening provided was too small. Second, there is a tremendous loss of energy to the flowing microconcrete due to the right-angle orientation of the opening and the restrictiveness of the mold being filled (i.e., thin wall space). Third, the abnormally high summer temperatures affected the set time of the microconcrete. Table 3-4 shows the temperatures for the days of pumping. It should be noted that the actual temperature at the pumping location could range from 5°F to 10°F higher than the temperature recorded. This was due to the greeenhouse effect of the building. Solutions for the three factors were to provide a larger opening and orientate the opening at an angle to allow a larger quantity of concrete to enter into the form at a lower energy loss and with a smoother flow. A set retarder was added to the design mix to delay the initial set of the concrete mixture, making it a better workable material.

The new orientation of the hose connection made a thirty degree angle to the facing plexiglass. To provide a larger opening, a

Table 3-4 Temperatures on Pumping Dates

Pumping Date	Hourly Temperatures, °F						
	6 a.m.	7 a.m.	8 a.m.	9 a.m.	10 a.m.	Max.	Min.
June 6, 1980	75	78	80	81	83	88	74
June 10, 1980	57	63	68	74	79	86	55
June 12, 1980	72	73	74	73	70	89	70
June 19, 1980	75	77	78	77	76	86	69
June 25, 1980	72	74	77	81	85	97	72
July 16, 1980	80	82	86	91	93	101	80
July 24, 1980	68	75	80	86	89	100	65
July 28, 1980	68	74	79	85	91	105	66
July 30, 1980	81	84	90	95	99	108	82

Note: Temperatures were recorded at K.S.U. Weather Data Library and are indicative of the temperatures for the surrounding area.
$°C = (°F - 32)\ 0.5\bar{5}$

rectangular funnel was designed and fabricated. The rectangular funnel connected to the mold can be seen in Figure 3.8. This modified connection enlarged the opening area by four times the previous opening. This can be seen by comparing Figure 3.9 and Figure 3.2. The set retarder utilized delayed the initial set by approximately sixty minutes, thereby allowing more time to work with the mix.

Two of the four molds designed were reworked to allow the possible connection of the rectangular funnel. These two molds were prepared for pumping as mentioned previously. The fifth attempt to fill the two molds previously prepared met with a certain degree of success.

The newly designed funnel was connected to the hose to be used during the pumping phase. Design Mix #2 was weighed, mixed and placed into the hopper. After achieving a continuous flow through the pump system the pump was shut off. The new funnel was connected to the first mold. This first mold was successfully filled with microconcrete while in a vertical position. After filling, the entire mold was placed in a horizontal position with the funnel engaged with the form. The funnel was then disconnected and the opening was covered with the capping system shown in Figure 3.9. Prior to placing the cover in the opening the periphery of the cover had grease applied to it to prevent any water seepage through the opening. The entire mold was then placed in a vertical position for twenty-four hours before the molds were stripped.

The second mold prepared did not meet with such a good degree of success. The funnel was placed in the mold opening. However after activating the pump the funnel was pushed outward and away from the

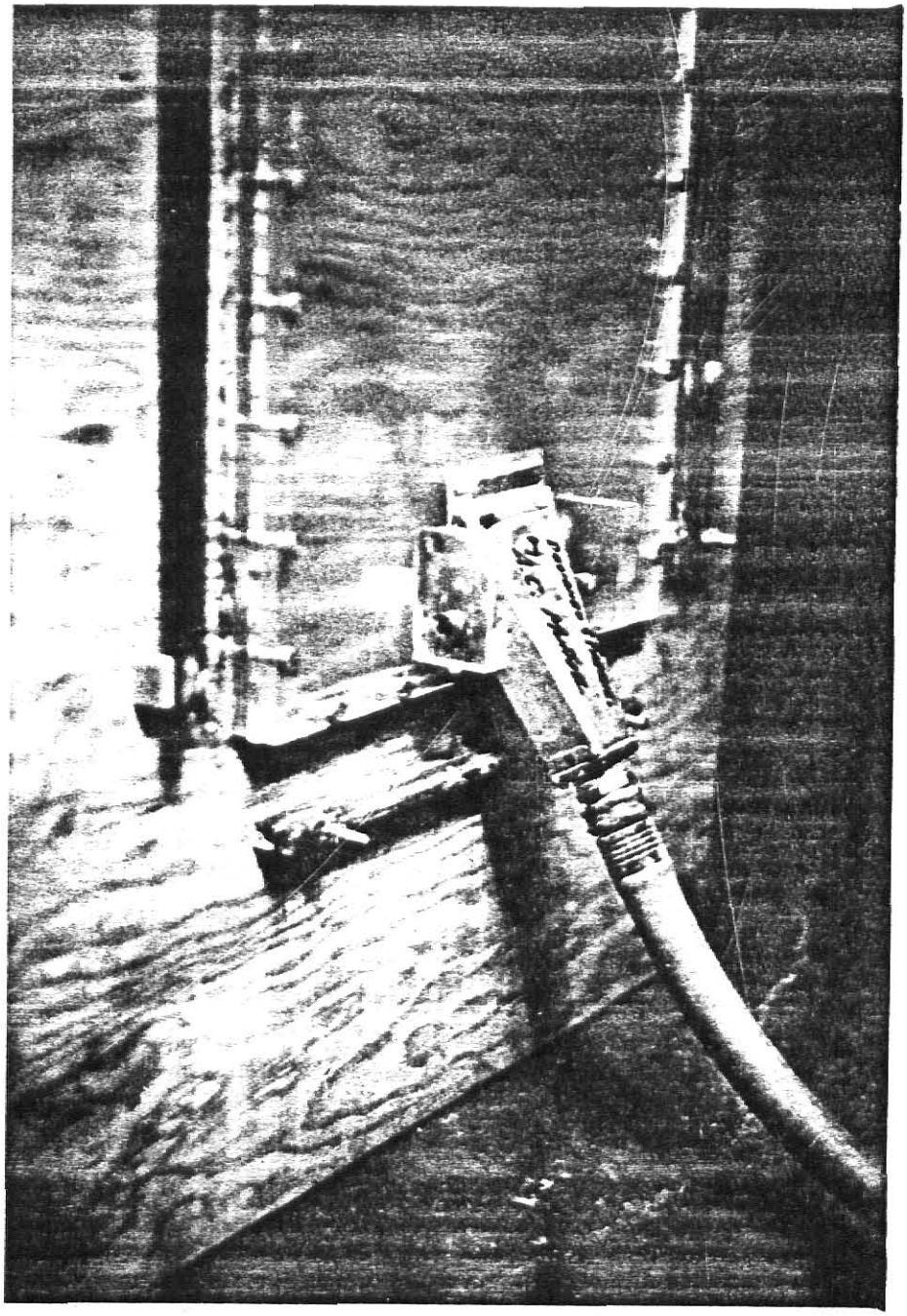

Figure 3.8 Rectangular Funnel Attached to Mold

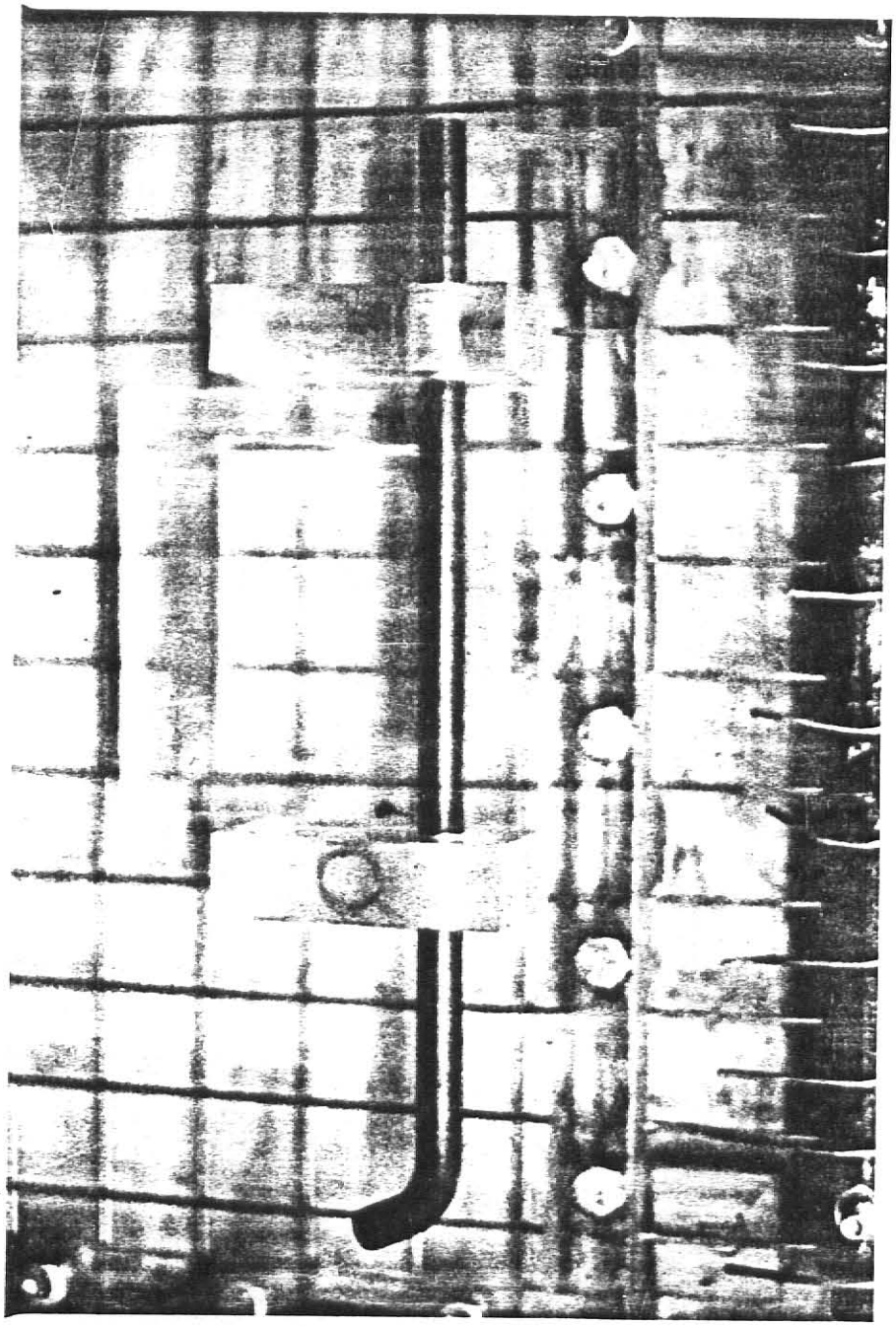

Figure 3.9 Modified Funnel Opening and Capping System

mold by the flowing microconcrete. After disengaging from the mold the hose plugged at the funnel connection.

The reason the funnel was pushed away from the mold was because the bottom edge was not sealed properly into the opening. The hose plugged at the funnel connection due to fatigue of the hose. It was noticed that with each use of the hose it would expand during the pumping phase of the molds. After the completion of pumping the hose would contract to its original diameter. However, continual use of the same hose weakened the hose wall. When the hose expands the inside diameter becomes greater than the inside diameter of the brass connection at the funnel. This creates a constriction through which the microconcrete would not flow, thereby plugging the system.

To prevent the hose from the constant plugging problems, a larger diameter hose was used. The switch to a 3/4 in. (19 mm) inside diameter hose from a 5/8 in. (16 mm) inside diameter hose proved to be the successful solution to the constant problem of plugging within the hose.

The amount of set retarder used in the mix was doubled. This delayed the initial set by more than two hours which allowed a longer work time with the mix. Also due to the abnormally high summer temperatures, the pumping phase for the molds was conducted in the early morning hours of the day prior to the temperature reaching a mid-morning high.

The sixth attempt to pump the molds proved to be the most successful of all previous attempts. The only modification from the fifth trial was the substitution of the larger diameter hose. The two molds were successfully filled with concrete. After filling the molds they were

placed in a horizontal position for twenty-four hour curing. This proved to be the only stumbling block for this attempt.

As the concrete cured it pulled from the front plexiglass surface, due to the shrinkage property of the microconcrete mix. This gave the specimen a textured surface instead of the smooth, glass-like surface desired. To prevent this type of surface fabrication, the remaining molds were cured in a vertical position.

The remaining required molds were pumped as previously described in sets of two and on separate dates. Table 3-5 indicates the date and number of panels fabricated. Having the confidence to successfully fill the molds an attempt was made to employ a different method of filling the molds. The attempt was to fill the mold through the top open end of the mold. For this attempt a fan-shaped funnel was designed and fabricated.

The fan-shaped funnel was connected to the hose then inserted into the top open end of the mold. The area of opening provided by the funnel was approximately 2 sq. in. (650 mm^2). A photo of the fan-shaped funnel inserted into the mold can be viewed in Figure 3.10.

The mix flowed through the hose and funnel then successfully into the mold. However, the surface adhesion of the concrete mix and the plexiglass mold overcame the momentum of the flowing mix. As a result the mold was not filled in the lower quarter section. An attempt was made to force the mix further into the mold by continually pumping the concrete into the mold. The front plexiglass mold plate began to bulge near the funnel connection due to the continual flowing of the micro-concrete. Suddenly, and without much warning, the plexiglass sheet

Table 3-5 Pumping Dates Test Panels were Fabricated

Pumping Date	No. of Molds Pumped	Test Panel No.
June 19, 1980	4	1
		2
		3
		4
July 24, 1980	2	5
		6
July 28, 1980	2	7
		8
July 29, 1980	2	9
		10

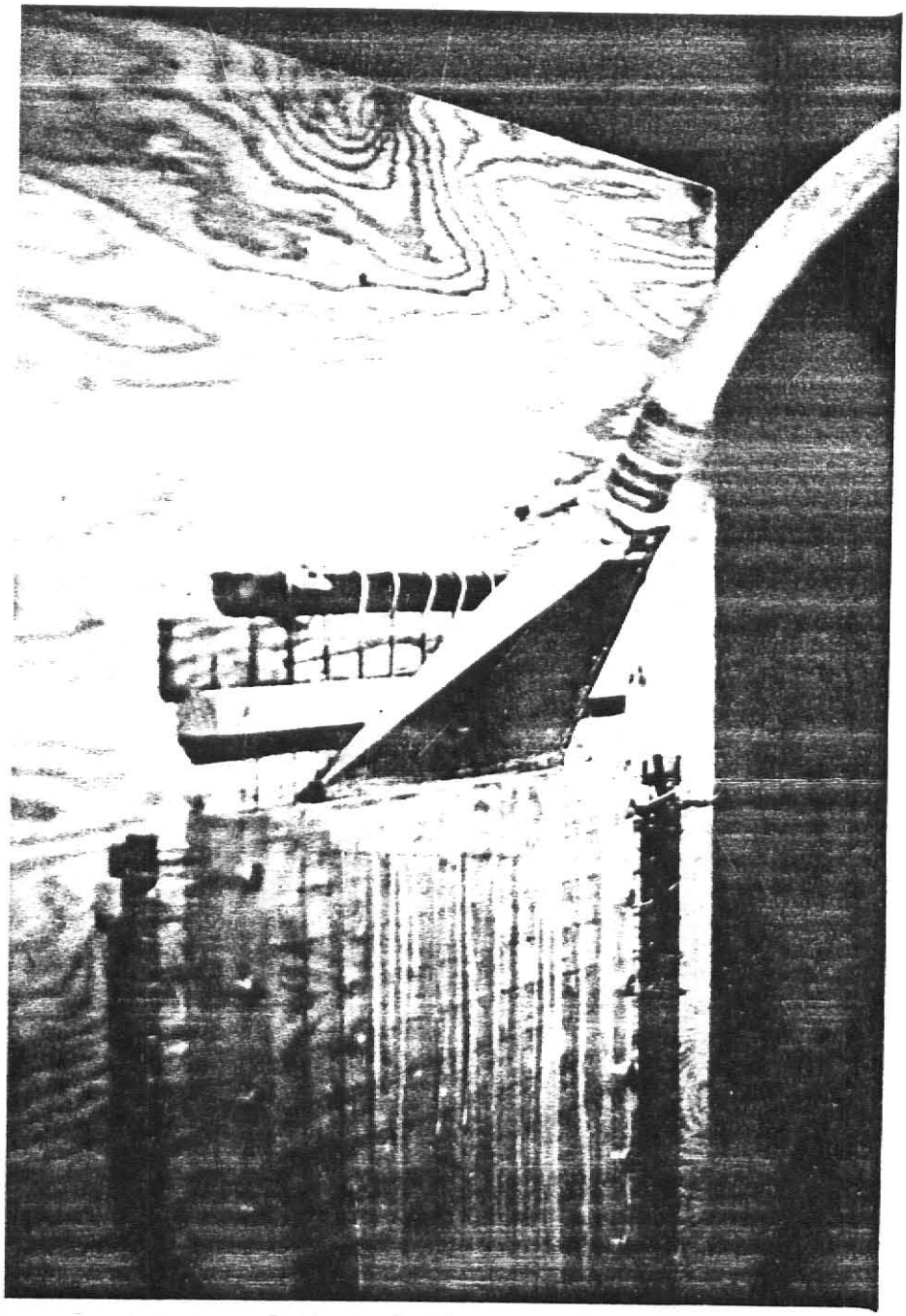

Figure 3.10 Fan-Shaped Funnel Inserted into Mold

fractured near the upper bolt connections. This method to fill the molds was aborted. However, the fan-shaped funnel will be incorporated for the pumping or filling of molds for other research projects.

The remaining sets of molds when filled were cured in a vertical position. This gave the specimens the smooth marble-like surface desired.

3.6 Stripping and Curing of the Specimens

Each test specimen was cured for twenty-four hours in the mold and at a controlled temperature. After the initial twenty-four hour curing time the molds were hand transported to the concrete laboratory. Each reinforcing wire was cut from the bar support holding it. All the bolts were loosened then removed from the mold. The front plexiglass plate was then removed from the mold and the smooth marble-like surface of the test specimen was revealed. The three plexiglass strips were then removed from the sides of the test specimen. It was a little difficult to remove the strips, however with the gain of experience their removal became effortless. The test specimen then was slidden off the back plexiglass plate and laid on a flat smooth surface. The remaining reinforcement ends were trimmed to be flush with the edge of the test specimen.

Each test specimen was then marked with its own individual number, date of casting, and date placed into the 100% moisture room. In the moisture room the test specimen was placed with its long edge on the floor. Room was provided for moisture to come in contact with both surfaces of the test specimen. This prevented the test specimen or test panel from warping while in the cure room. Each test panel was cured for twenty-eight days in the cure room before it could be tested.

After the test panel was placed in the cure room the molds were cleaned and prepared for another test panel fabrication as stated in Section 3.3. A total of ten test panels were fabricated for testing.

3.7 Test Cylinders

Three 3 in. x 6 in. (7.6 cm x 15.2 cm) were cast for each test panel fabricated. One cylinder per mixed batch was used for the determination of the stress-strain curve for that particular micro-concrete mix. The remaining cylinders were tested in compression to determine the compressive strength of the mix. All test cylinders were cured in the same environment that the test panels were cured.

3.8 Design and Fabrication of Test Frame

The function of the test frame was to apply a uniform, uniaxial, in-plane load through the test panel without any eccentricity. Since only one test frame would be constructed it had to be versatile in order to change the support conditions for the test panels. There were basically two test panel support conditions tested. For the first support condition the test panel was simply supported on all four sides. Figure 3.11 shows this support condition. The second support condition used simple supports on the top and bottom of the test panel and also small clip angles along the long sides of the test panel. This condition is depicted in Figure 3.12. The tests conducted on this type of support system also included the varying of the number of clip angles used per side.

Figure 3.13 is a photo of the completed test frame with a sample specimen. This sample specimen is simply-supported on all four edges.

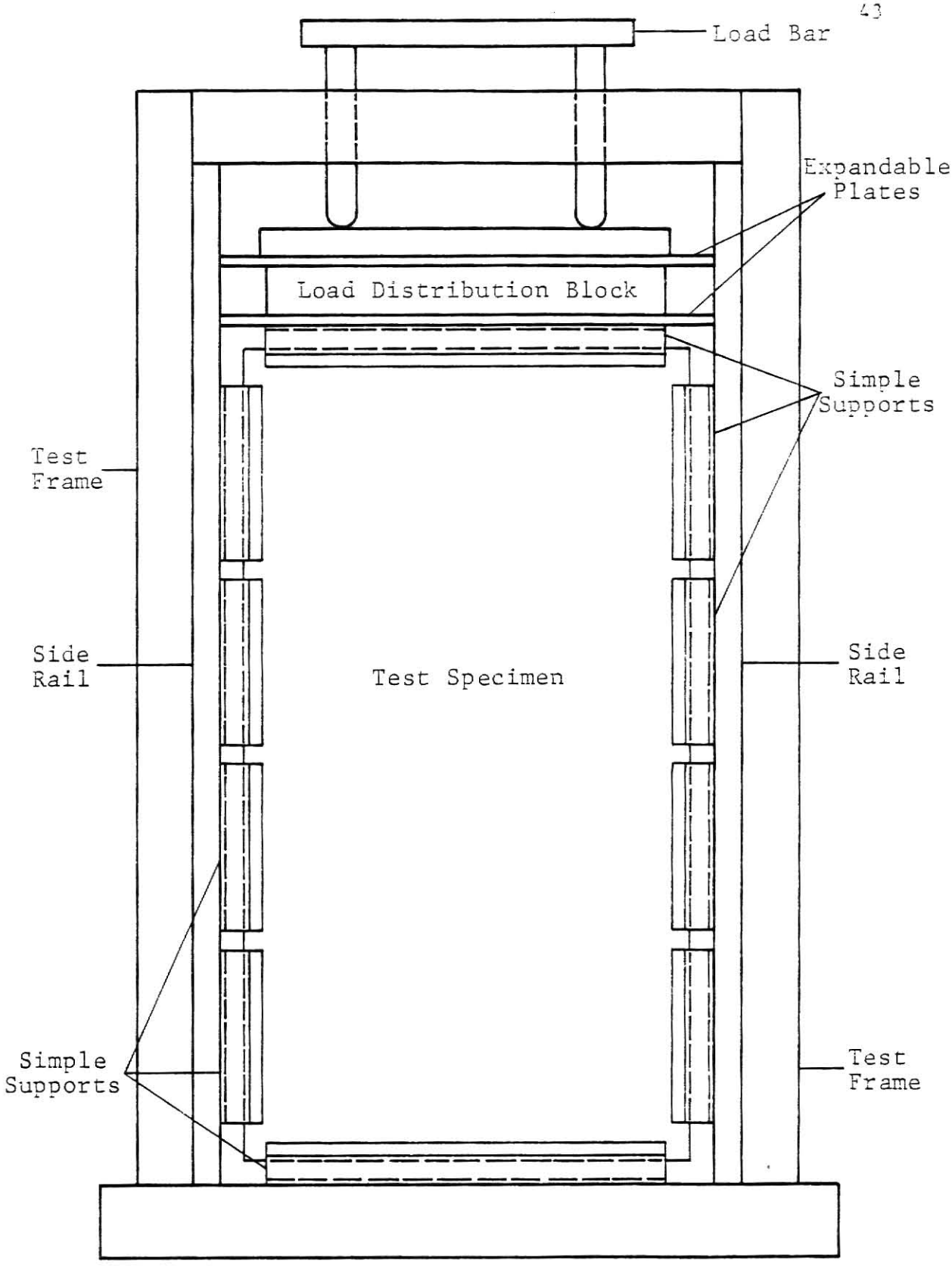

Figure 3.11 Simply-Supported Test Panel

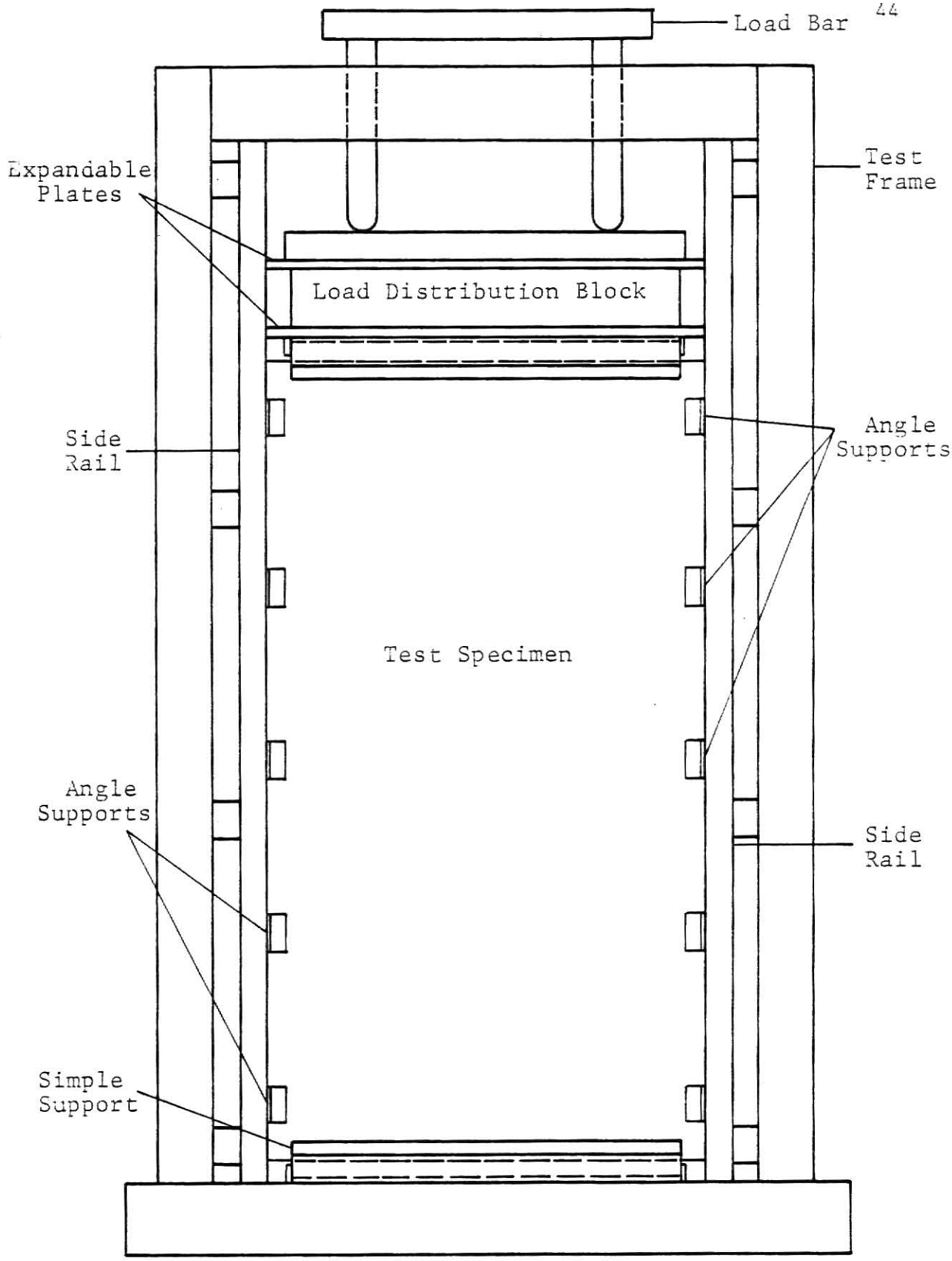

Figure 3.12 Test Panel with Clip Angle Supports

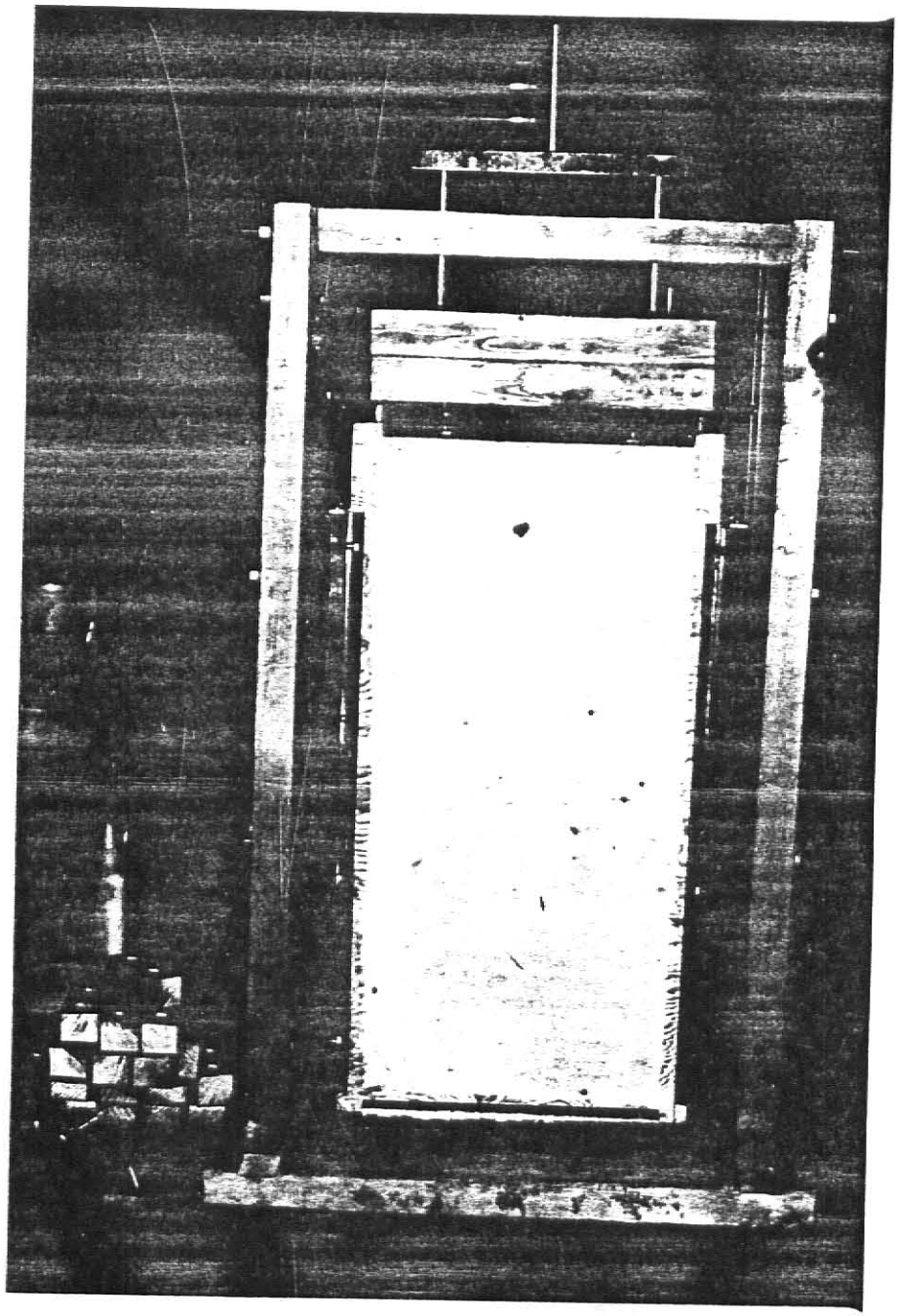

Figure 3.13 Completed Test Frame

Some of the important parts which made up the test frame are the metal side rails, load bar, load distribution block, and simple supports, depicted in Figure 3.11 and Figure 3.12.

The load bar transferred the load from the testing machine to the load distribution block. The load distribution block was made of 3 in. x 3 in. x 11 in. (7.6 cm x 7.6 cm x 28 cm) wood. This block transferred the point load into a uniform load and through the plate.

Attached to the top and bottom of the block was a set of expandable plates with tabs milled at the ends in an outward direction. These tabs were located on both top and bottom plates of the distribution block. The side rail was made of a section of steel 3 in. x 3/4 in. x 33 in. (7.6 cm x 2.0 cm x 84 cm). This section of steel had a slot 1/4 in. (6.4 mm) down the center of the 3 in. (7.6 cm) dimension running the entire length of the bar. Drawings of the side rail are shown in Figure 3.14.

Into this slot the tabs of the plates on the distribution block were inserted. This assured that the test panel would be loaded with minimum eccentricity. Also attached to the bottom of the load block was a simple support. Their fabrication will be discussed later. In the center of the wood base for the frame was a 1 in. (25.4 mm) diameter alignment pin. This pin was inserted into the base of the testing machine to align the loading head of the testing machine and the test frame. The top of the test frame was braced to the sides of the testing machine to prevent any sidesway movement of the frame during the testing phase.

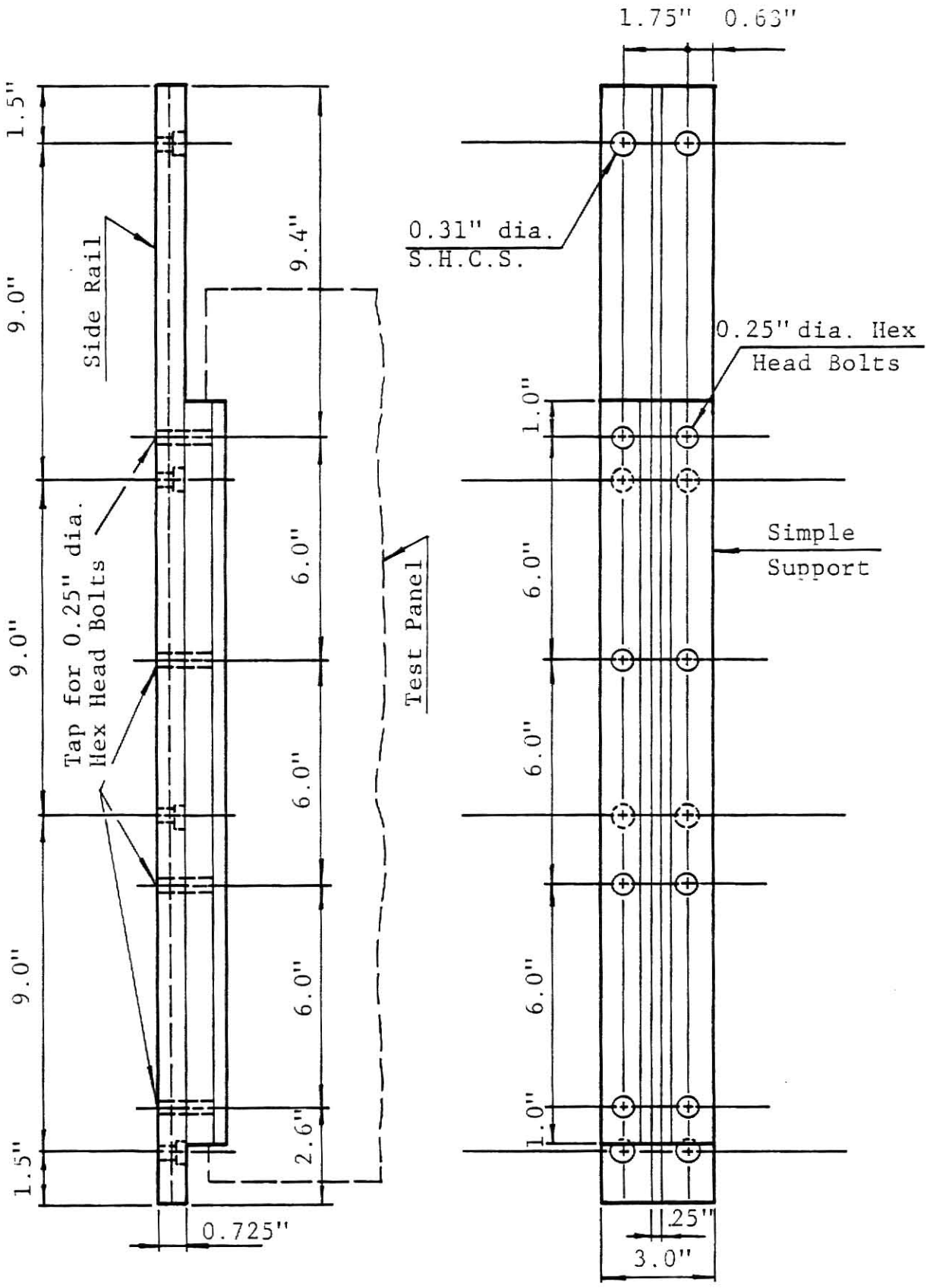

1 in. = 2.54 cm.

Figure 3.14 View of Simple Support Attached to Side Rail

3.9 Fabrication of Supports

The base of the simply supported system was fabricated from a section of steel 3 in. x 3/4 in. (76 mm x 19 mm) in cross-section. Through the center of the 3 in. (76 mm) dimension was a semi-circular slot 1 in. (25.4 mm) in diameter and 1/2 in. (12.7 mm) in depth. To complete the simple support a 1 in. (25.4 mm) diameter bar was cut into small disks. Both surfaces of the disks were then milled until the length of each disk was 1/2 in. (12.7 mm). A 1/4 in. (6.4 mm) slot was then milled into each disk. This slot started at the center of the disk and extend outward in a radial direction. These disks were then placed in series and inserted into the 3 in. (7.6 cm) base previously discussed. Drawings for the fabrication of the simple supports can be viewed in Figure 3.15. The simple supports were then attached to the side rails (shown in Figure 3.14), wood base and load distribution block. A drawing showing the test frame with a test panel simply supported on all edges is pictured in Figure 3.11. This figure shows the modified simple supports on the slide rails of the test frame.

The clip angles were made from angle iron 1/2 in. x 1/2 in. x 1/8 in. (12.7 mm x 12.7 mm x 3.2 mm). The angle iron was cut into 1 in. (25.4 mm) lengths. These angles were then glued to the test panels at the locations shown in Figure 3.12.

The simple supports were attached to the frame by hex head bolts while the clip angles were attached by friction retainers attached to the side rails of the test frame.

3.10 Preparation of Test Panels

Each test panel was prepared for testing separately. Three days prior to the scheduled testing date the test panel was removed from

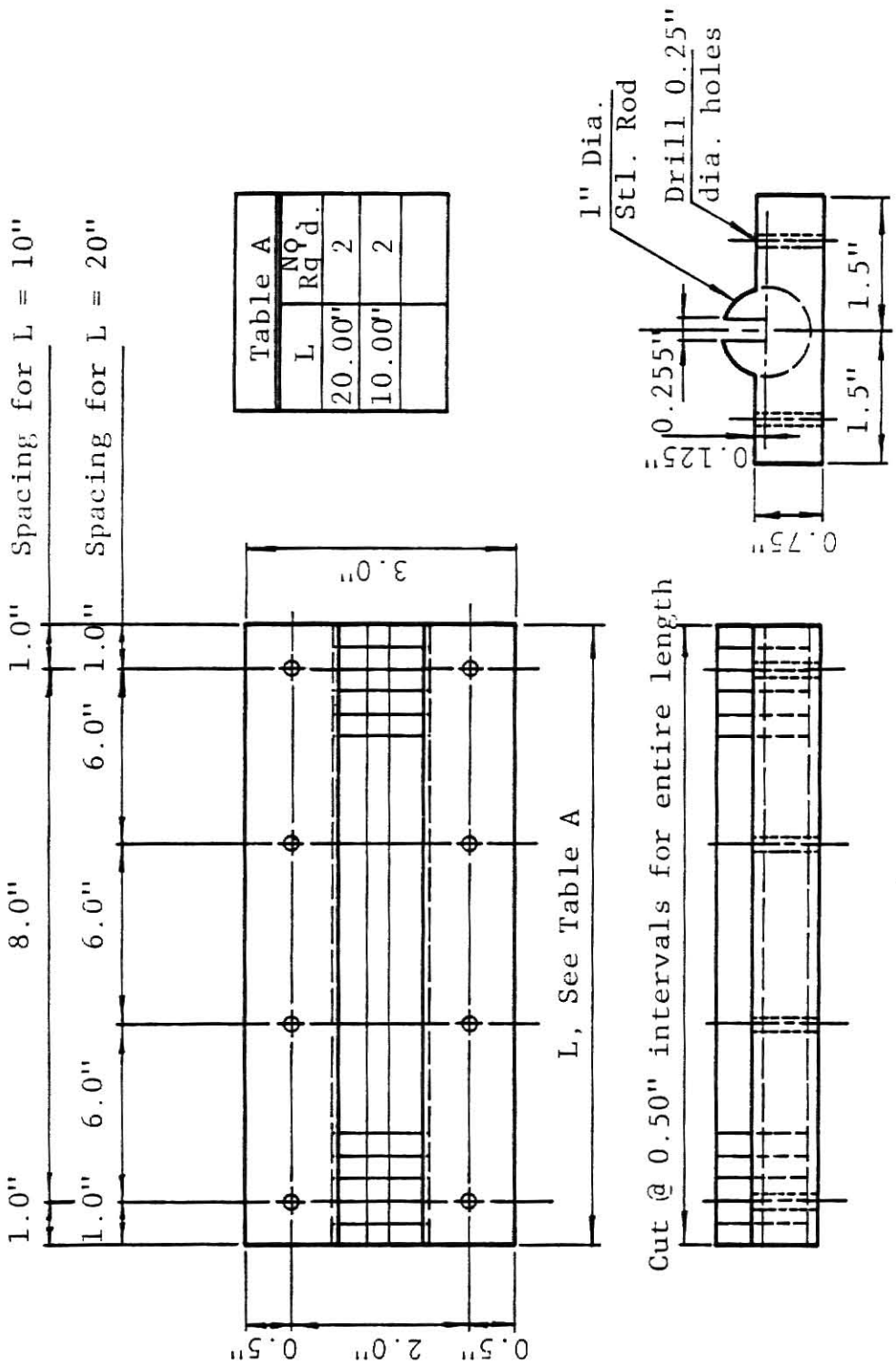

1 in. = 2.54 cm.

Figure 3.15 Drawing of Simple Support

the moisture room. The panel was set on edge to dry properly. The locations for the strain gages and dial indicator gages were marked directly on each panel after the panel had been cleaned. Cleaning the panel was an effortless task of removing, by wiping, any residue the panel may have collected while in the cure room.

After the panel had dried for twenty-four hours the strain gages were mounted onto the panel. The strain gages were located 1/2 in. (12.7 cm) to the left of the center of the panel to prevent any disturbance which may occur from the dial gages. The locations for the strain gage and dial gages are depicted in Figure 3.16. The strain gages were orientated in parallel with the long dimension of the panel. They were placed in the same locations but on opposite surfaces to measure the tension or compression strain of the particular surface. Table 3-6 shows the type and properties of the strain gage used.

Table 3-6 Strain Gage Properties for Test Panel

Strain Gage	University Precision Resistance
Type	Wire Type W32
Gage Length	0.32 in. (0.81 cm)
Gage Resistance	120 Ω
Gage Factor	1.95

The wire strain gages were bonded to the test specimen with Duco-cement by DuPont. First a small quantity of the bonding agent was spread over the area where the strain gage was to be placed. The gage was then properly placed on the location and firmly set into place. Then another small quantity of Duco-cement was applied over the gage to prevent it from peeling off from the test specimen.

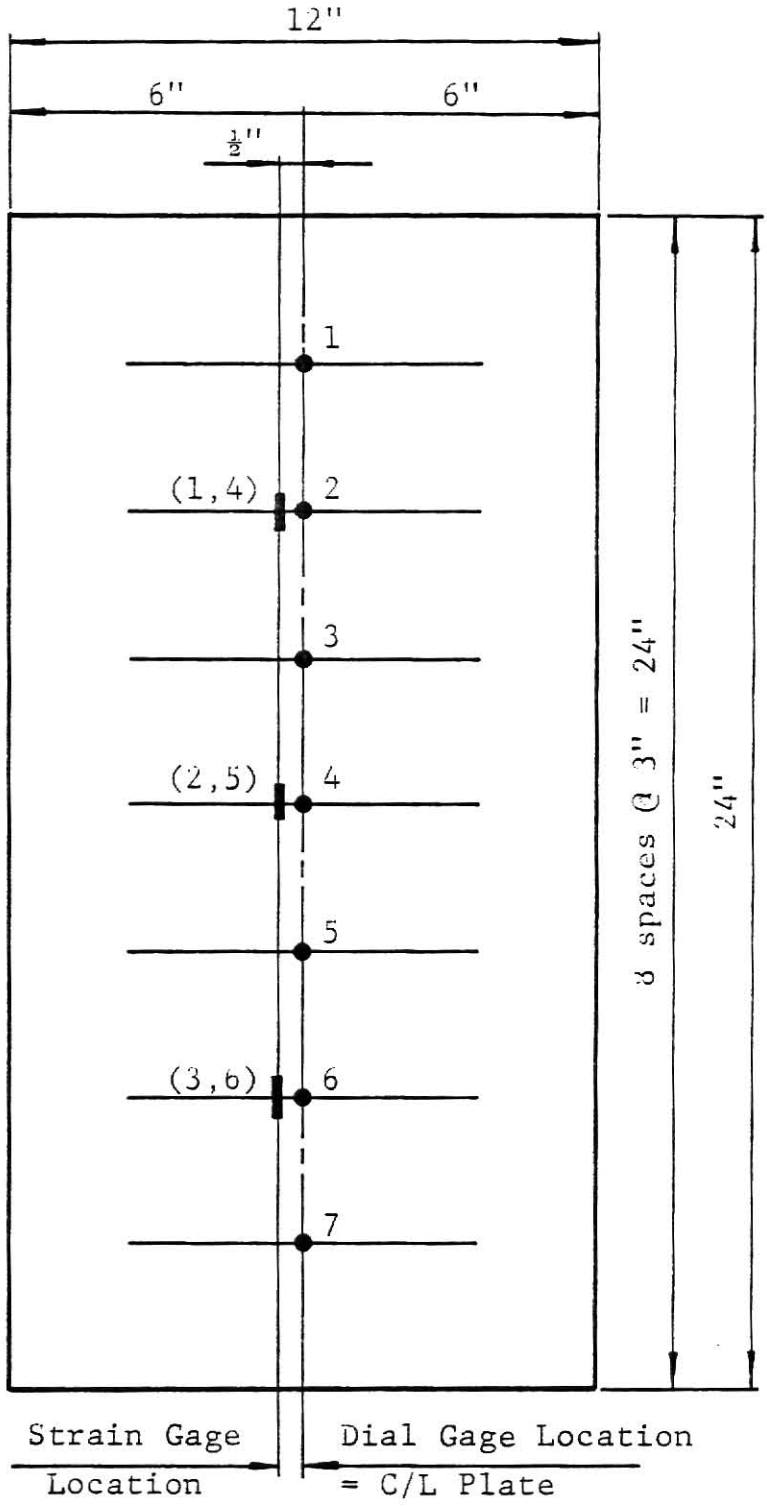

Figure 3.16 Gage Locations on Test Panel

After a three hour drying time the lead wires were soldered to the strain gages. Tape was then placed on the strain gages and the wires were taped down onto the test panel to prevent them from pulling the strain gages during handling.

3.11 Test Set-up

The 20,000 lb. (90 kN) Riehle Compression Testing Machine was used for testing the panels. The testing frame was properly orientated on the machine then securely braced to prevent movement during the testing phase. With the proper supports attached the test specimen was maneuvered to the correct position. The load distribution block was then placed on the test panel. Figures 3.11, 3.12, and 3.13 show test panels set in the test frame ready for testing. The strain gage lead wires were then connected to the Budd Switch and Balance Unit in an ascending order. The switch and balance unit was then wired to a Strainsert Strain Indicator. The strain indicator was set in a half-bridge mode. A temperature compensating gage consisting of a metal foil gage mounted on a sample concrete cylinder was also wired into the strain indicator. Seven Soil Test LC-10 dial gages securely fastened to a metal stand were then located at the positions shown in Figure 3.16. The dial gages measured the deflection of the center of the panel. Figure 3.17 shows the dial gages used to measure the panel deflection. The gages have a range of 2.000 in. (5.1 cm) with an accuracy of 0.001 in. (0.03 mm).

3.12 Testing Procedure

With the test panel properly situated in the testing machine as mentioned in Section 3.11, the panel was loaded to properly seat the

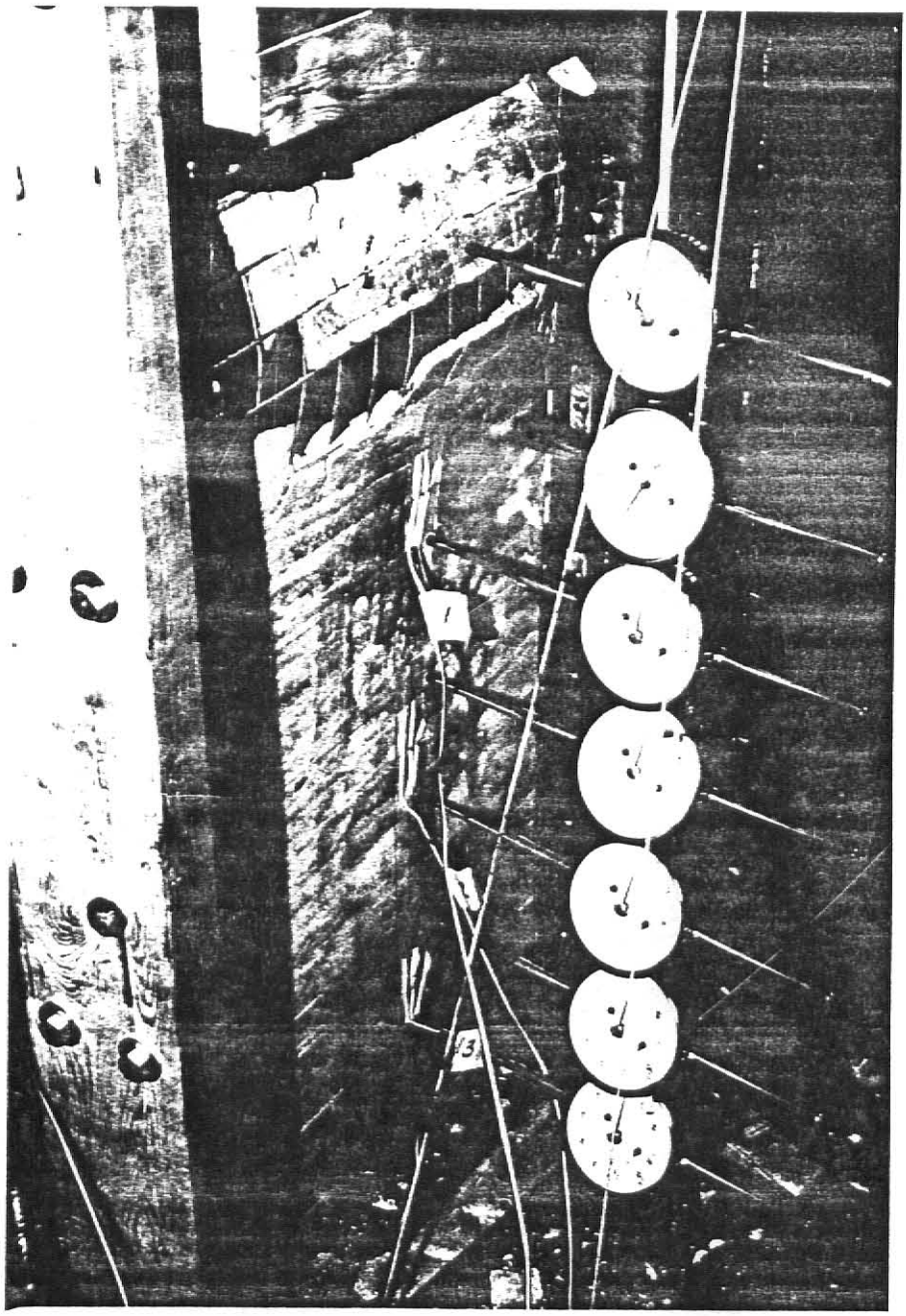

Figure 3.17 Deflection Gages Mounted to Stand

load distribution block containing the top simple support on the panel. To reduce the effects of hysteresis, zero shift, and deviation from linearity the gages may have acquired during installation strain cycling was conducted on each test panel prior to performing the actual tests. After several strain cycles, the strain gages were rebalanced to zero. At this point the dial gage readings were recorded. The test panel was then incrementally loaded to failure with strain and dial gage readings being manually recorded after each incremental increase of load. Table 3-7 depicts the type of support conditions for each panel tested. The testing of the cylinders occurred on the same date the test panel was tested. The cylinders were also removed from the cure room on the date the test panel was removed. There was a total of four batches of mix #2 made. Therefore, four cylinders were tested to determine the stress-strain properties of the mix. The properties for the gages mentioned are depicted in Table 3-8. The gages were located at mid-height of the cylinder. The top of the cylinder was marked into four equal wedge sections, i.e., two diameter lines 90° ($\pi/4$ rad.) apart. Where these lines intersected the circumference of the cylinder they were drawn downward to intersect the mid-height line of the cylinder. At these intersections is where the strain gages were located. The gages were glued onto the cylinder with Duco-cement in a similar fashion as the gages for the test panel. A total of four gages were used per cylinder. They were orientated in a horizontal, vertical, horizontal, vertical pattern. The lead wires were soldered to the gages and taped to the cylinder to prevent damage to the gages while being handled. Sulfur caps were then applied to the ends of the

Table 3-7 Panel Number and Support Conditions

Support Conditions			Panel No.	Pumping Date
Top	Bottom	Sides		
S.S.	S.S.	S.S.	1	6-19
S.S.	S.S.	S.S.	2	6-19
S.S.	S.S.	2A/side	3	6-19
S.S.	S.S.	2A/side	4	6-19
S.S.	S.S.	3A/side	5	7-24
S.S.	S.S.	3A/side	6	7-24
S.S.	S.S.	3A/side	9	7-30
S.S.	S.S.	5A/side	7	7-28
S.S.	S.S.	5A/side	8	7-28
S.S.	S.S.	5A/side	10	7-30

S.S. = Simple Support A = Angle

Table 3-8 Strain Gage Properties for Cylinder

Strain Gage	BLH Electronics SR-4
Type	A-5-1-S6
Gage Resistance	120Ω ± 0.2
Gage Factor	2.01 ± 1%

Table 3-9 Actual Panel Thickness Based on 18 Data Points

Plate No.	Design Thickness	Fabrication* Thickness	Standard Deviation	Coefficient of Variation (%)	Percent Difference
1	0.250"	0.299"	0.004	1.338	+19.6
2	0.250"	0.308"	0.005	1.623	+23.2
3	0.250"	0.254"	0.004	1.575	+ 1.6
4	0.250"	0.280"	0.005	1.786	+12.0
5	0.250"	0.244"	0.003	1.230	- 2.4
6	0.250"	0.231"	0.006	2.597	- 7.6
7	0.250"	0.309"	0.007	2.265	+23.6
8	0.250"	0.327"	0.012	3.670	+30.8
9	0.250"	0.251"	0.004	1.595	+ 0.4
10	0.250"	0.238"	0.010	4.202	- 4.8

*From a compilation at 18 data points per panel.

1 in. = 25.4 mm

cylinder to enhance the distribution of applied load. To determine the stress-strain properties of the mix, the gaged cylinders were tested in the Southwark Compression Testing Machine. The gage lead wires were connected to the Budd Switch and Balance Unit in a similar fashion as the gage wires were for the test panel. This unit was then wired to the Strainsert Transducer Strain Indicator. The Half-Bridge series with the temperature compensating gage previously described also were connected. Strain cycling was also conducted on these gages to reduce the effects of hysteresis, zero shift and deviation from linearity. They were then balanced to zero. After balancing the gages the cylinder was loaded incrementally until the cylinder failed. The strain gages readings were recorded manually after each incremental load. The remaining twenty-six cylinders without strain gages were tested in compression to determine the nominal strength of the test panels. These are indicated on Figure 4.21 through Figure 4.24.

3.13 Panel Thickness Measurements

After testing of the test panels the thicknesses were measured. This was accomplished by using two Soil Test LC-10 dial gages. The gages were connected in a manner which allowed both movable ends to move simultaneously. The instrumentation set-up is shown in Figure 3.18. Prior to inserting the panel between the two gages a grid pattern of 3 in. (7.6 cm) squares were marked on the panel. The initial difference of the two dial gages were recorded. The test panel was then placed between the gages. Eighteen readings were taken per test panel. Table 3-9 shows the results of the measurements taken on each test panel.

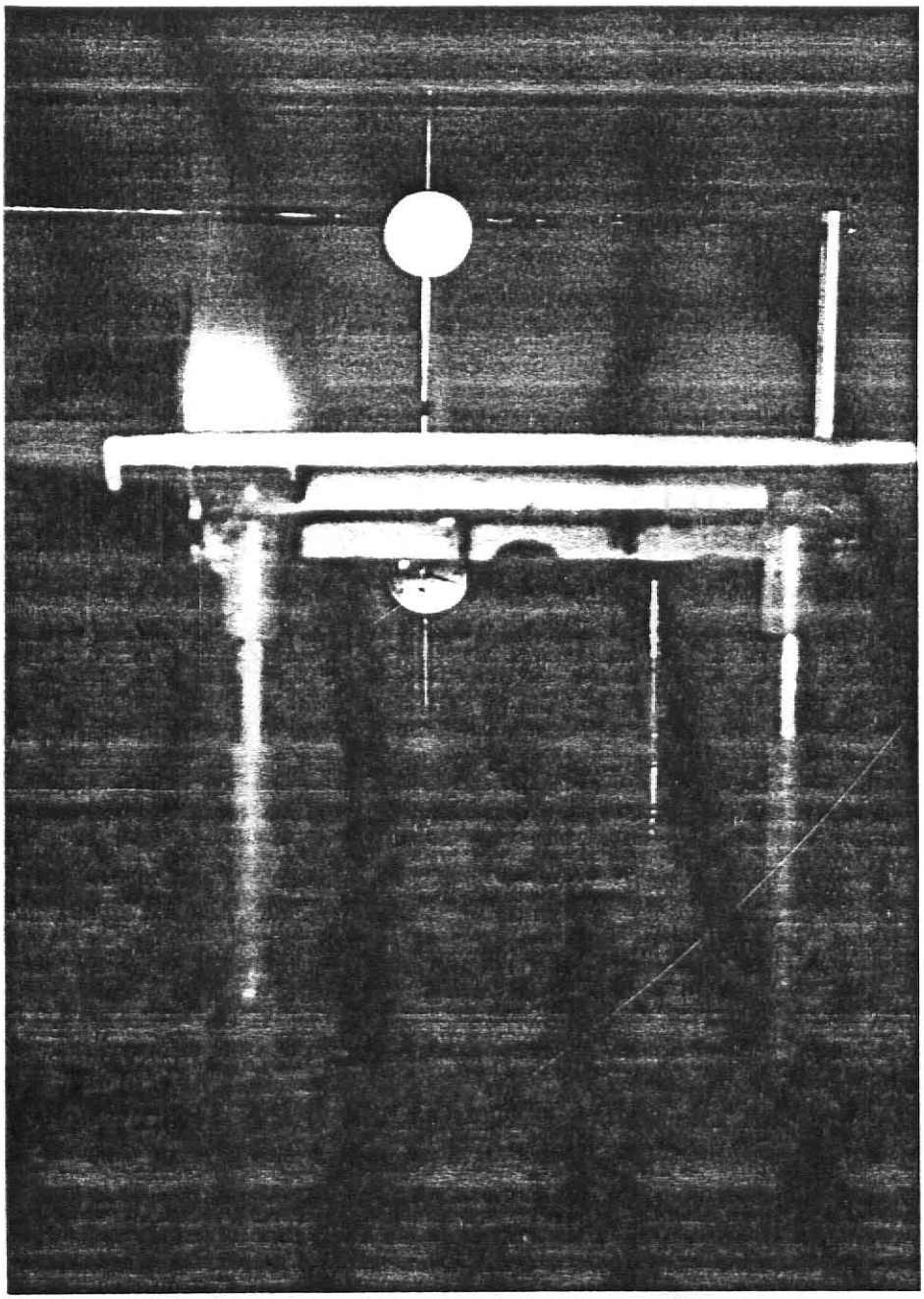

Figure 3.18 Test Panel Thickness Measuring Device

Chapter 4

TEST RESULTS

4.1 Test Summary

A total of ten test panels were fabricated. These panels were tested in uniaxial in-plane compression through the center of the panel thickness. The testing frame was designed and constructed to prevent any appreciable amount of moment from being applied to the panel. Of the ten test panels fabricated, two were tested with a simple support condition on all four edges. Two panels were tested with the combination of simple supports on the short dimension of the panel and two angles (one each near the top and bottom) fastened per side to the panel. The remaining six panels were tested in a similar fashion except for increasing the number of angles fastened to the panel. Three panels had three angles fastened per side (top, mid-section and near bottom). The last three panels had five angles fastened per side (near the top, bottom, and at quarter points. See Figure 3.13). Panel number and type of support conditions are depicted in Table 3-7.

Mix Design #2 was used four times to fill the molds. Three cylinders were cast for each test panel fabricated. A total of thirty cylinders were cast. Test panels one through four were made from the first batch of Mix #2, therefore twelve cylinders were cast. Two test panels were fabricated from each of the other three batches. Six cylinders were cast from each batch making a total of thirty 3 in. x 6 in. (7.6 cm x 15.2 cm) cylinders.

One cylinder from each of the four batches was used to determine the stress-strain relationship for that particular batch. This

cylinder was tested after the last panel from the particular batch was tested. The remaining twenty-six cylinders were tested on the same date the plates were tested (three per plate) to determine the strength of the plate.

4.2 Test Results

The data recorded from each test is graphically shown in Figures 4.1a,b,c through Figures 4.10a,b,c. The figures graphically compare the load-strain properties for the gages at the same location but on opposite surfaces. The buckling load for the test panel is indicated by the change of strain direction as the panel is increasingly loaded.

The deflection profiles for the center of the test panel are displayed in Figures 4.11 through 4.20. The profiles were made from the collection of data recorded by the dial gage readings. The panels deflected in one or two waves depending on the support conditions.

From the information collected from the compression testing of the cylinders in Figures 4.21 through 4.28 were constructed. Figures 4.21 through 4.24 are the stress-strain curves for the data collected and for the calculated curve using Equation (2.3a). As can be seen, these two curves are in close agreement. This is proof that Equation (2.3a) is a justifiable equation. Figures 4.25 through 4.28 graphically depict the variance in Poisson's Ratio with increasing load. The average cylinder compressive strengths are shown in Table 4-1.

Two sets of calculations were made to determine the buckling load of the test panels. The first set of calculations utilized the theoretical panel thickness to determine the critical load. These

calculations are summarized in Tables 4-2, 4-3, and 4-4. After measuring the panel thickness, as mentioned in Chapter 3, the critical panel load was recalculated using the actual panel thickness. The critical loads are summarized in Tables 4-5 through 4-7.

Also shown are Figures 4.29 and 4.30 which graphically show the comparison of the Experimental Critical Load (P_{crE}) to the Calculated Critical Load (P_{crT}) ratio vs the panel number. Note how the mean is lower for the ratio calculated by using the actual panel thickness in Figure 4.30.

Table 4-8 is a summary of the critical loads due to theoretical and actual panel thickness. Also included are the values obtained from experimental results.

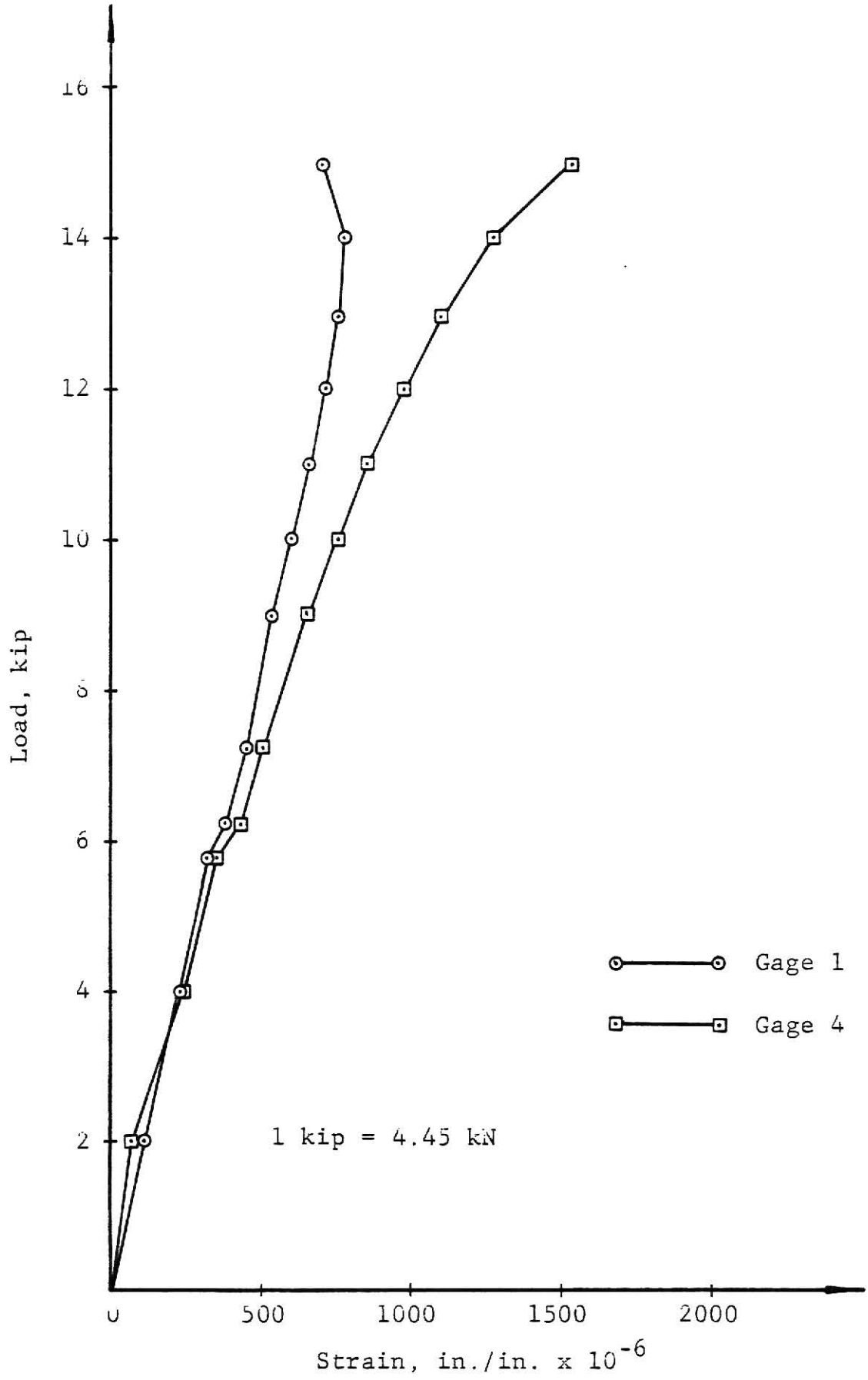

Figure 4.1a Load vs. Strain, Plate 1, Gage 1 & Gage 4

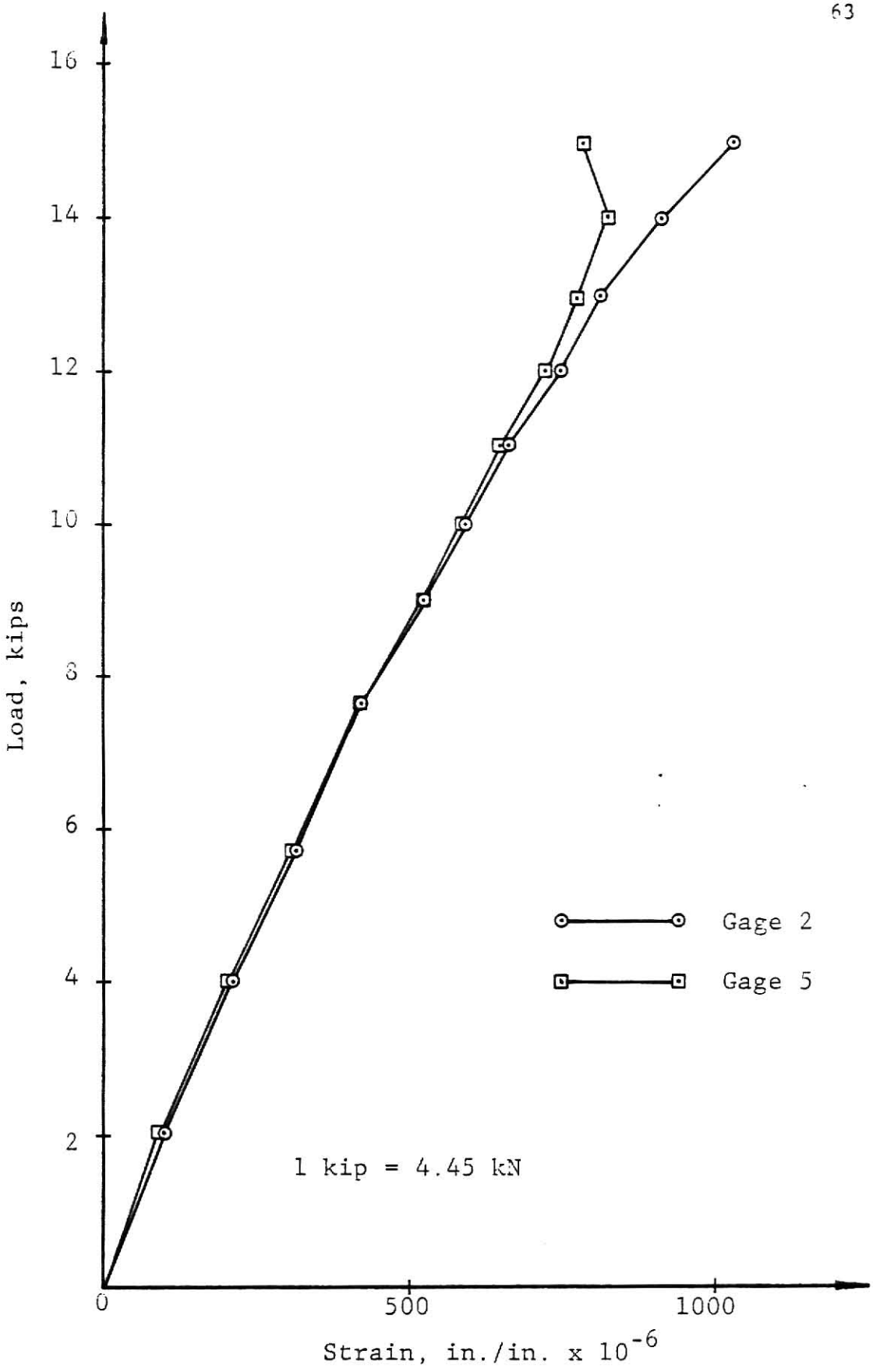

Figure 4.1b Load vs. Strain, Plate 1, Gage 2 & Gage 5

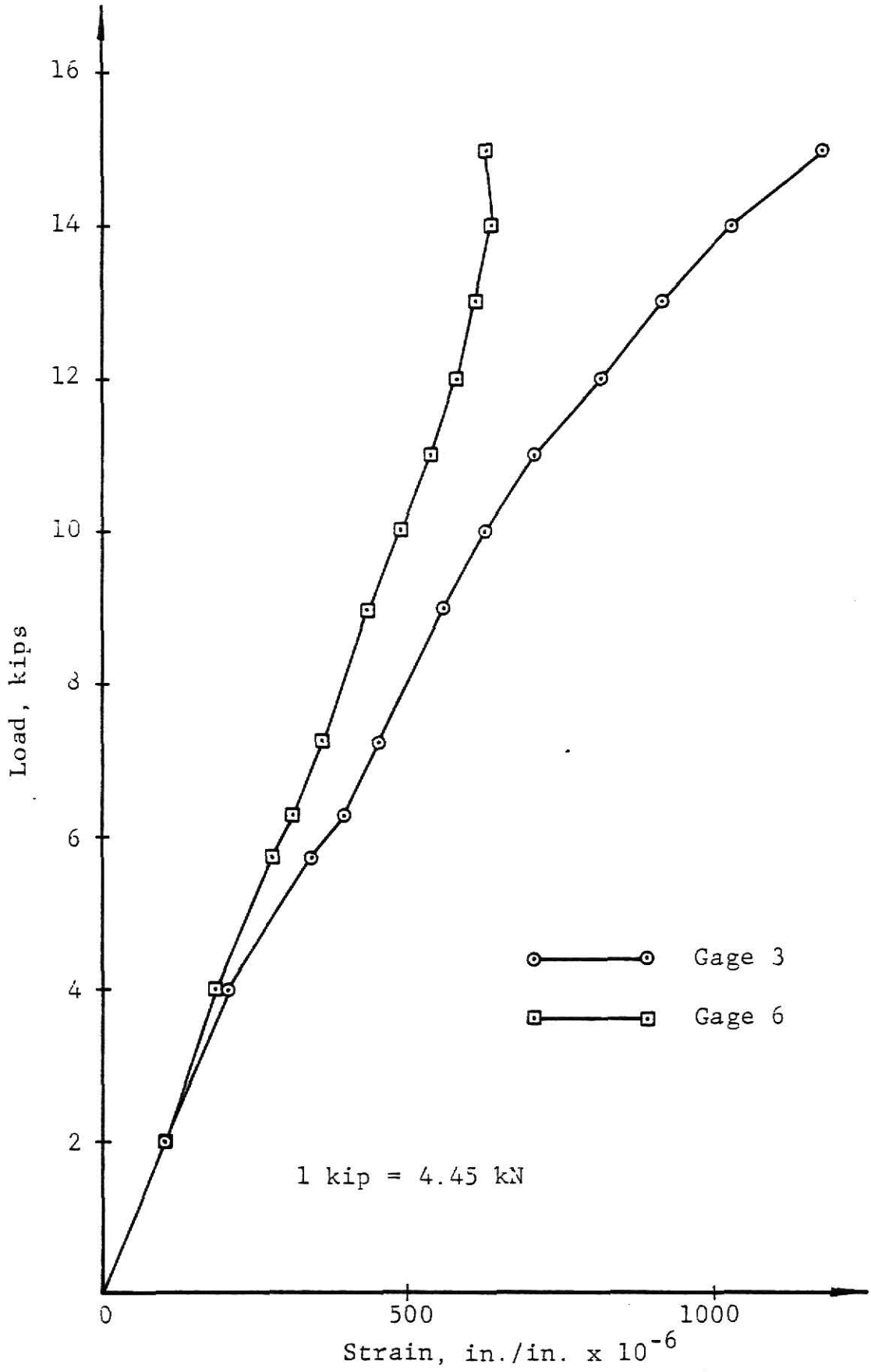

Figure 4.1c Load vs. Strain, Plate 1, Gage 3 & Gage 6

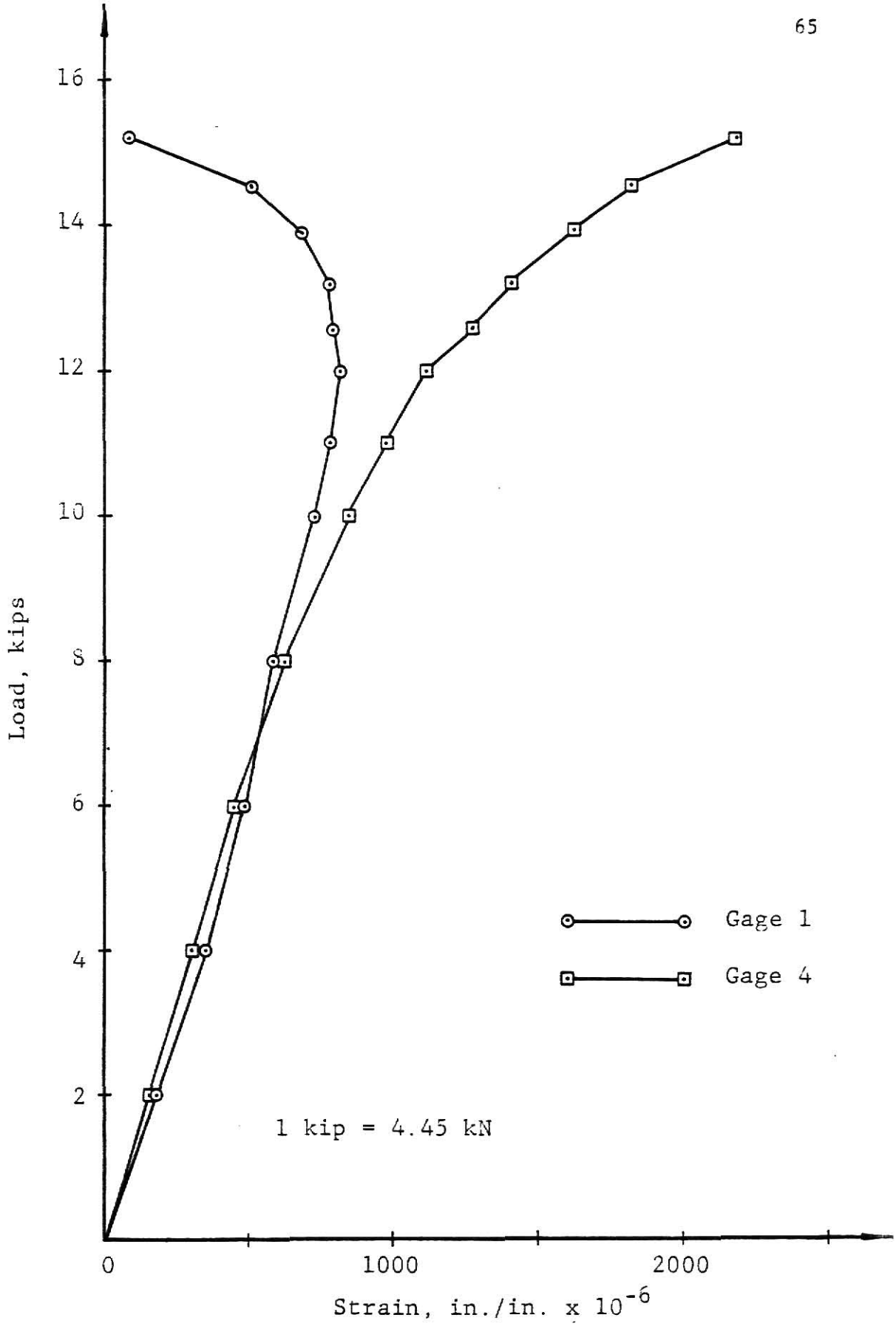

Figure 4.2a Load vs. Strain, Plate 2, Gage 1 & Gage 4

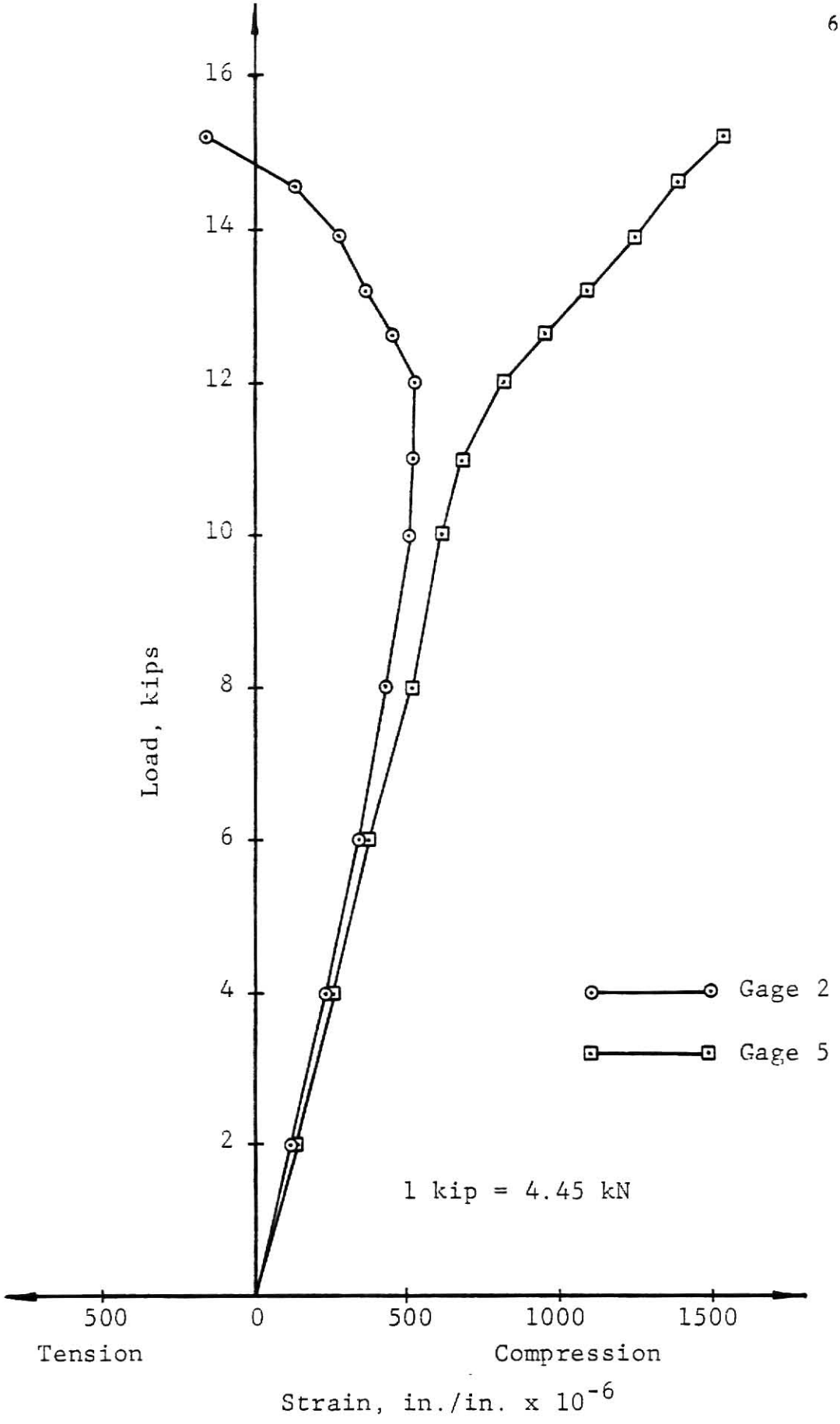

Figure 4.2b Load vs. Strain, Plate 2, Gage 2 & Gage 5

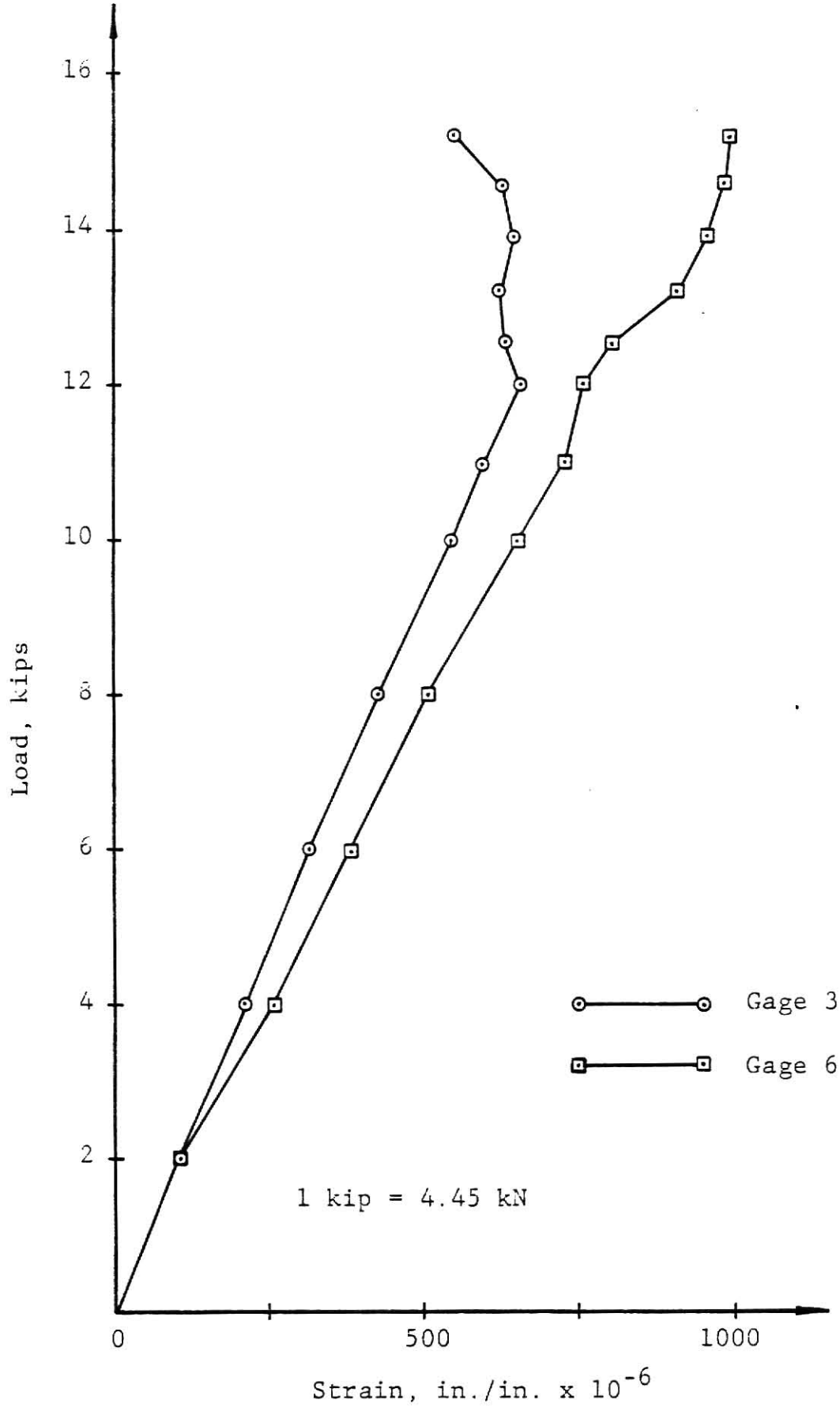

Figure 4.2c Load vs. Strain, Plate 2, Gage 3 & Gage 6

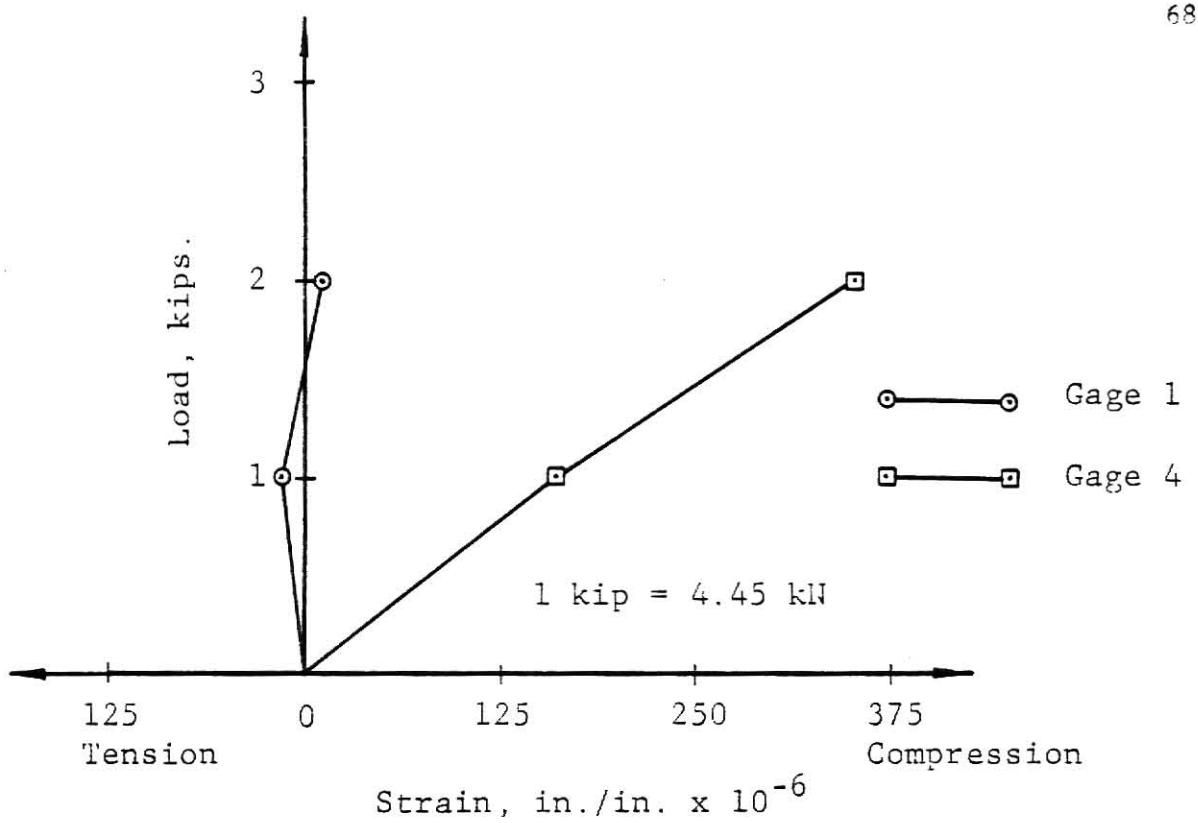

Figure 4.3a Load vs. Strain, Plate 3, Gage 1 & Gage 4

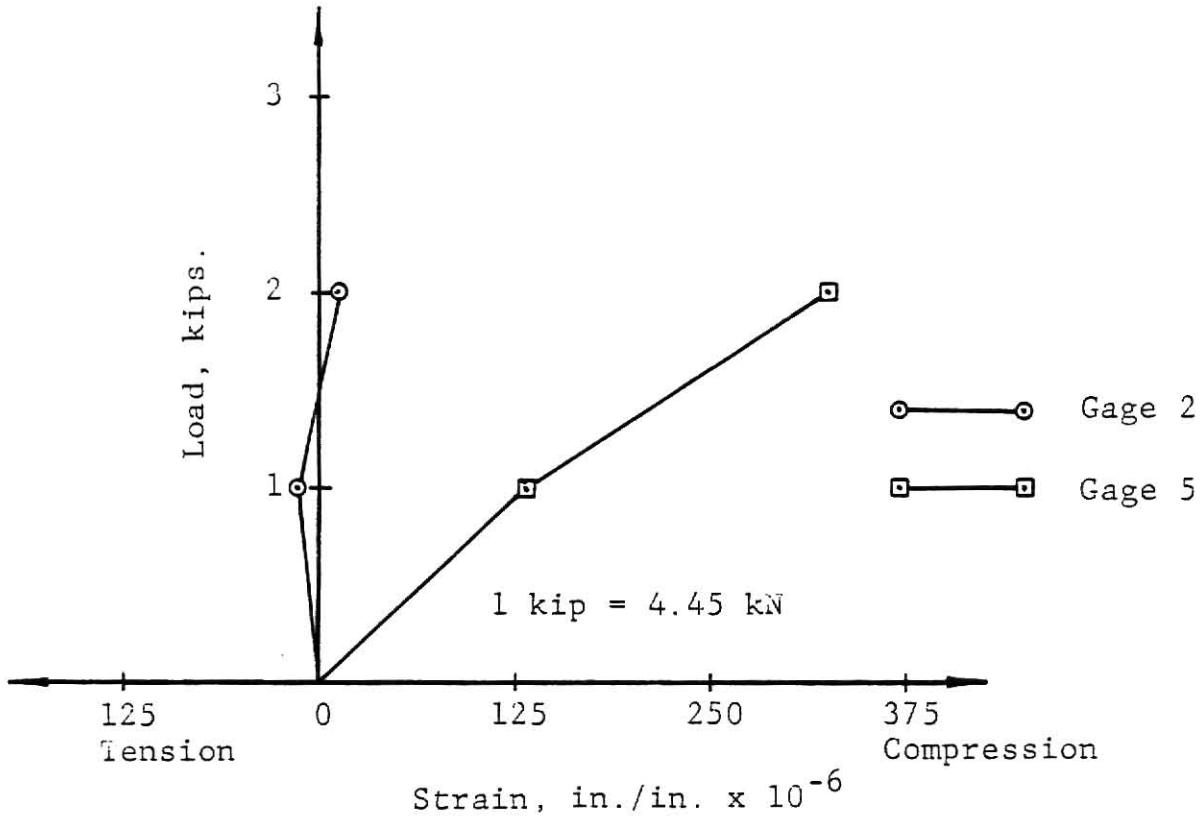

Figure 4.3b Load vs. Strain, Plate 3, Gage 2 & Gage 5

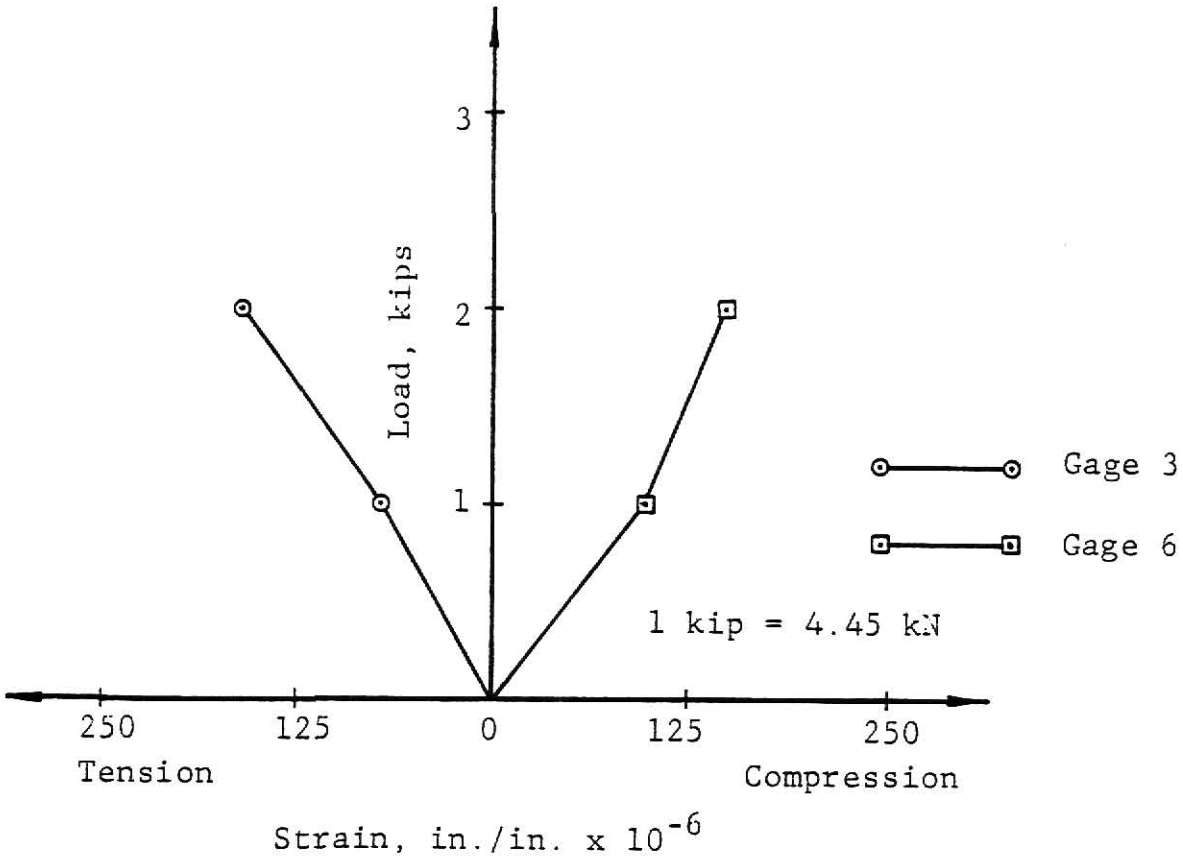

Figure 4.3c Load vs. Strain, Plate 3, Gage 3 & Gage 6

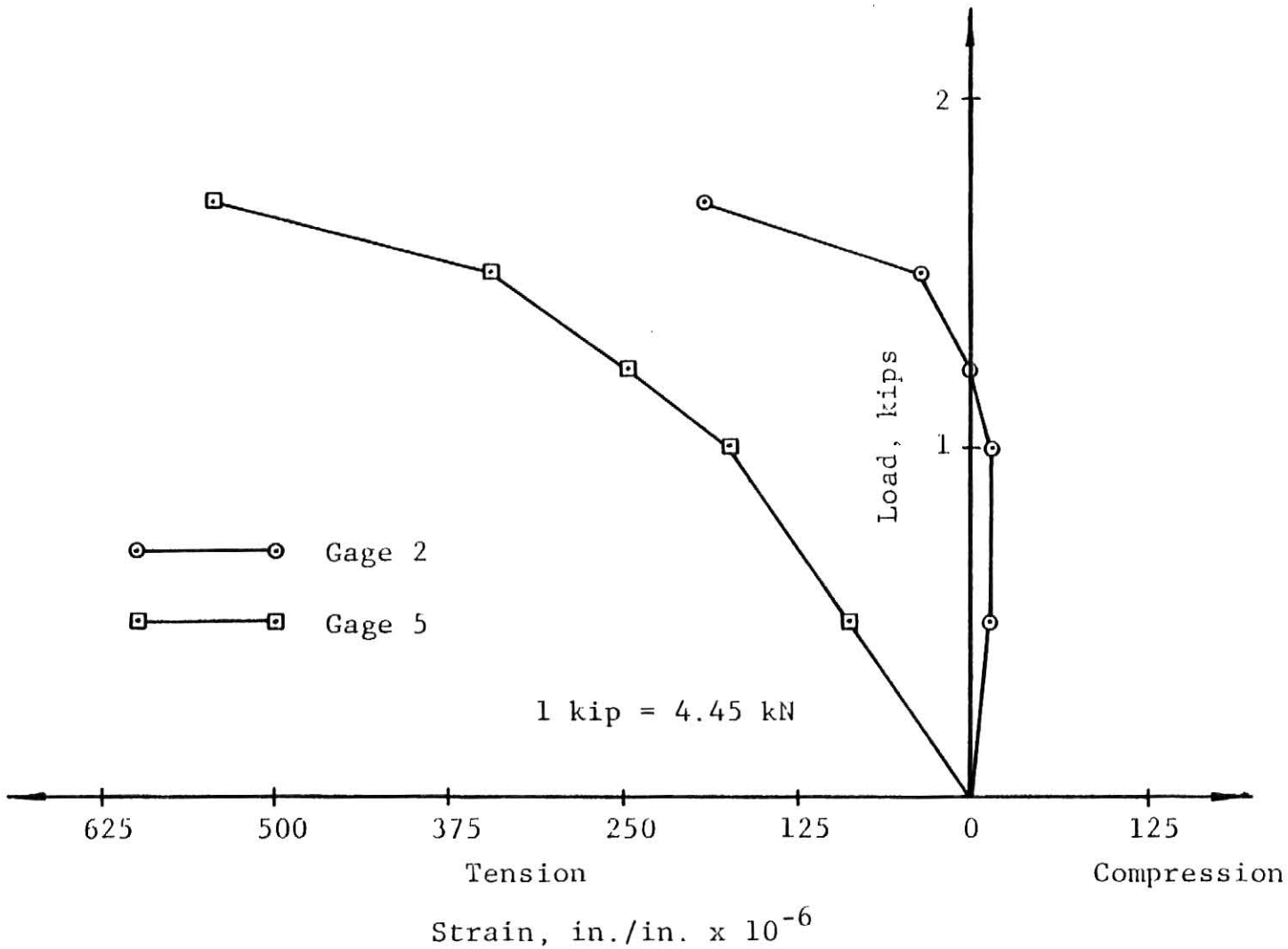

Figure 4.4b Load vs. Strain, Plate 4, Gage 2 & Gage 5

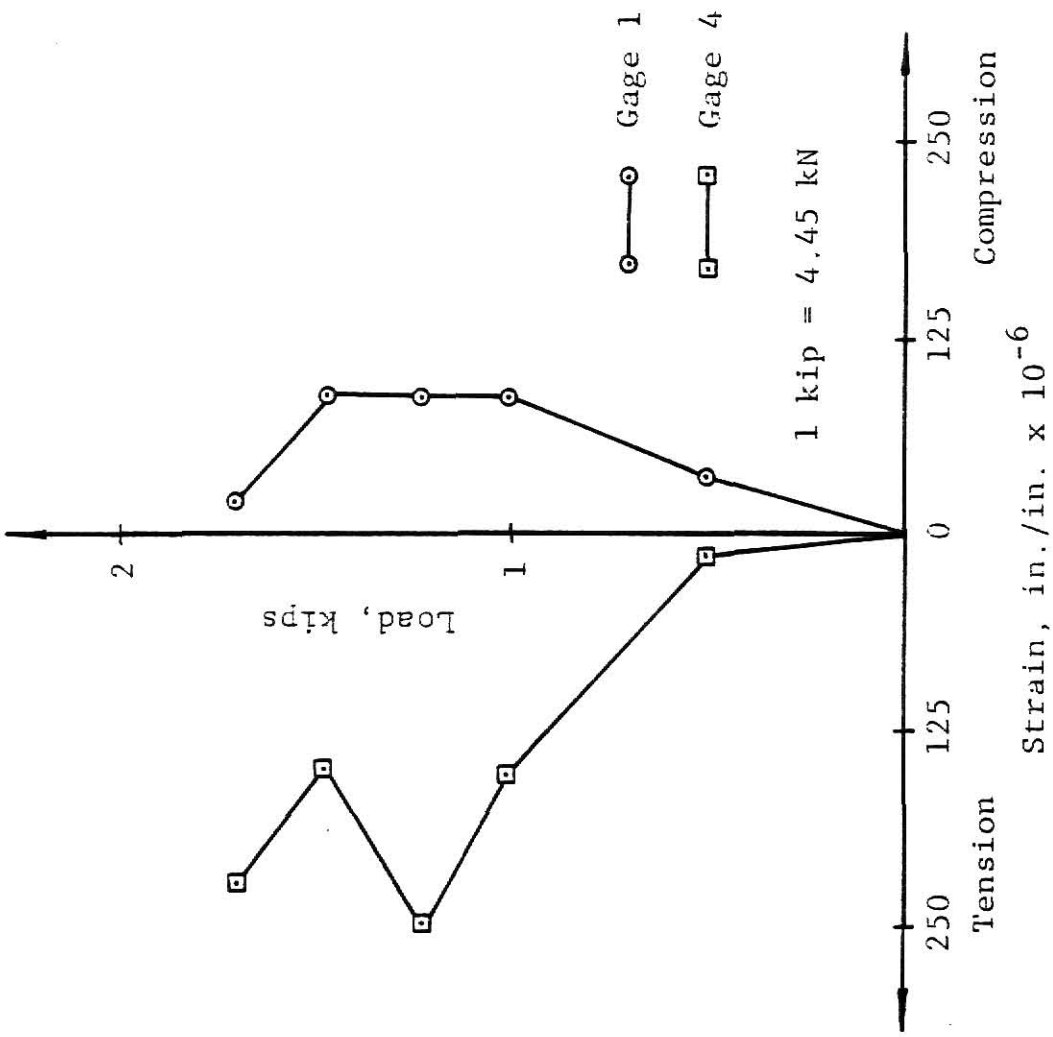

Figure 4.4a Load vs. Strain, Plate 4, Gage 1 & Gage 4

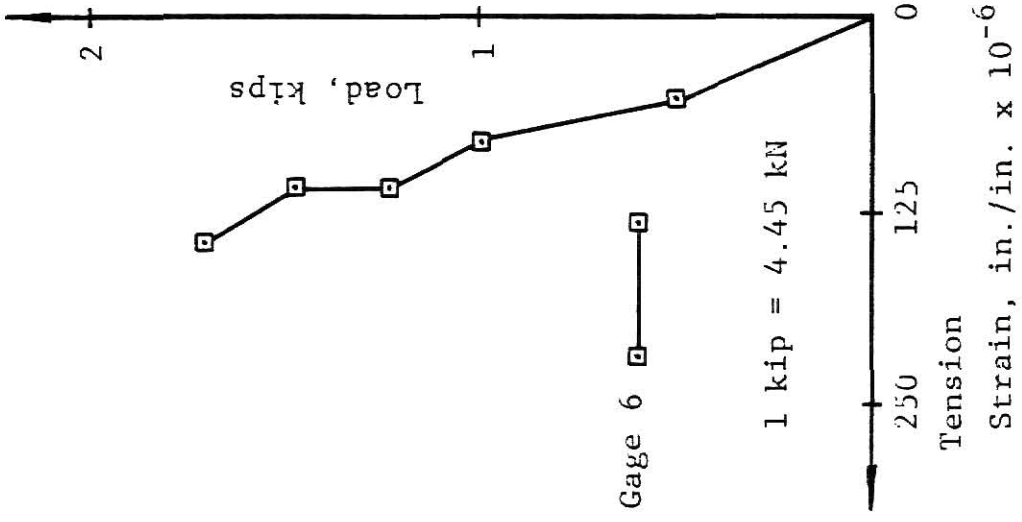

Figure 4.4c Load vs. Strain, Plate 4, Gage 6

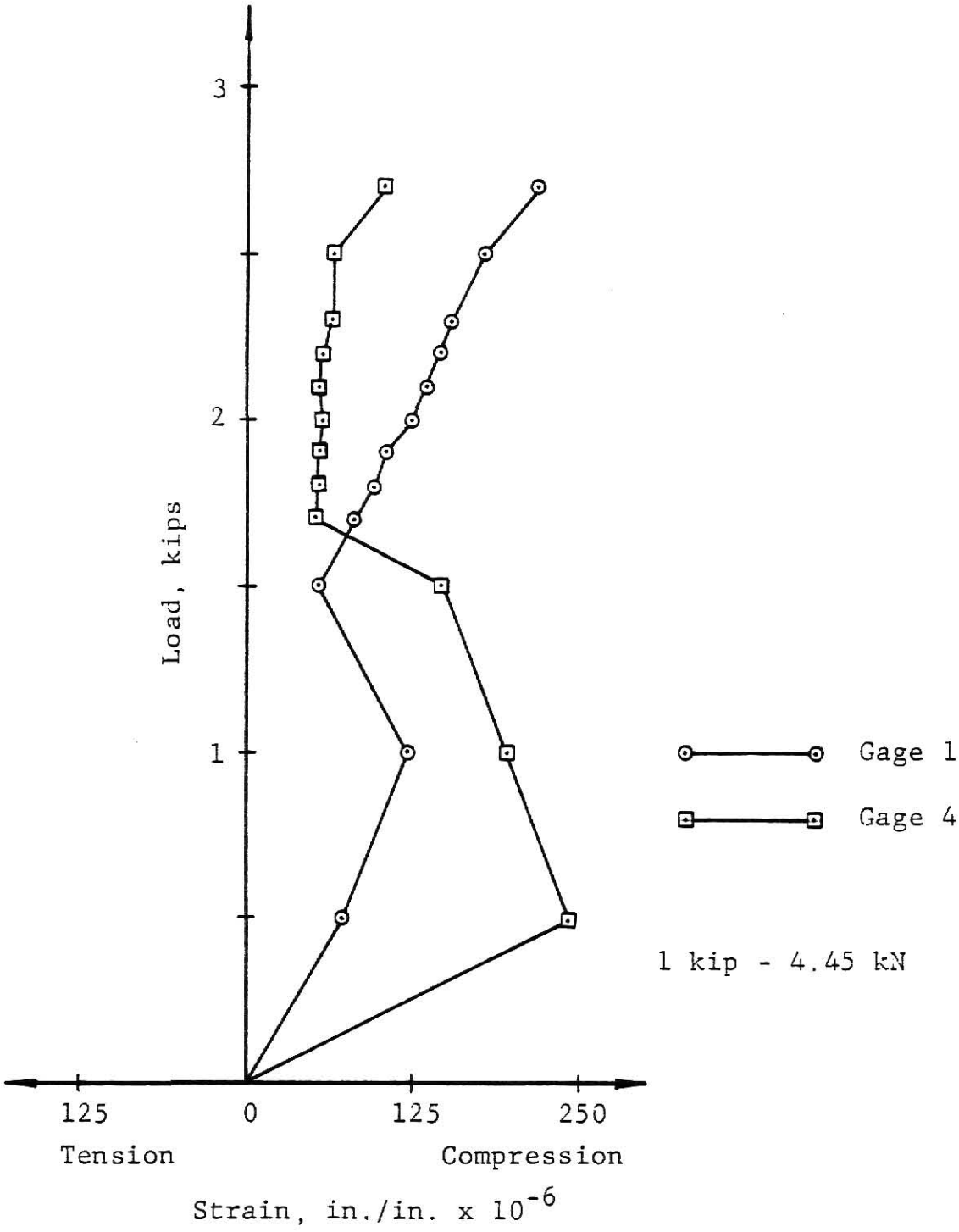

Figure 4.5a Load vs. Strain, Plate 5, Gage 1 & Gage 4

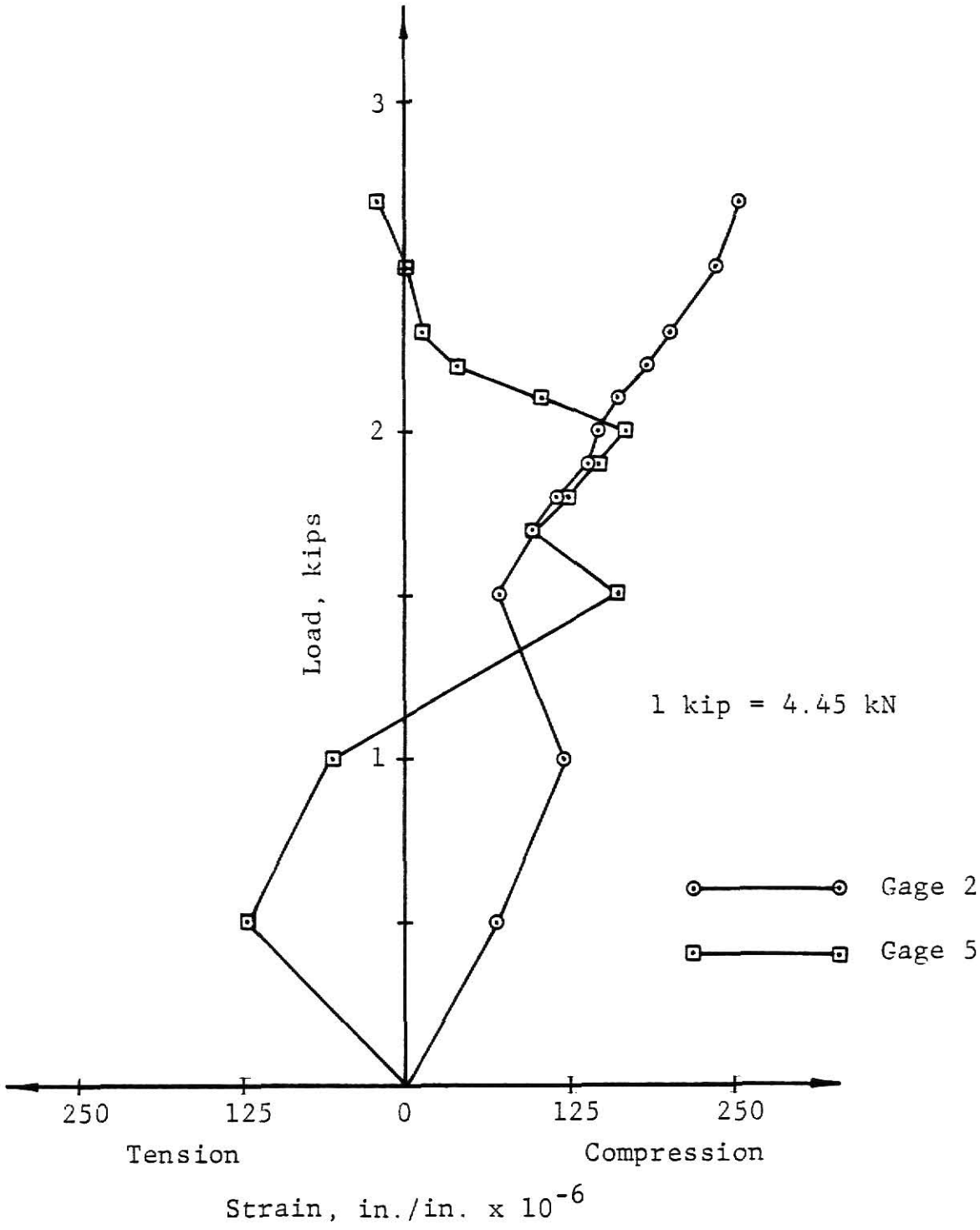

Figure 4.5b Load vs. Strain, Plate 5, Gage 2 & Gage 5

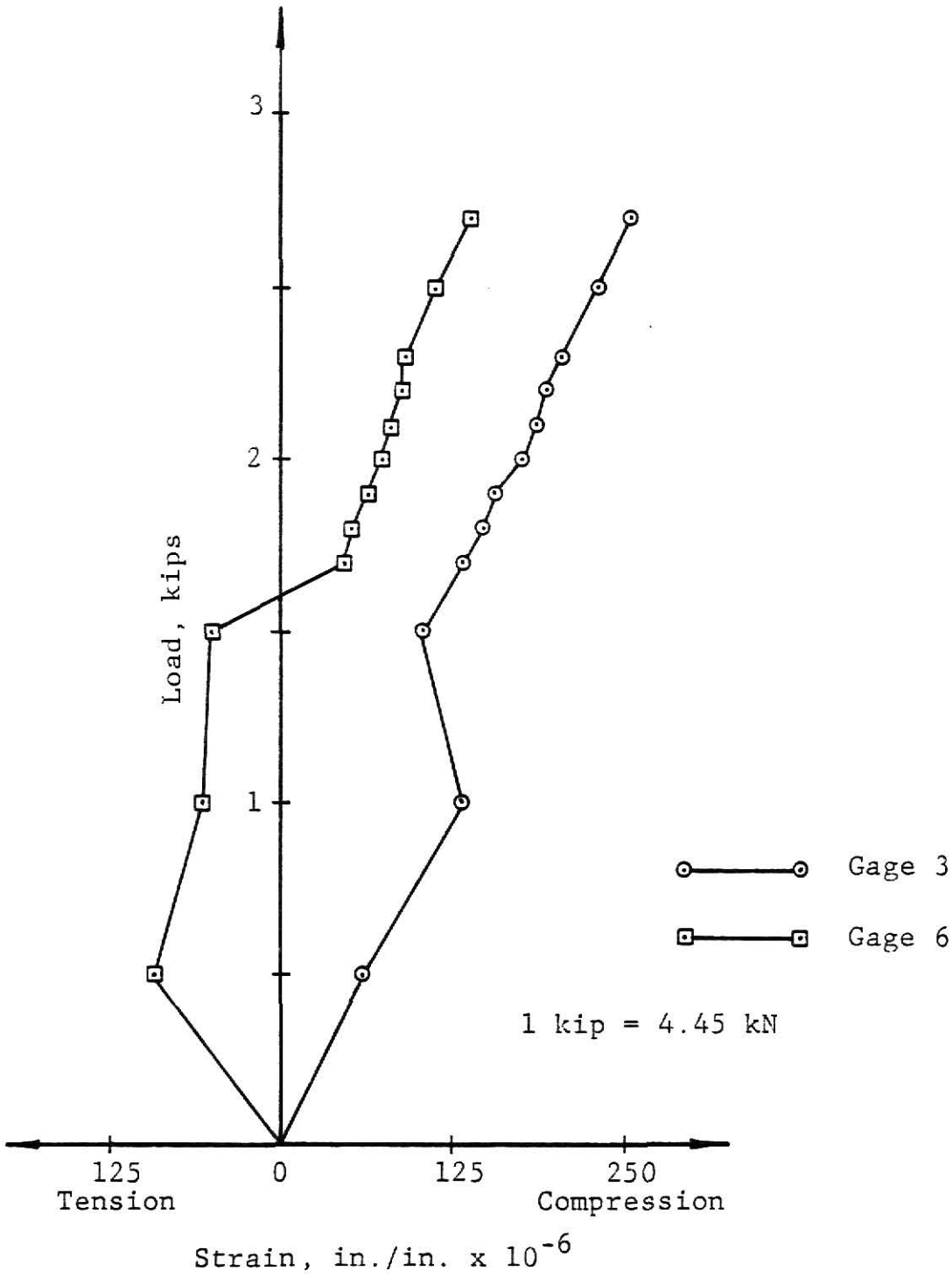

Figure 4.5c Load vs. Strain, Plate 5, Gage 3 & Gage 6

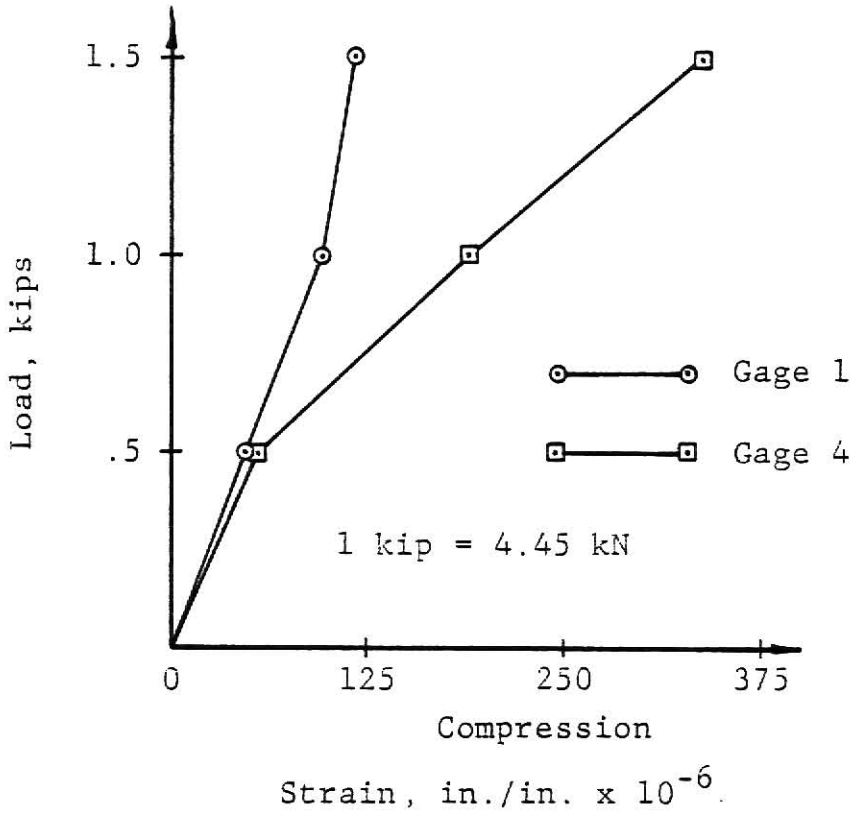

Figure 4.6a Load vs. Strain, Plate 6, Gage 1 & Gage 4

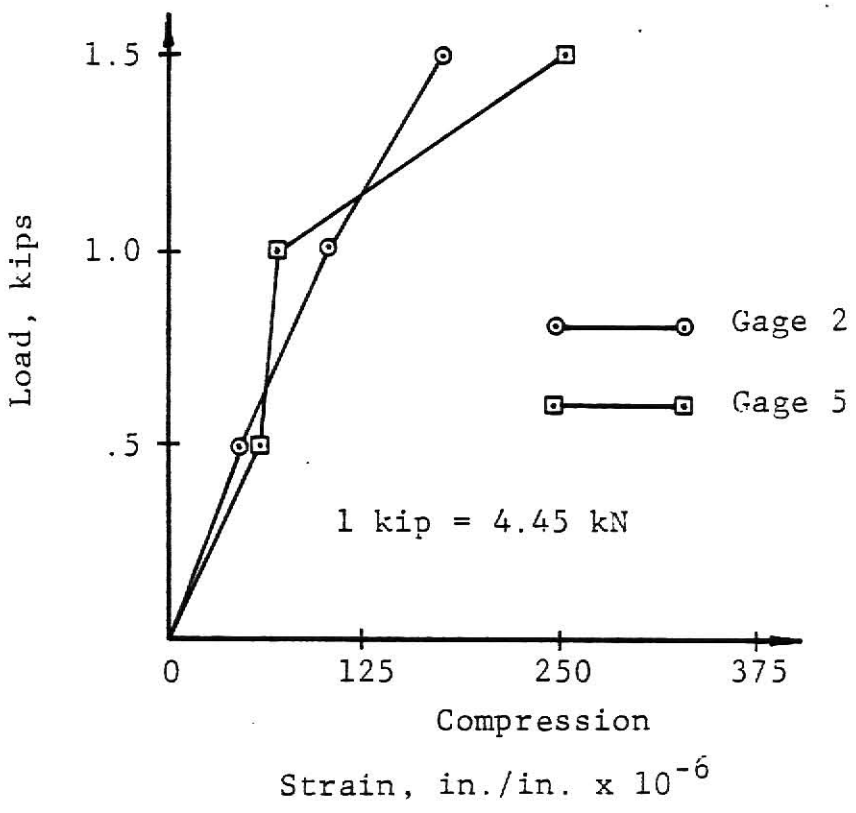

Figure 4.6b Load vs. Strain, Plate 6, Gage 2 & Gage 5

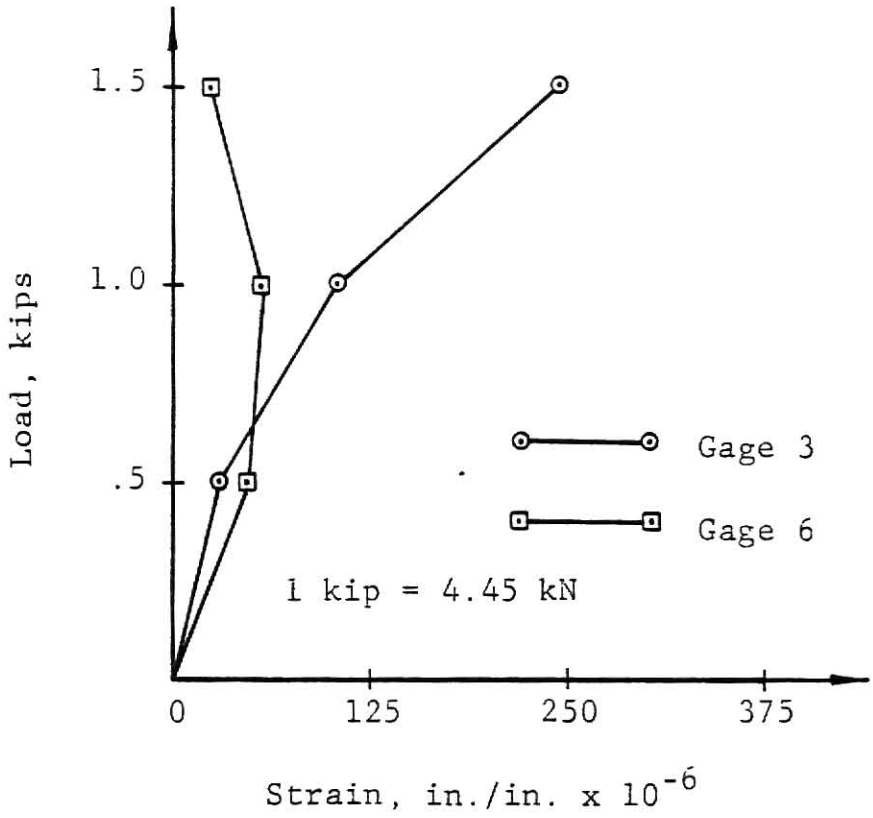

Figure 4.6c Load vs. Strain, Plate 6, Gage 3 & Gage 6

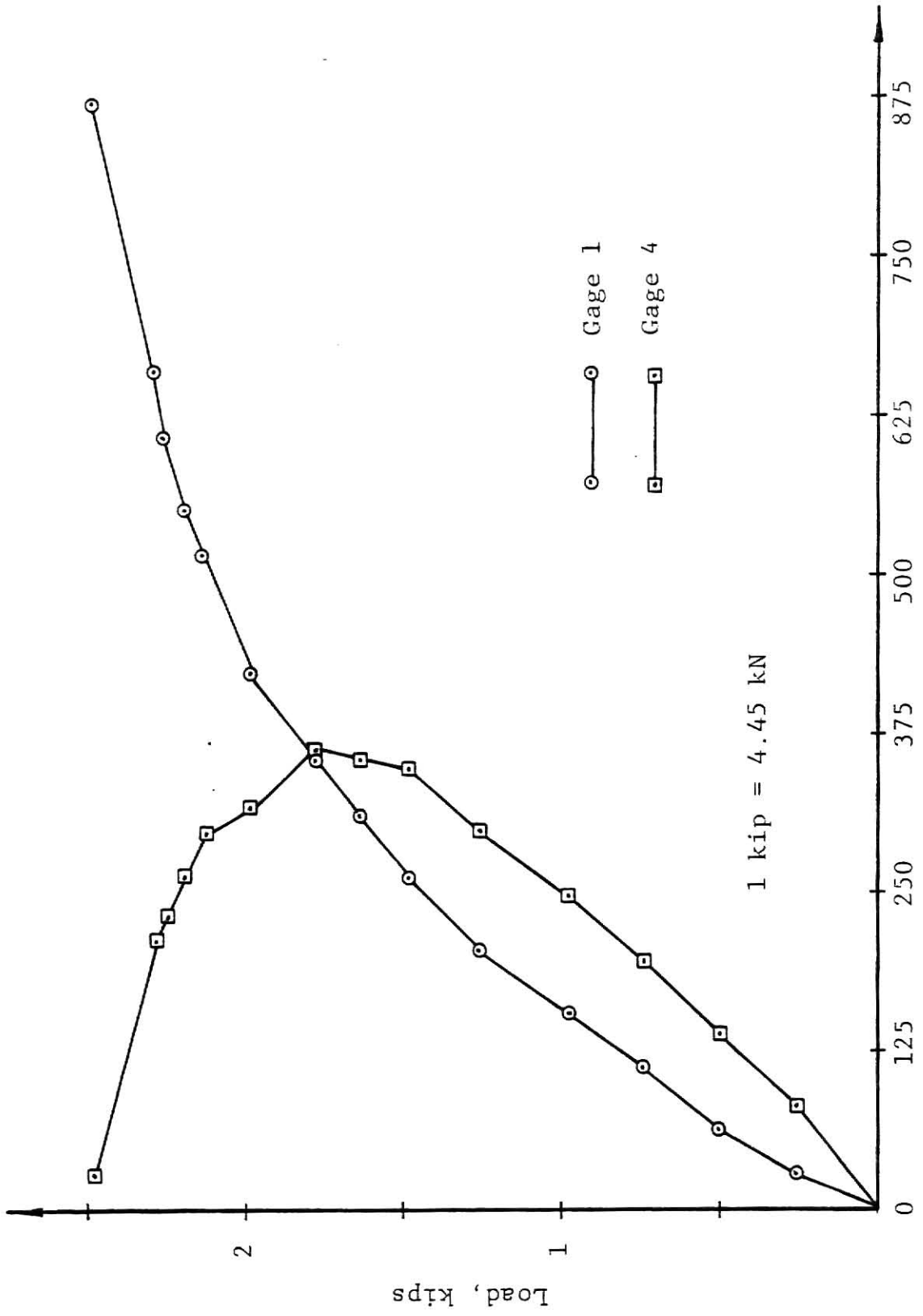

Figure 4.7a Load vs. Strain, Plate 9, Gage 1 & Gage 4

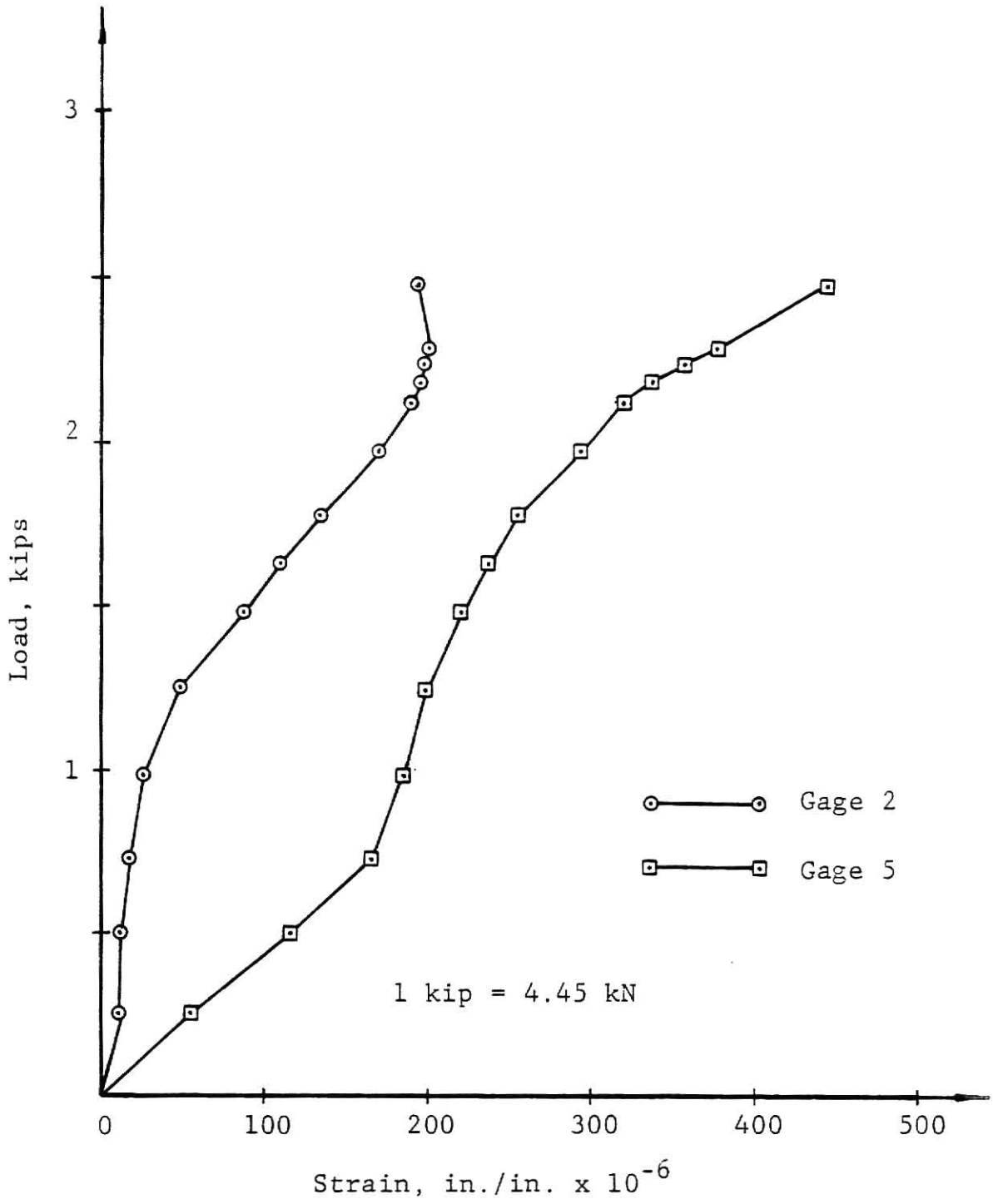

Figure 4.7b Load vs. Strain, Plate 9, Gage 2 & Gage 5

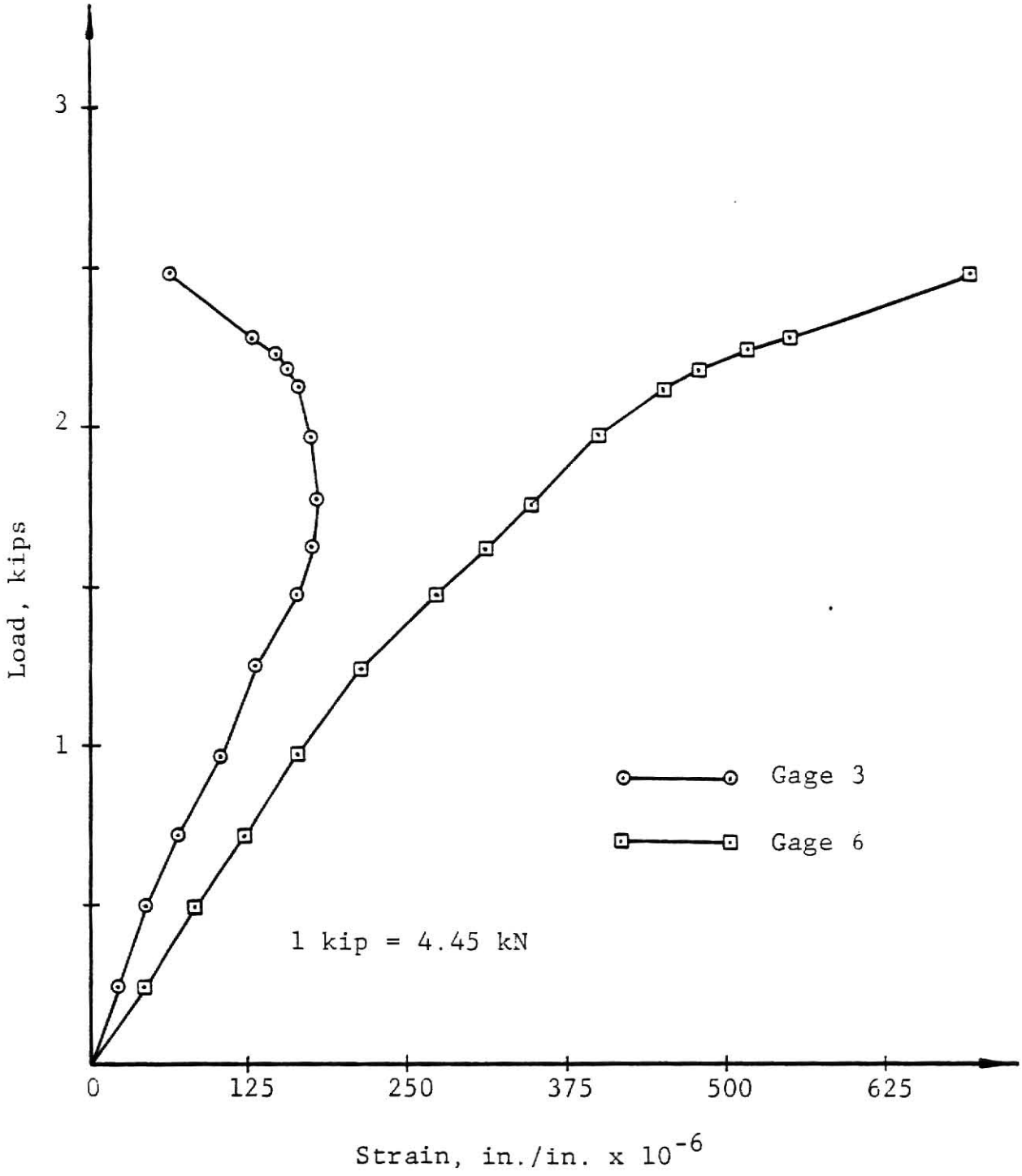

Figure 4.7c Load vs. Strain, Plate 9, Gage 3 & Gage 6

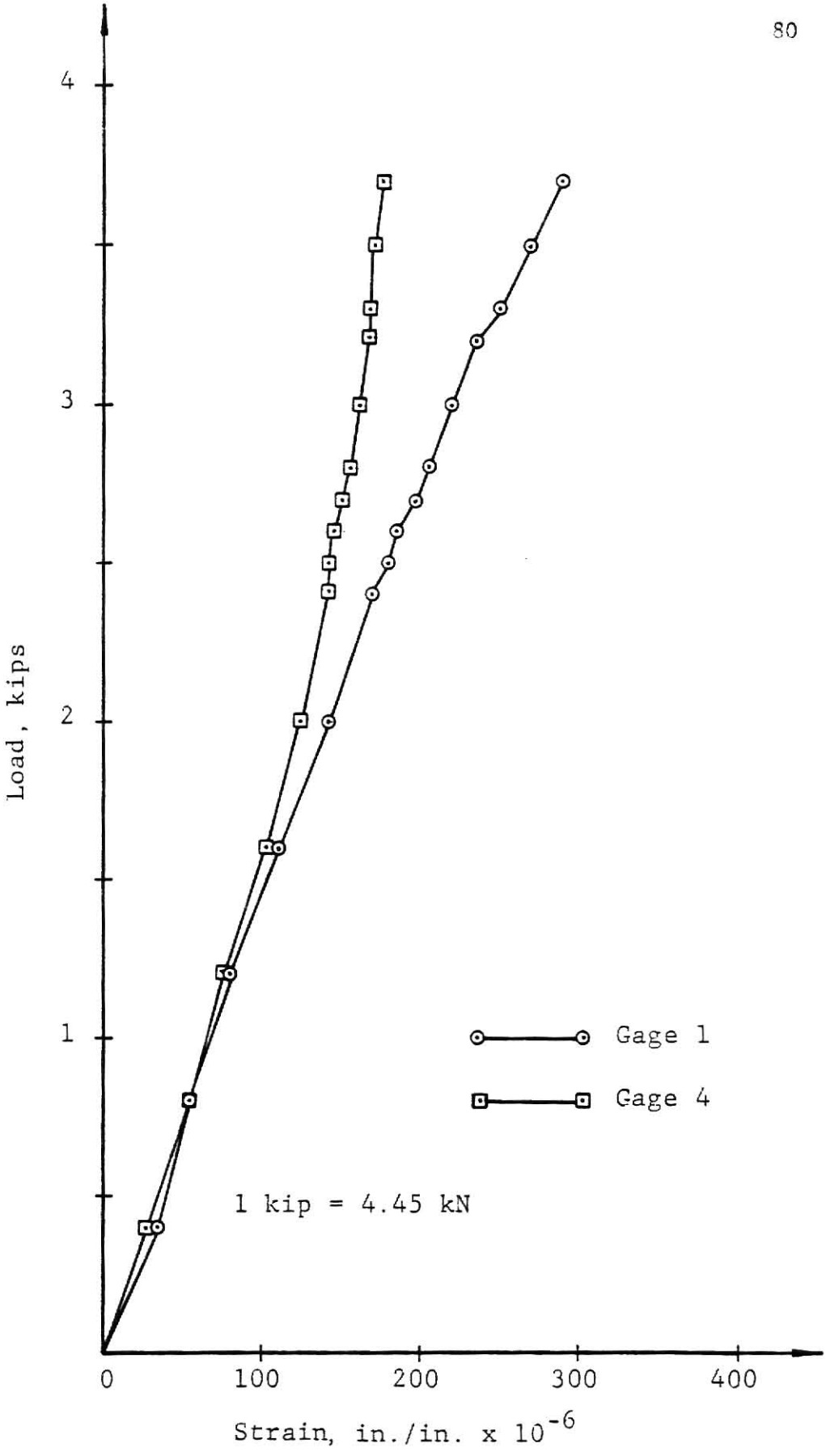

Figure 4.8a Load vs. Strain, Plate 7, Gage 1 & Gage 4

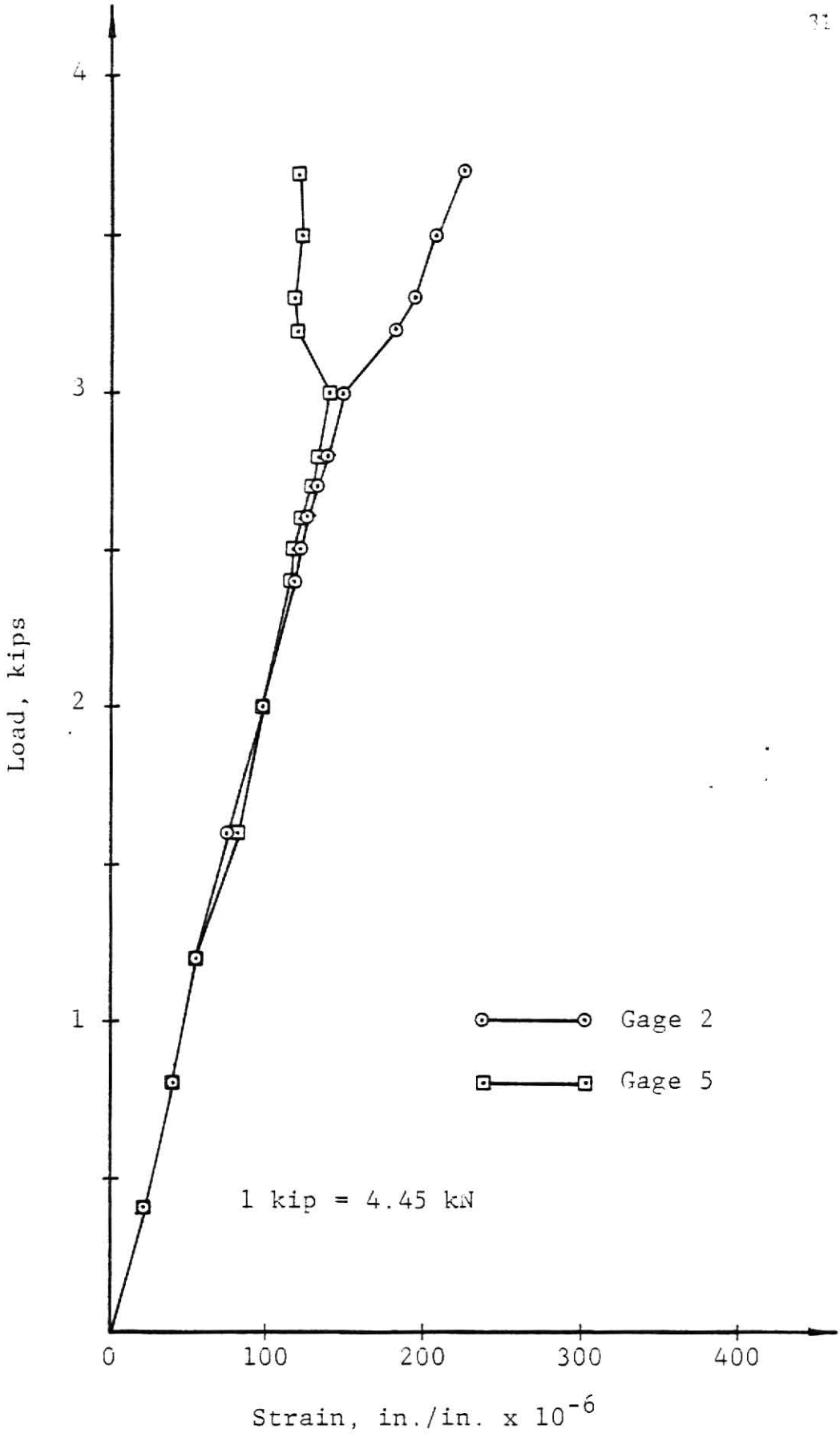

Figure 4.8b Load vs. Strain, Plate 7, Gage 2 & Gage 5

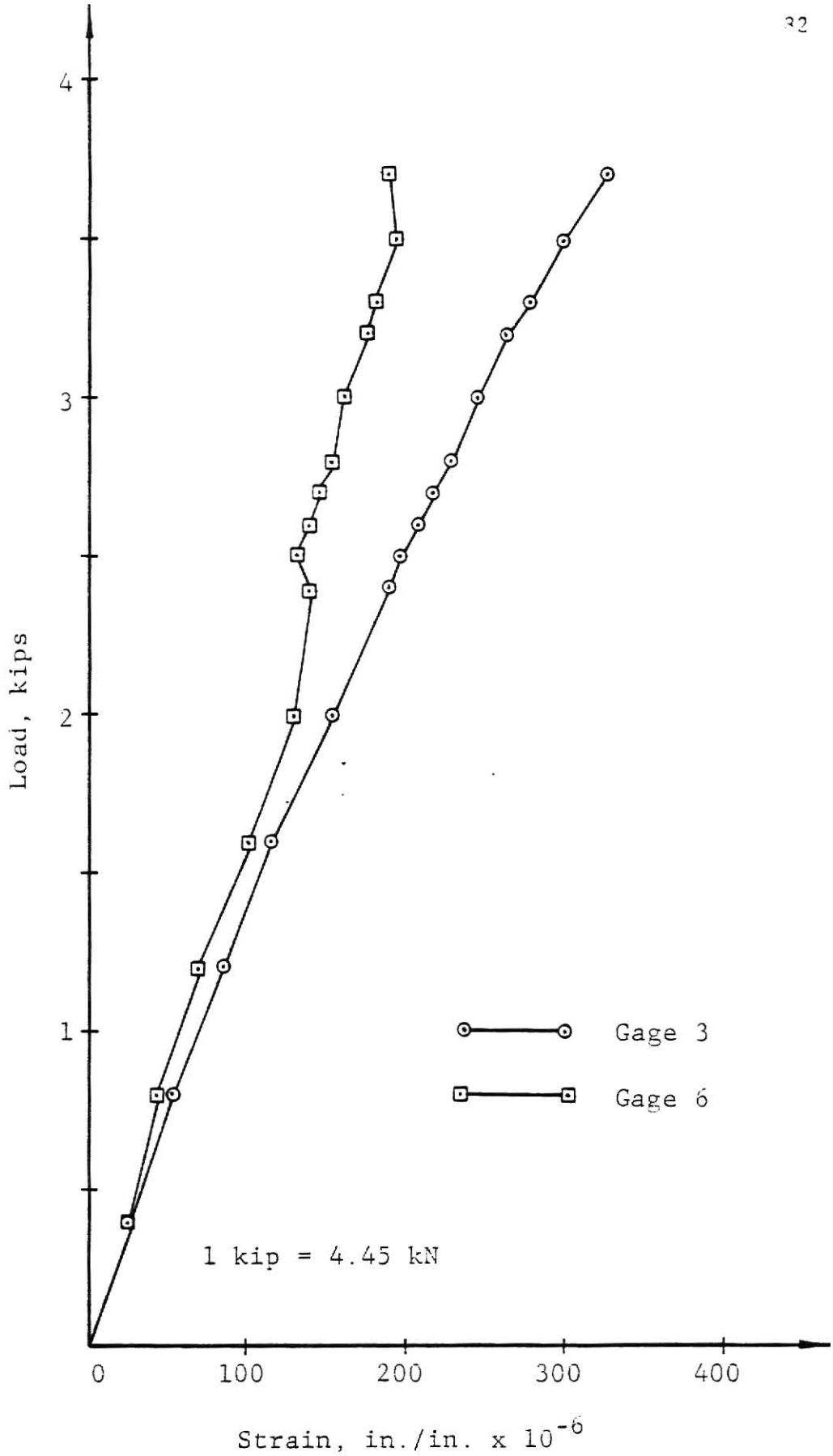

Figure 4.8c Load vs. Strain, Plate 7, Gage 3 & Gage 6

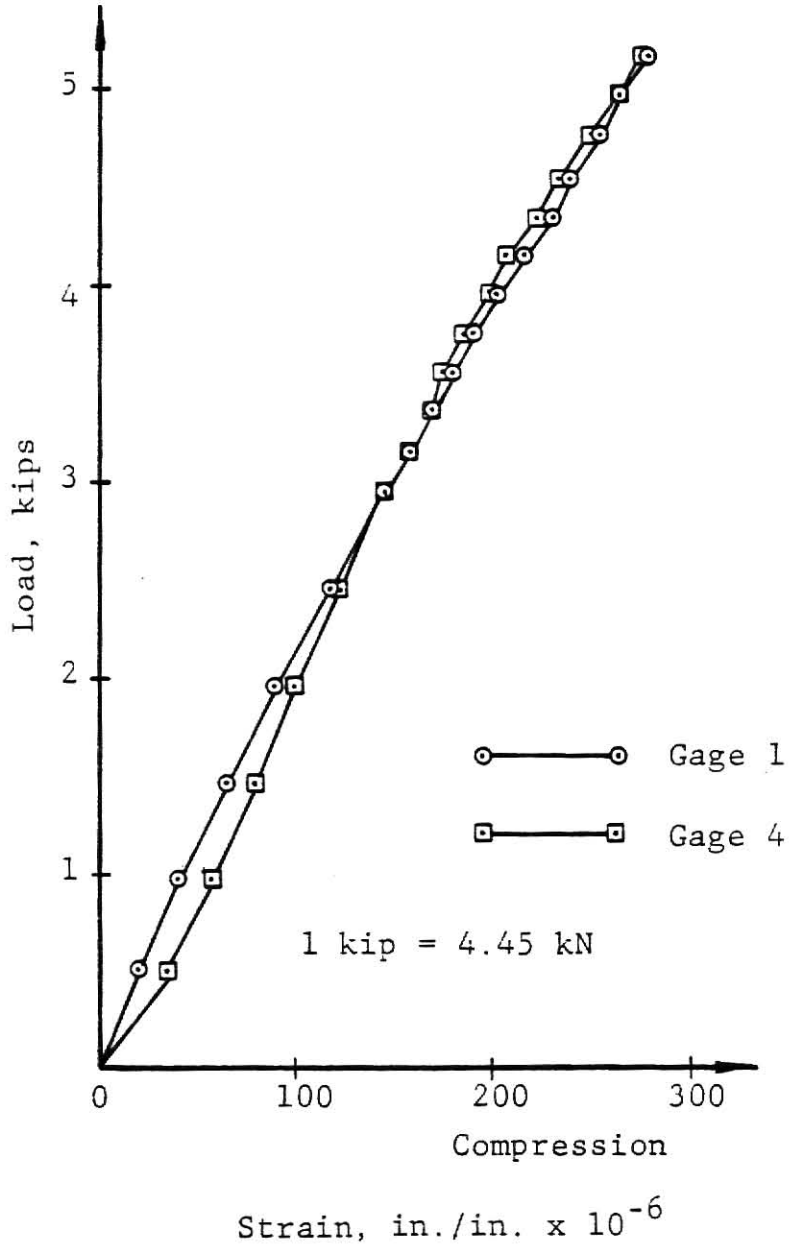

Figure 4.9a Load vs. Strain, Plate 8, Gage 1 & Gage 4

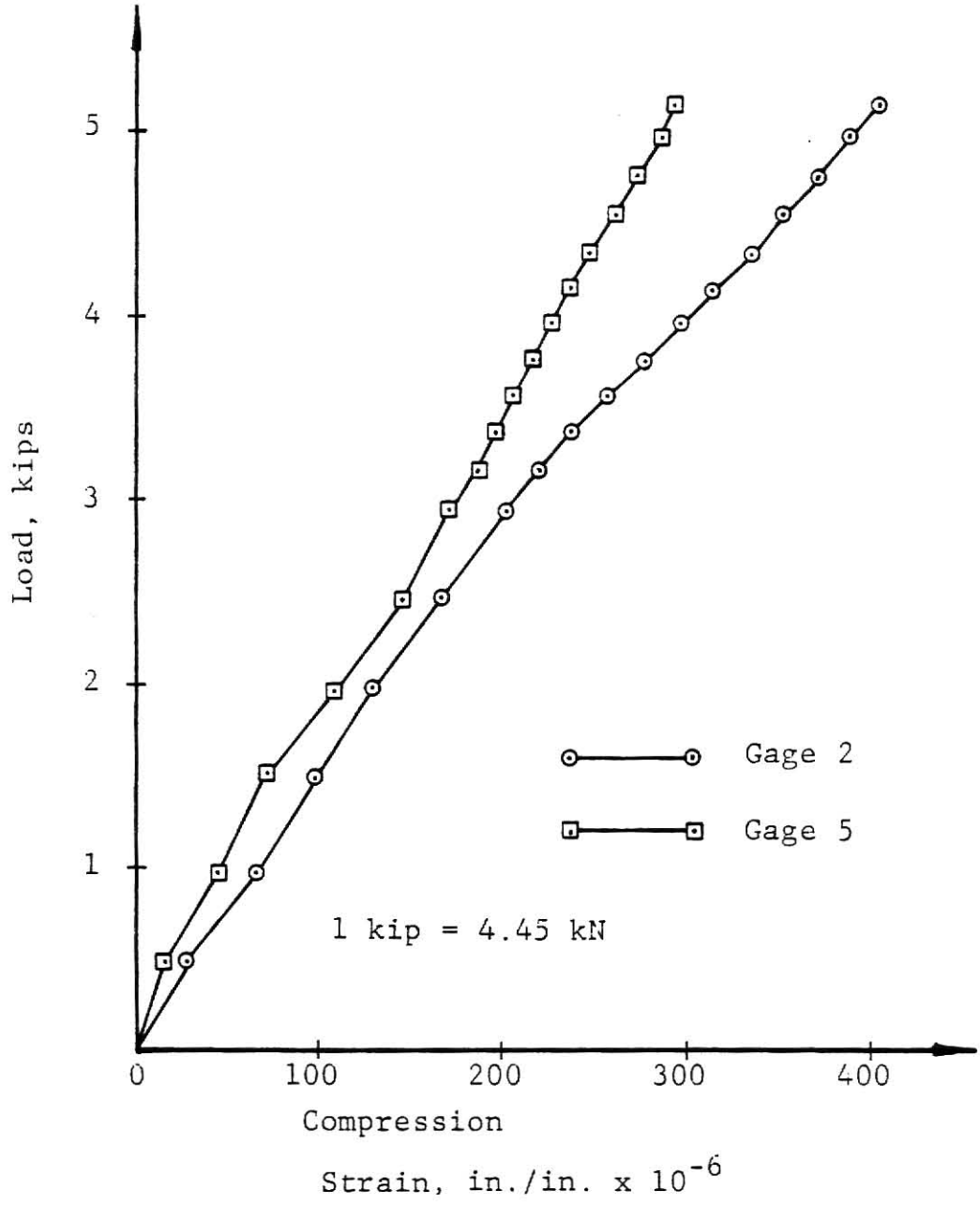

Figure 4.9b Load vs. Strain, Plate 8, Gage 2 & Gage 5

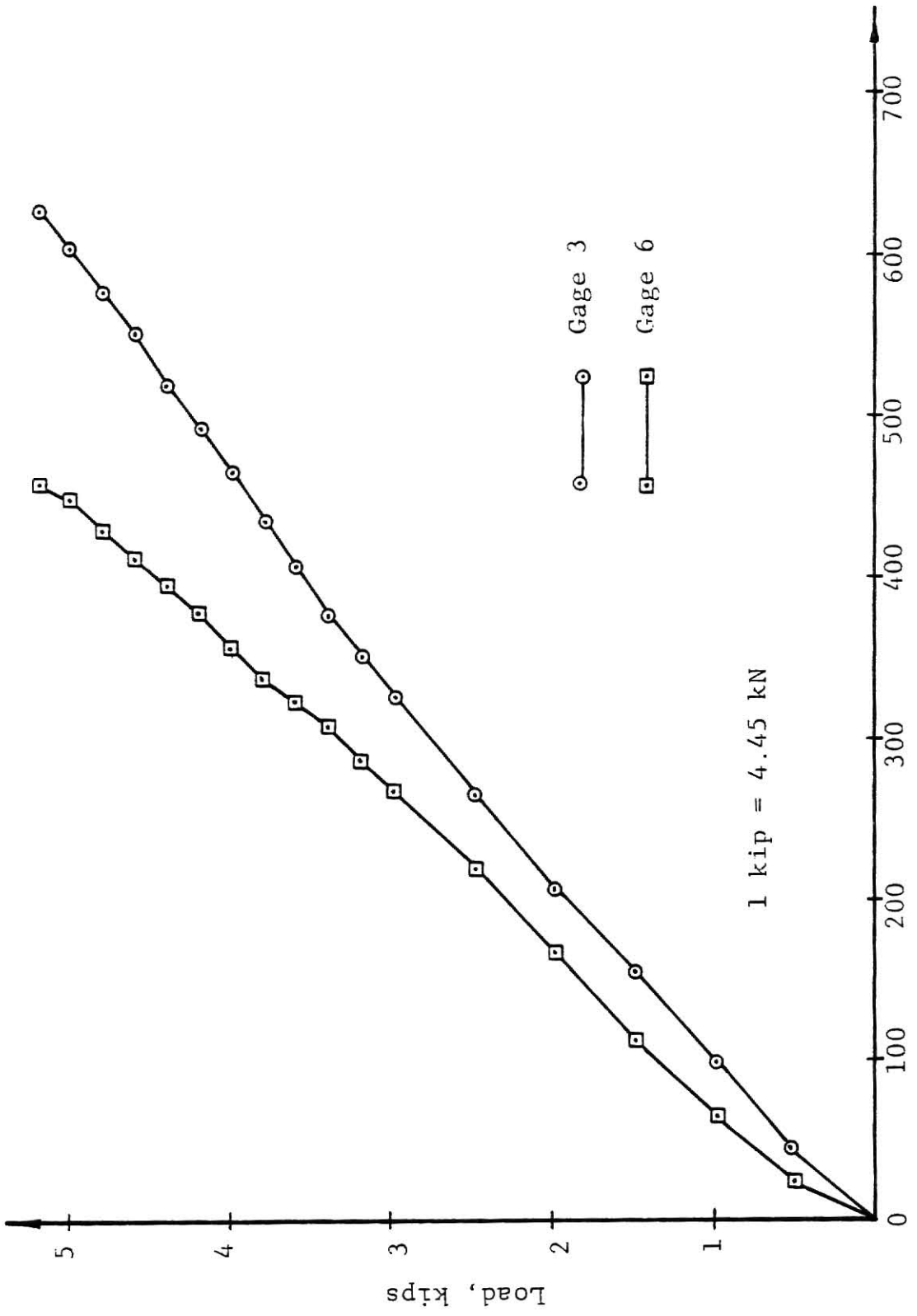

Figure 4.9c Load vs. Strain, Plate 8, Gage 3 & Gage 6

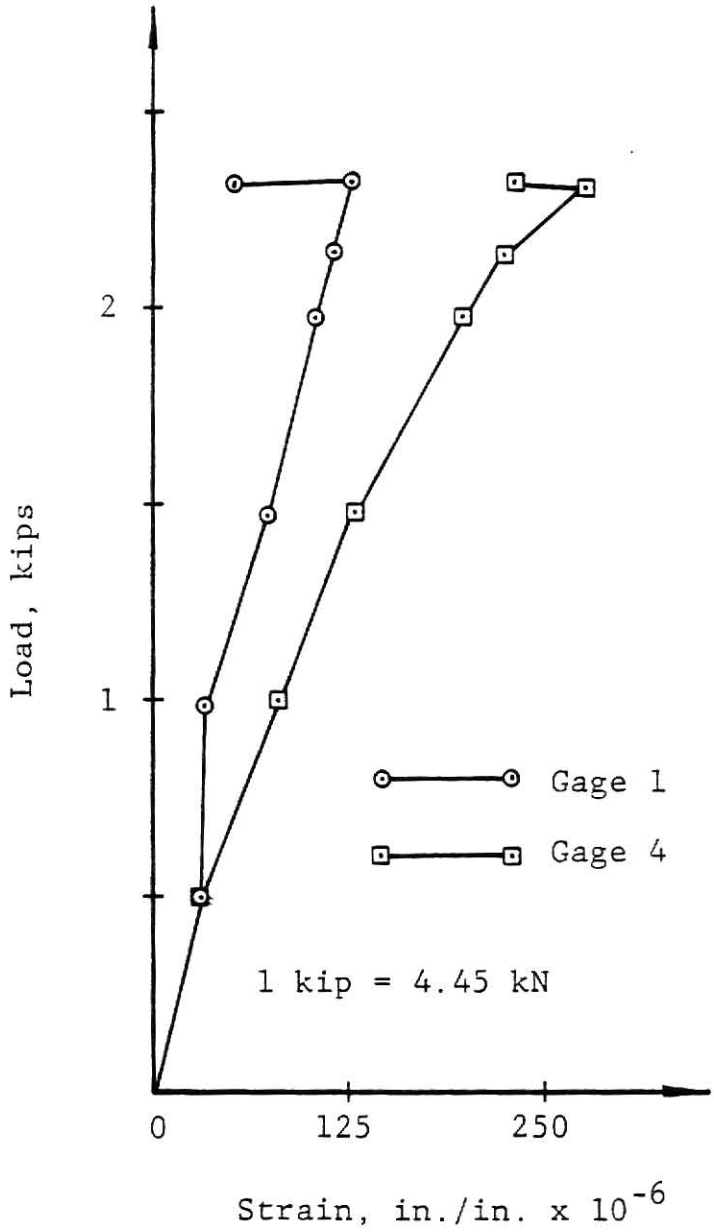

Figure 4.10a Load vs. Strain, Plate 10, Gage 1 & Gage 4

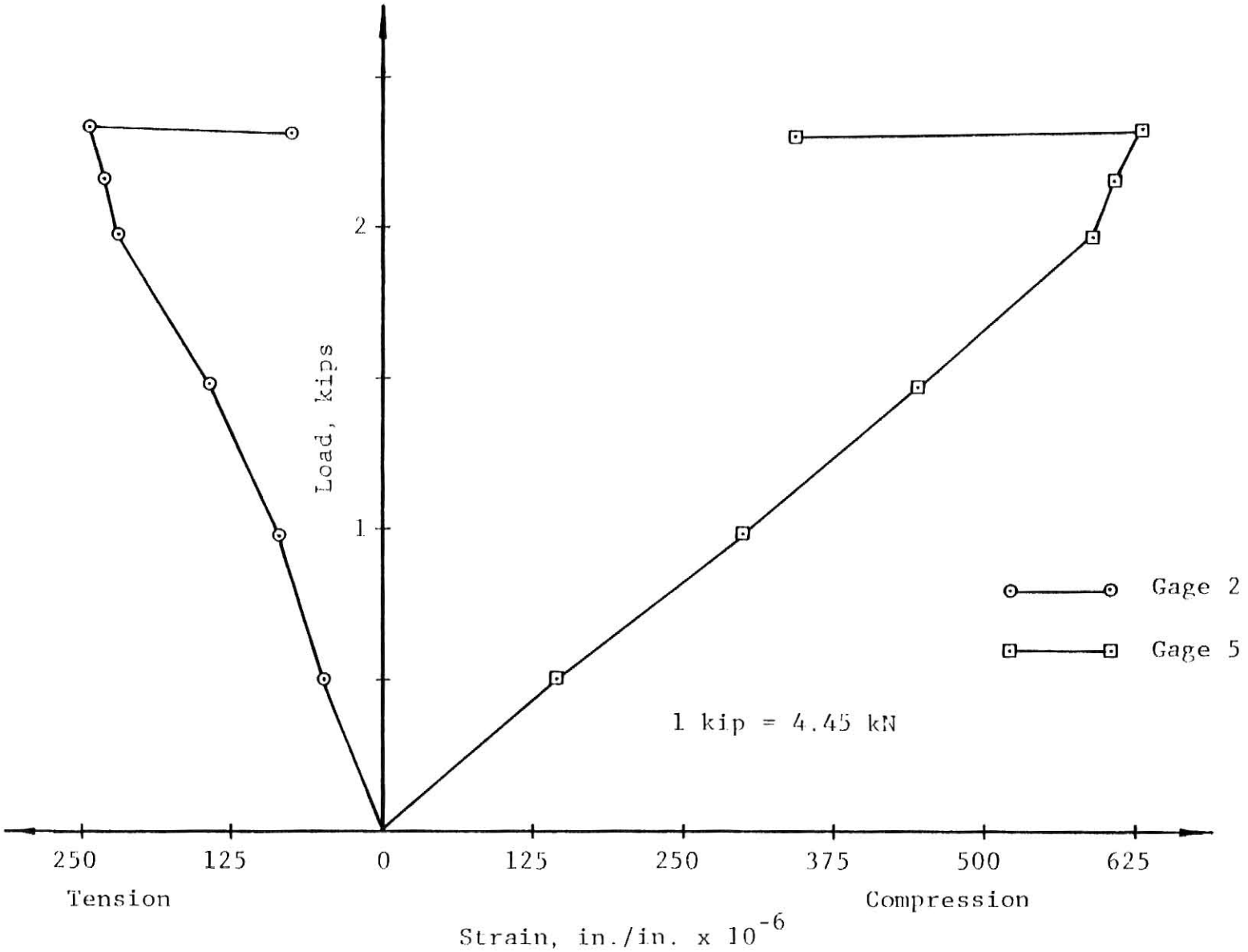

Figure 4.10b Load vs. Strain, Plate 10, Gage 2 & Gage 5

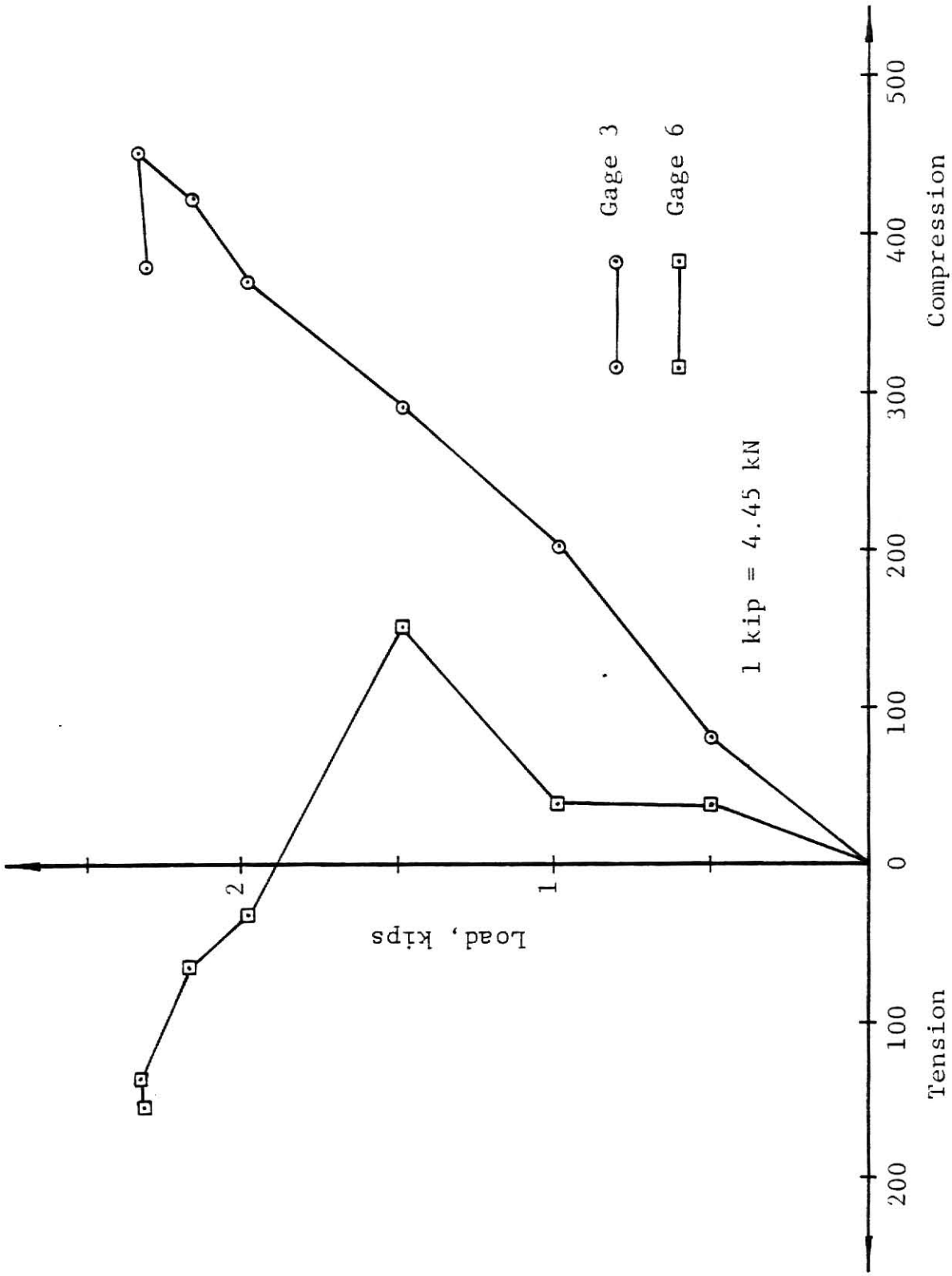

Figure 4.10c Load vs. Strain, Plate 10, Gage 3 & Gage 6

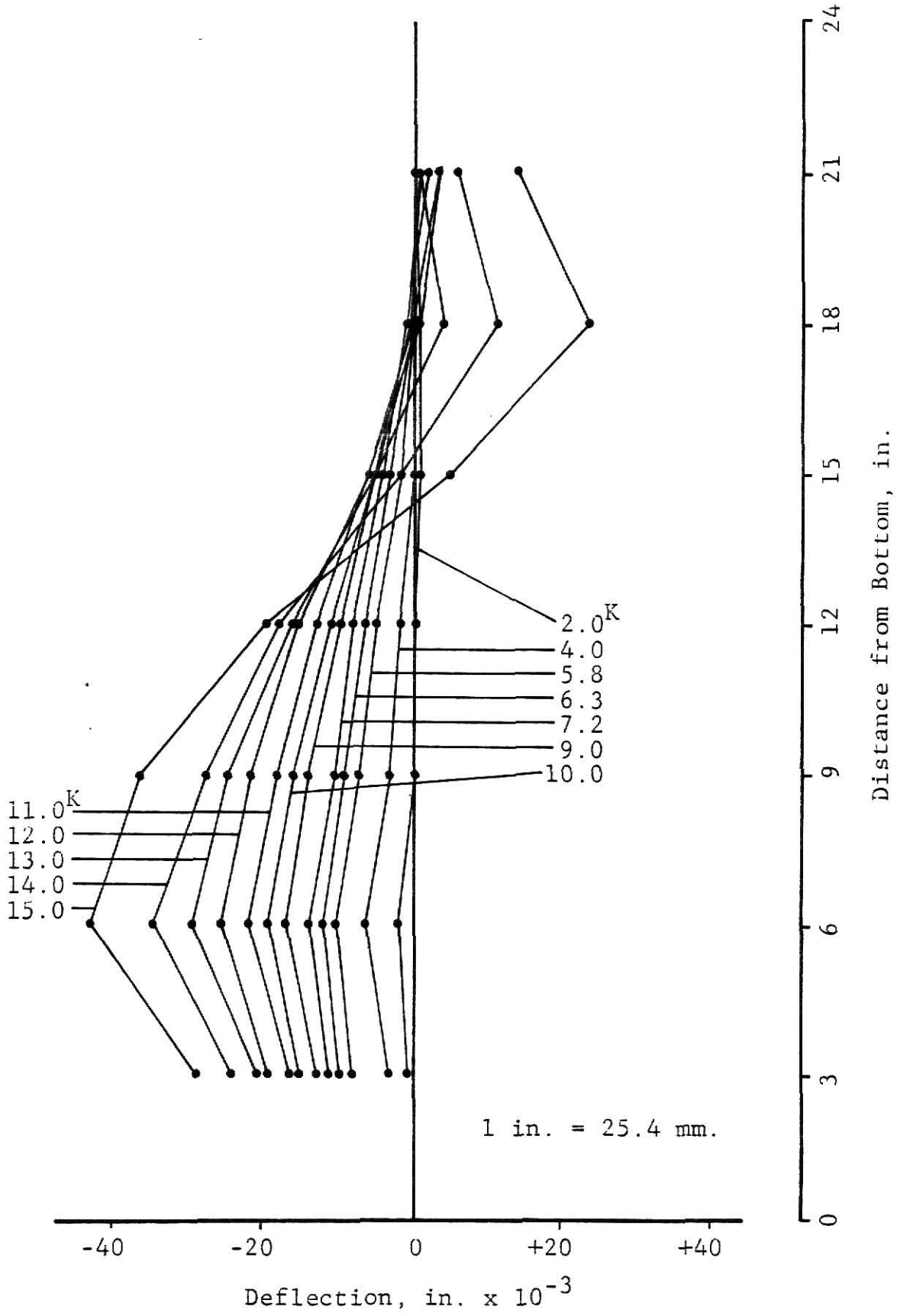

Figure 4.11 Deflection Profiles for Panel 1

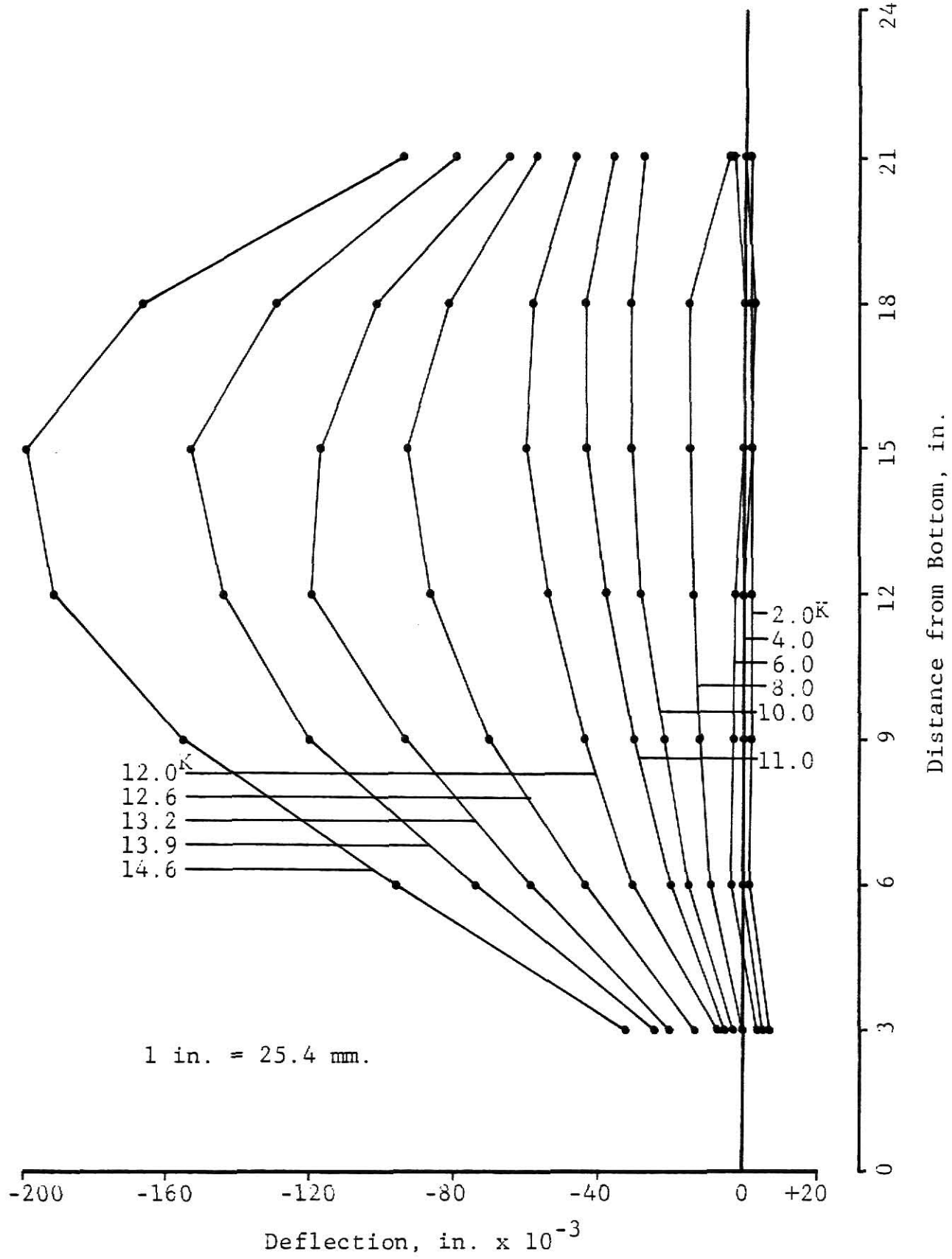

Figure 4.12 Deflection Profiles for Panel 2

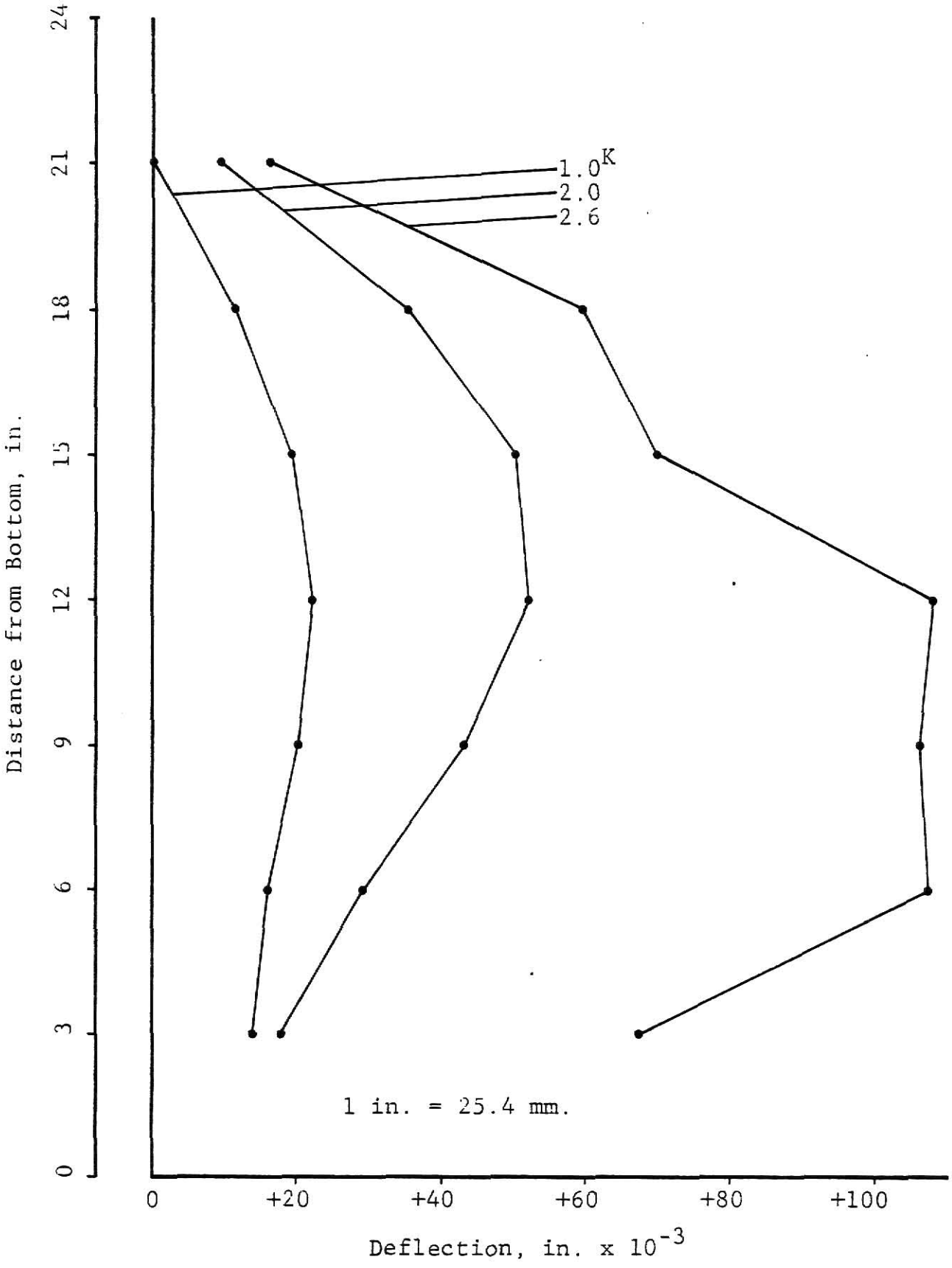

Figure 4.13 Deflection Profiles for Panel 3

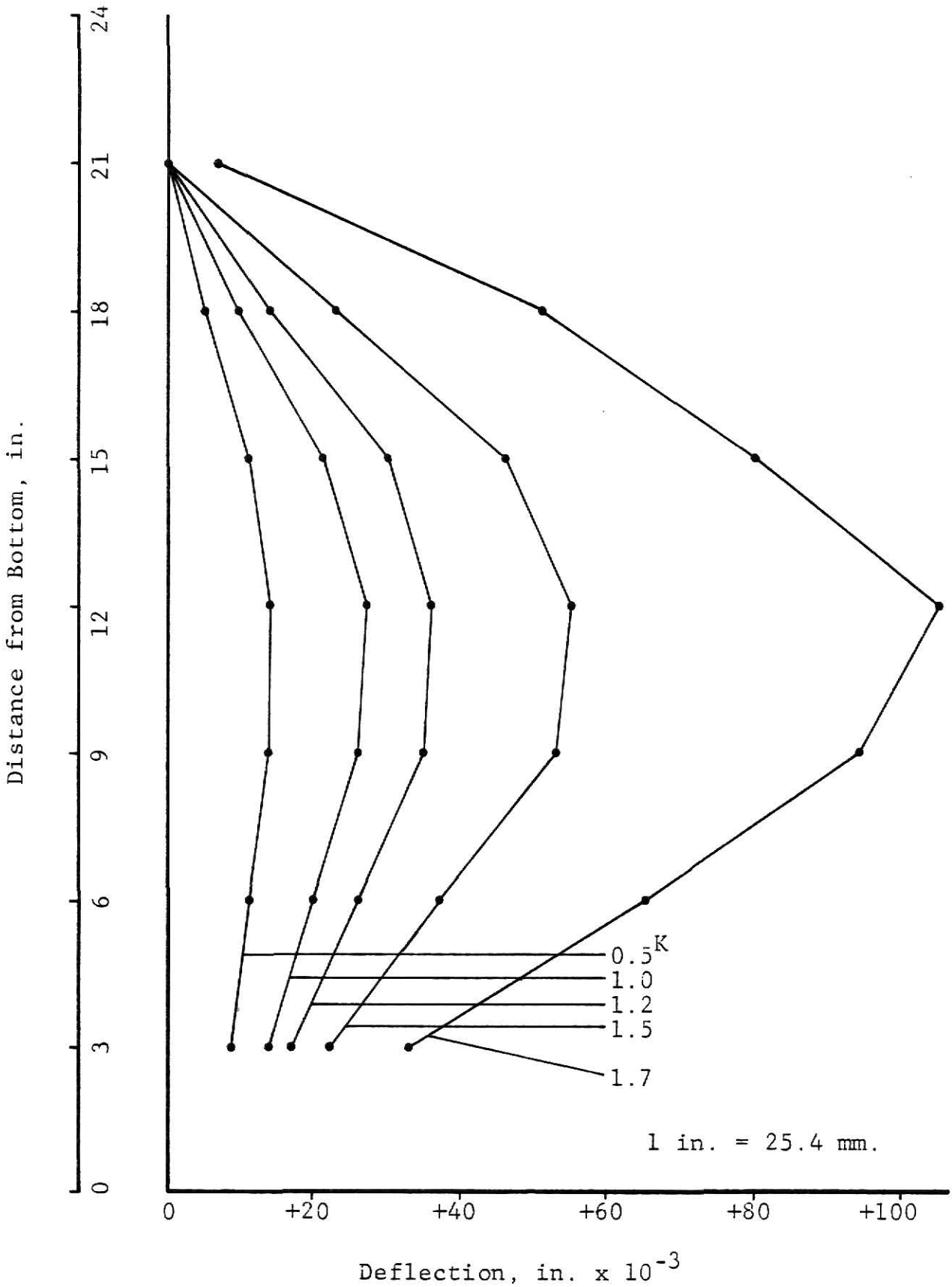

Figure 4.14 Deflection Profiles for Panel 4

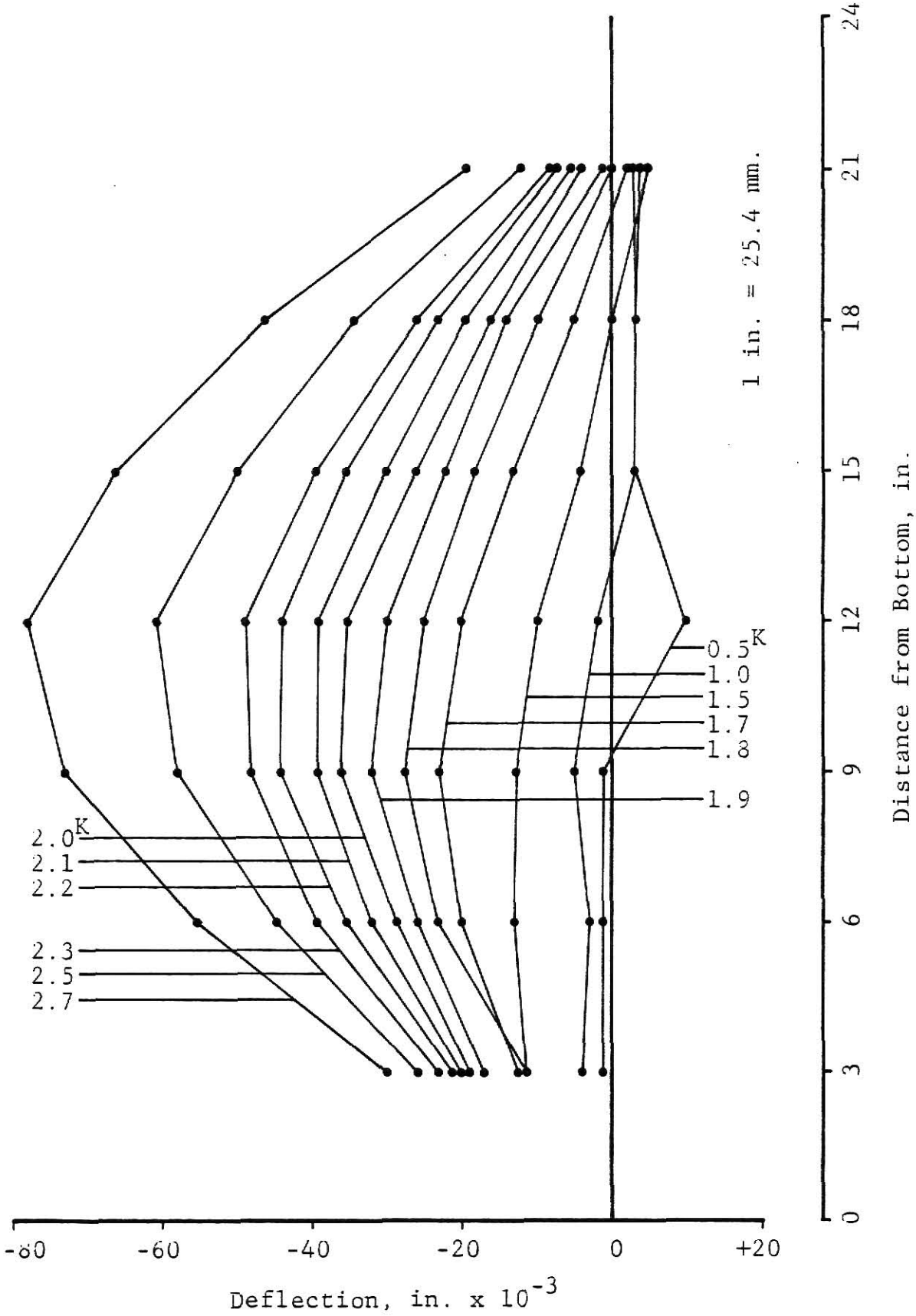

Figure 4.15 Deflection Profiles for Panel 5

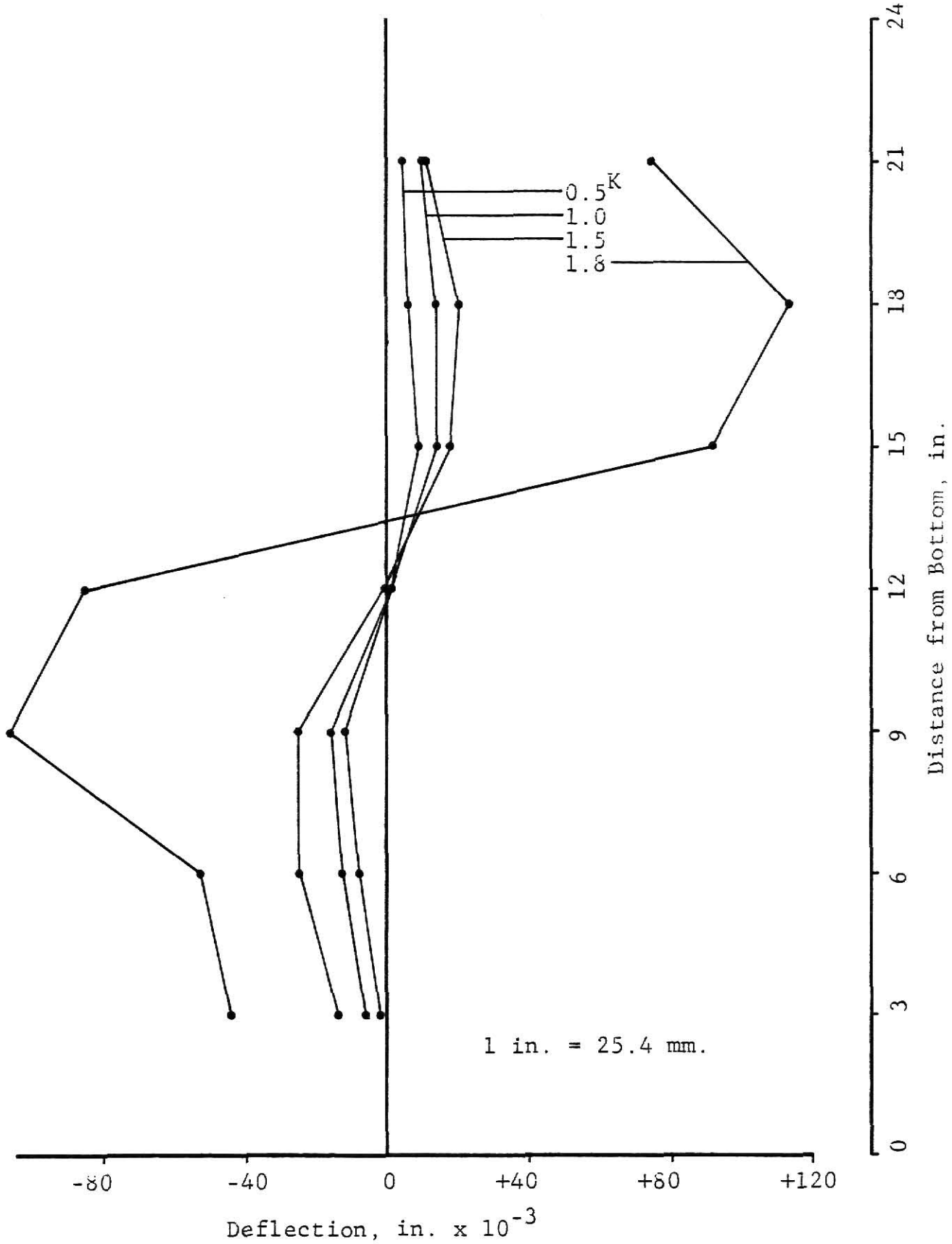

Figure 4.16 Deflection Profiles for Panel 6

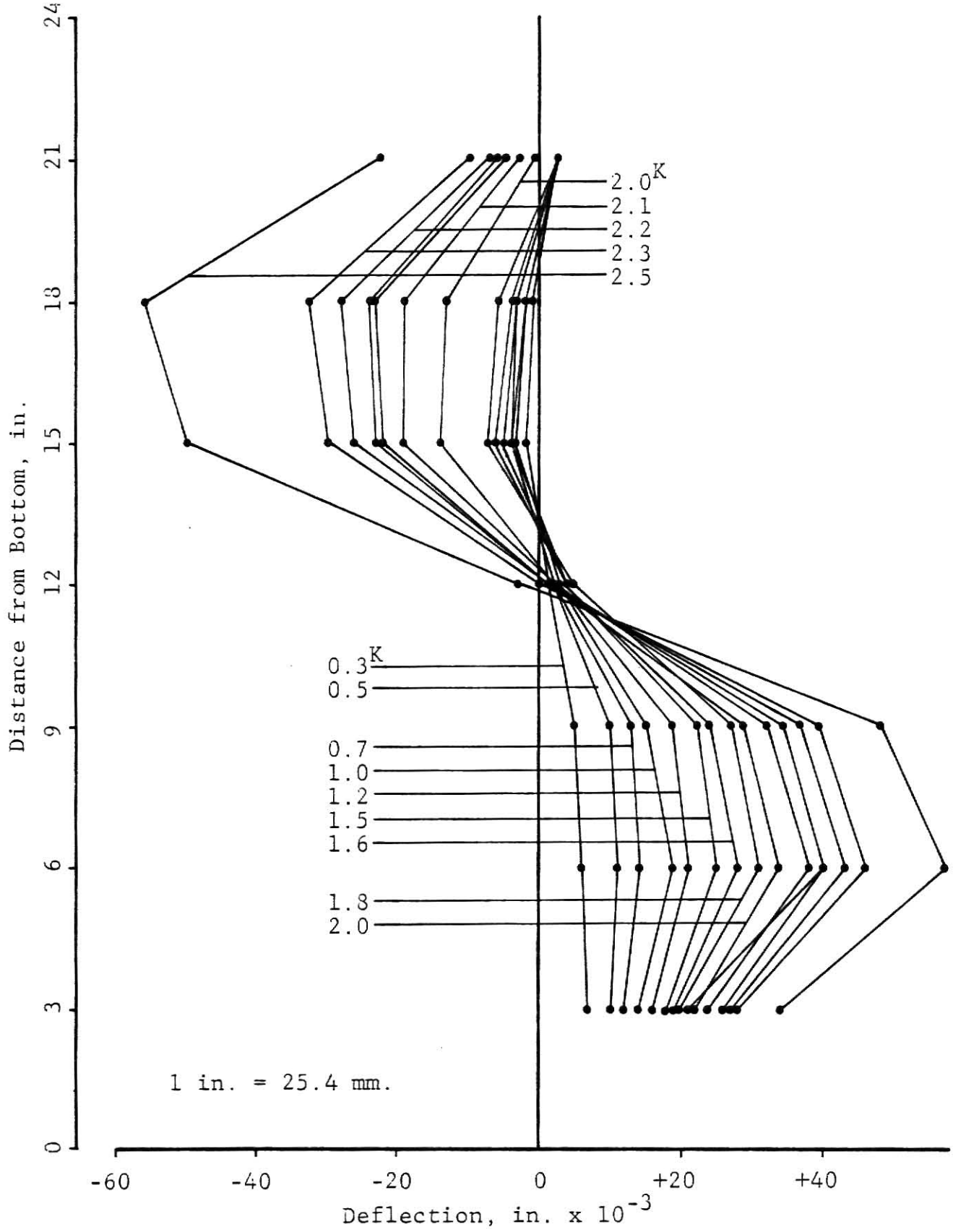

Figure 4.17 Deflection Profiles for Panel 9

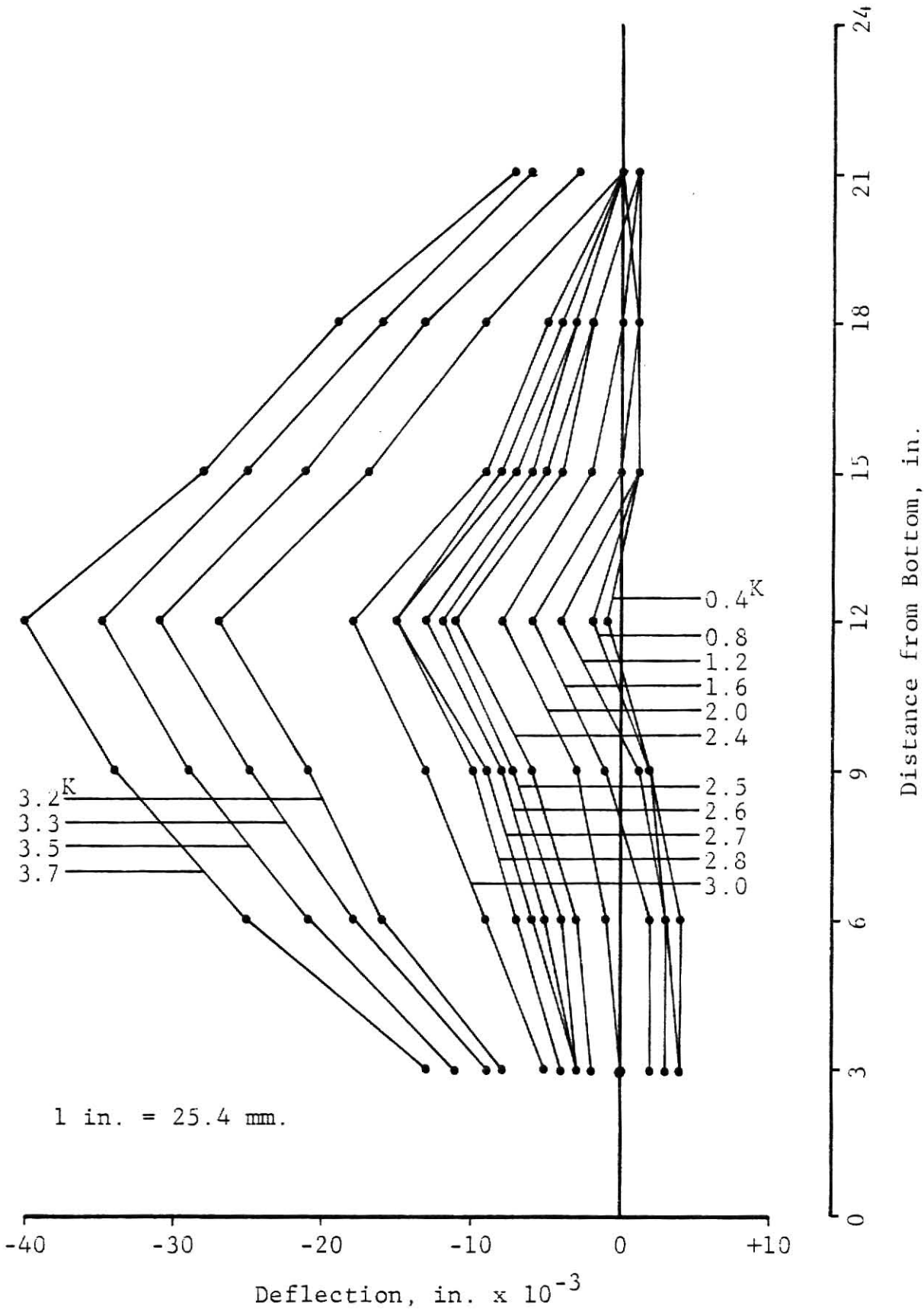

Figure 4.18 Deflection Profiles for Panel 7

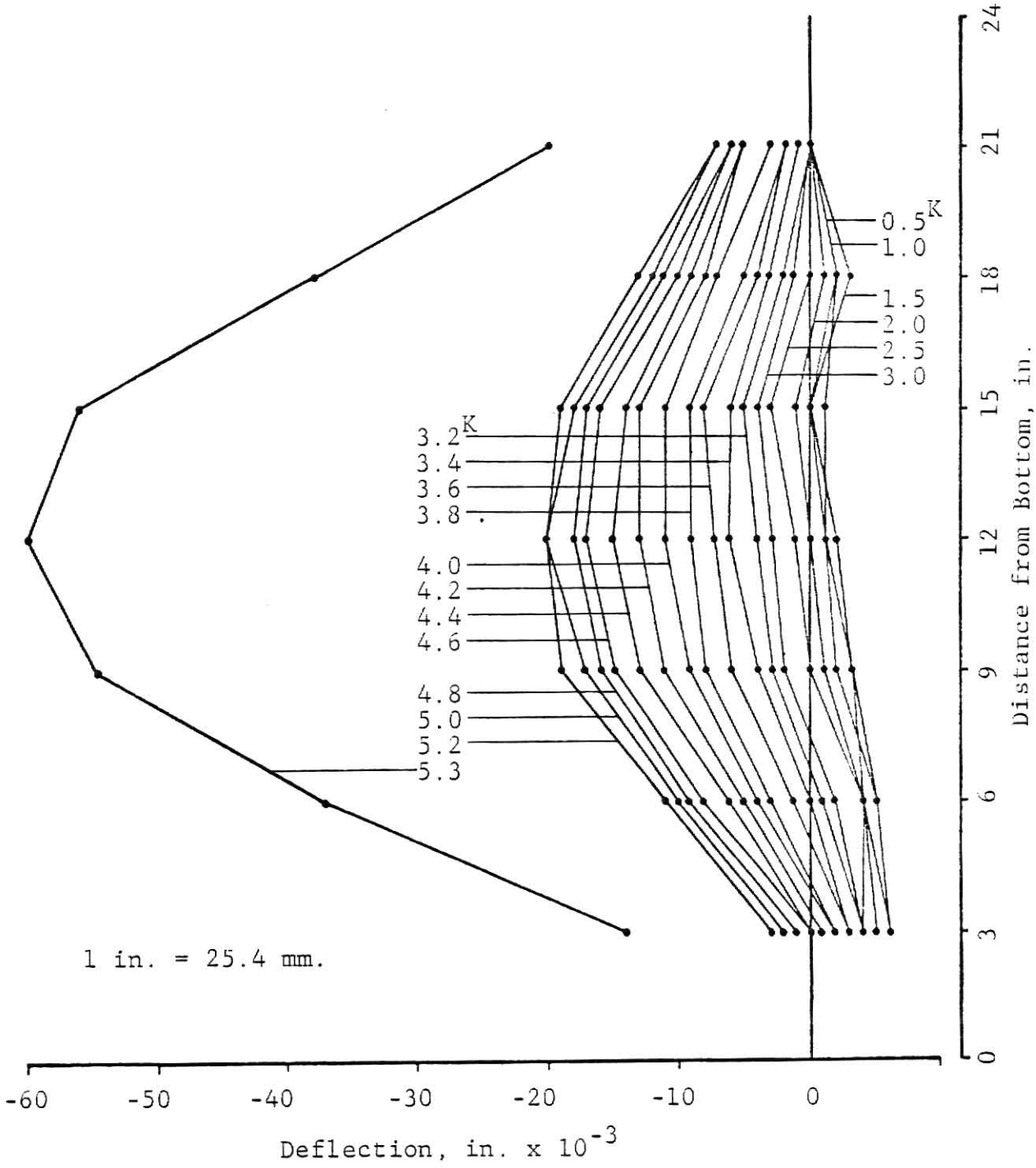

Figure 4.19 Deflection Profiles for Panel 8

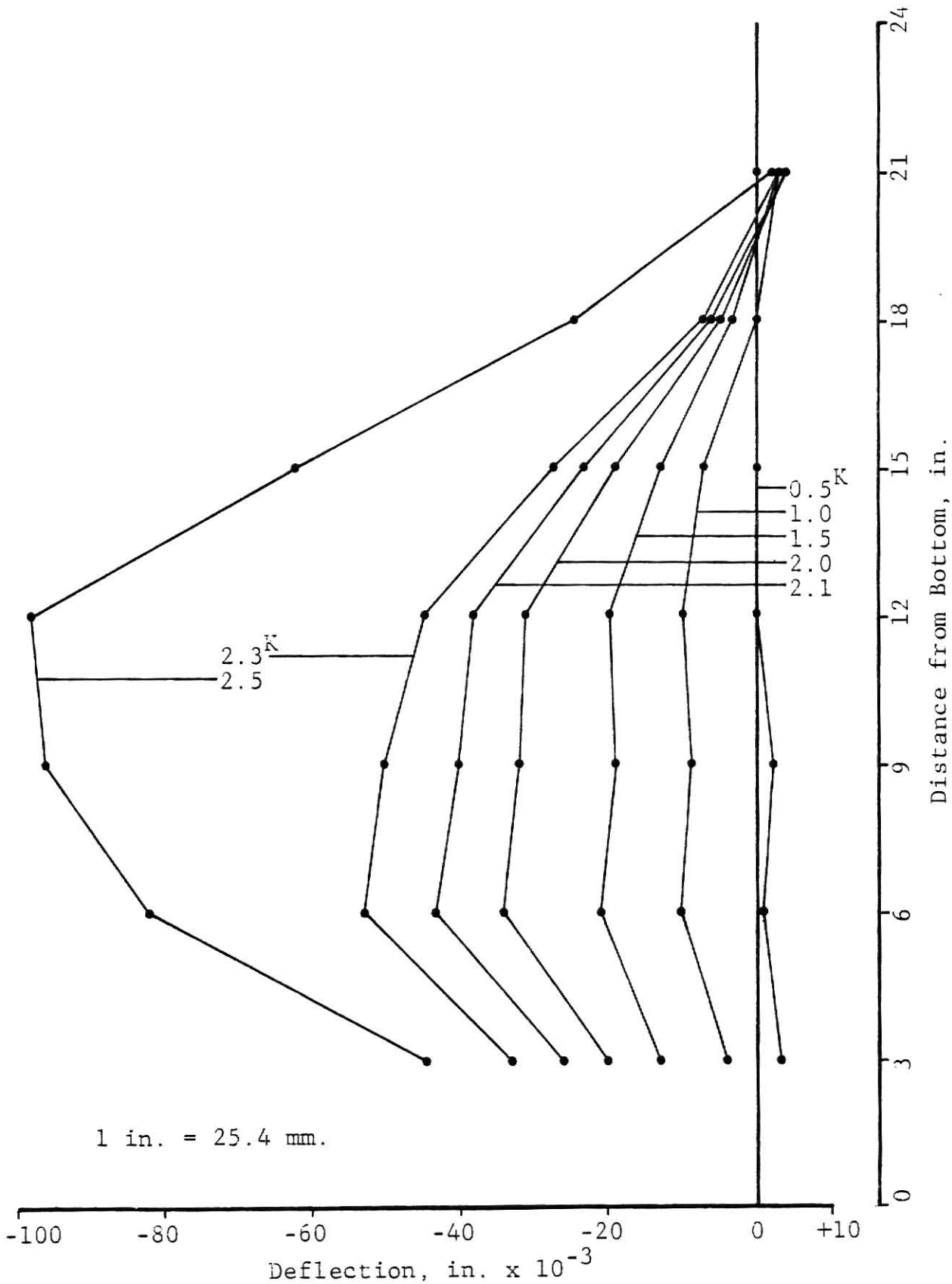

Figure 4.20 Deflection Profiles for Panel 10

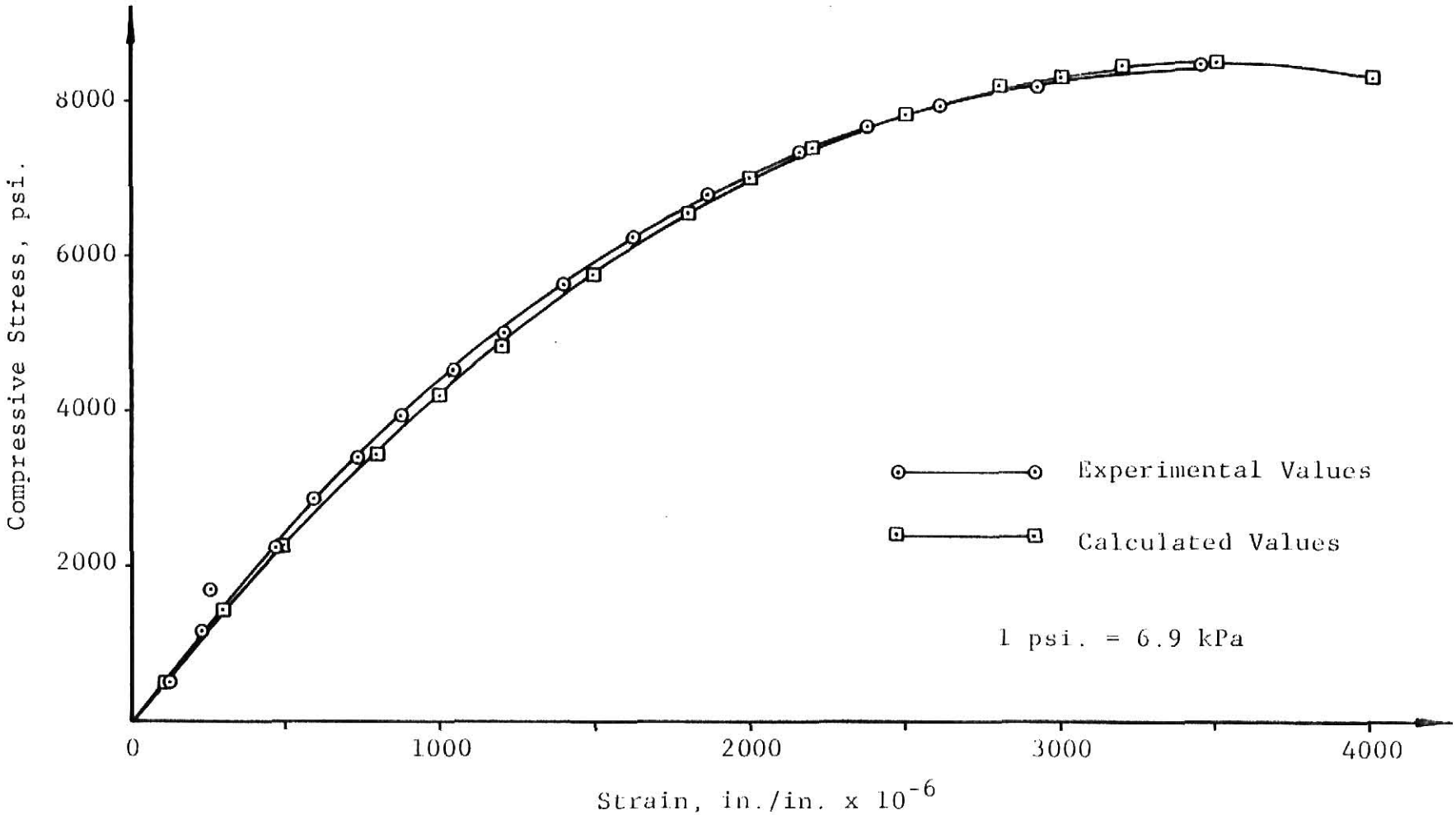

Figure 4.21 Stress-Strain Curve for Panel 1,2,3,4

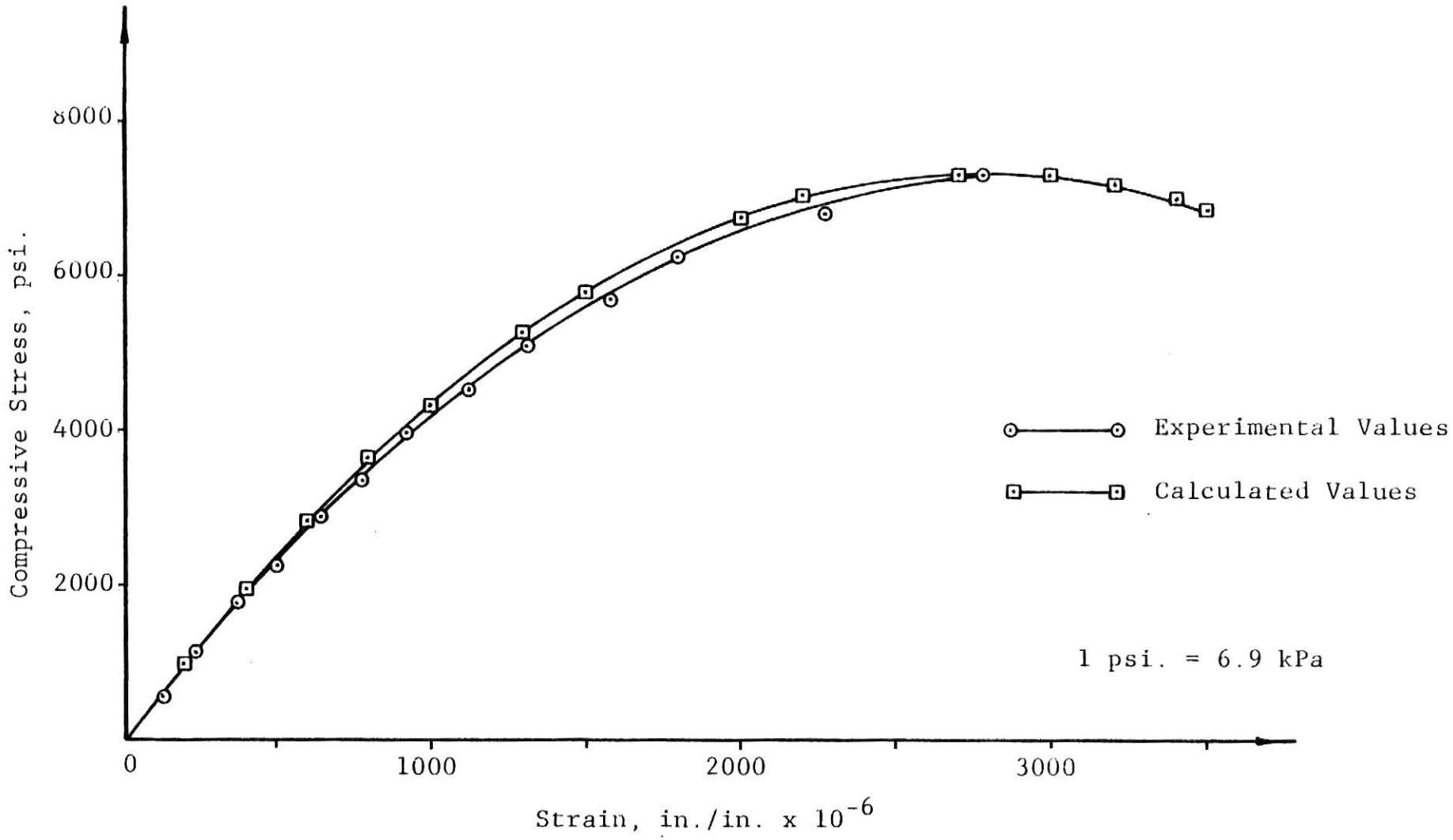

Figure 4.22 Stress-Strain Curve for Panel 5,6

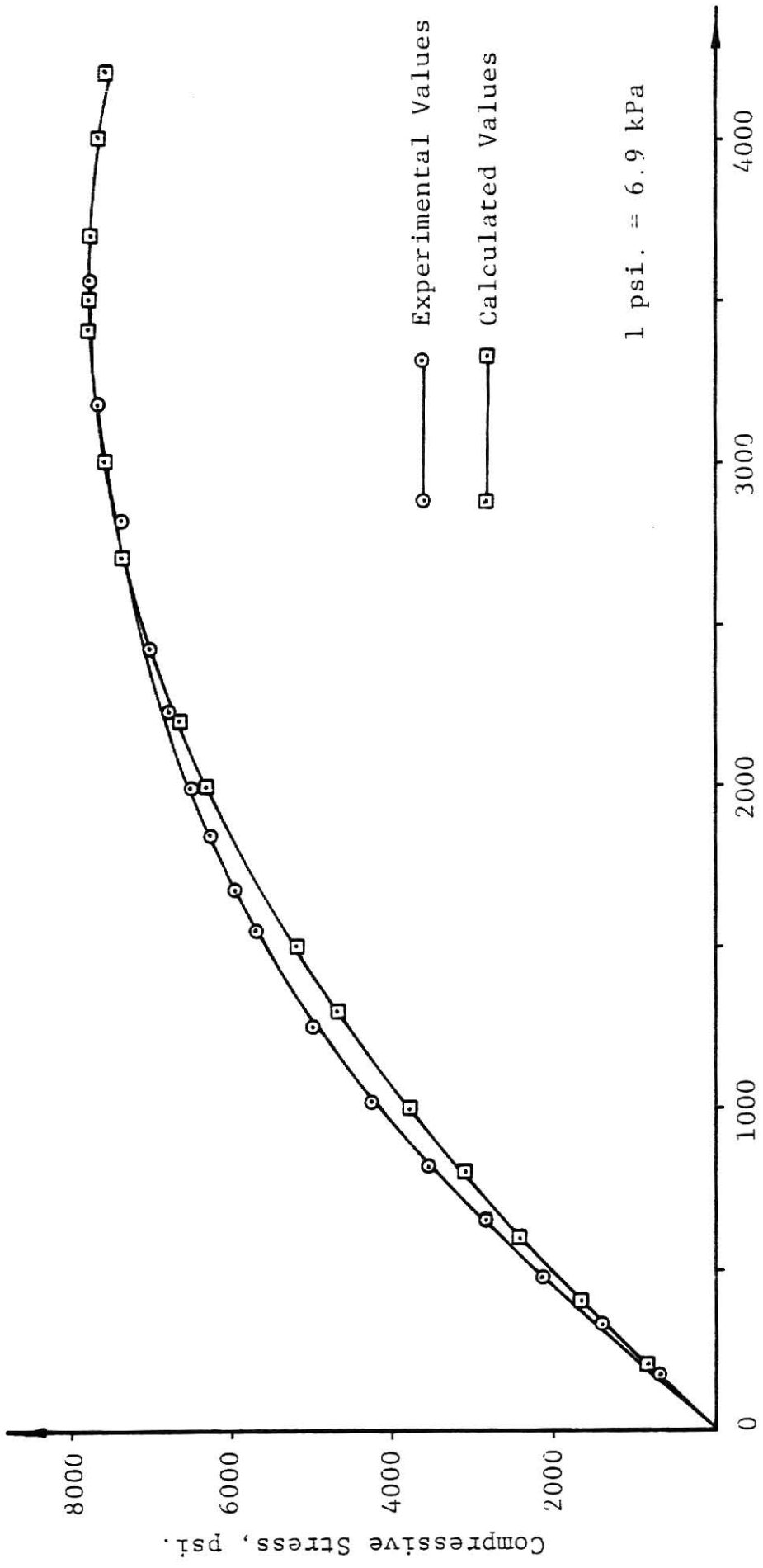

Figure 4.23 Stress-Strain Curve for Panel 7,8

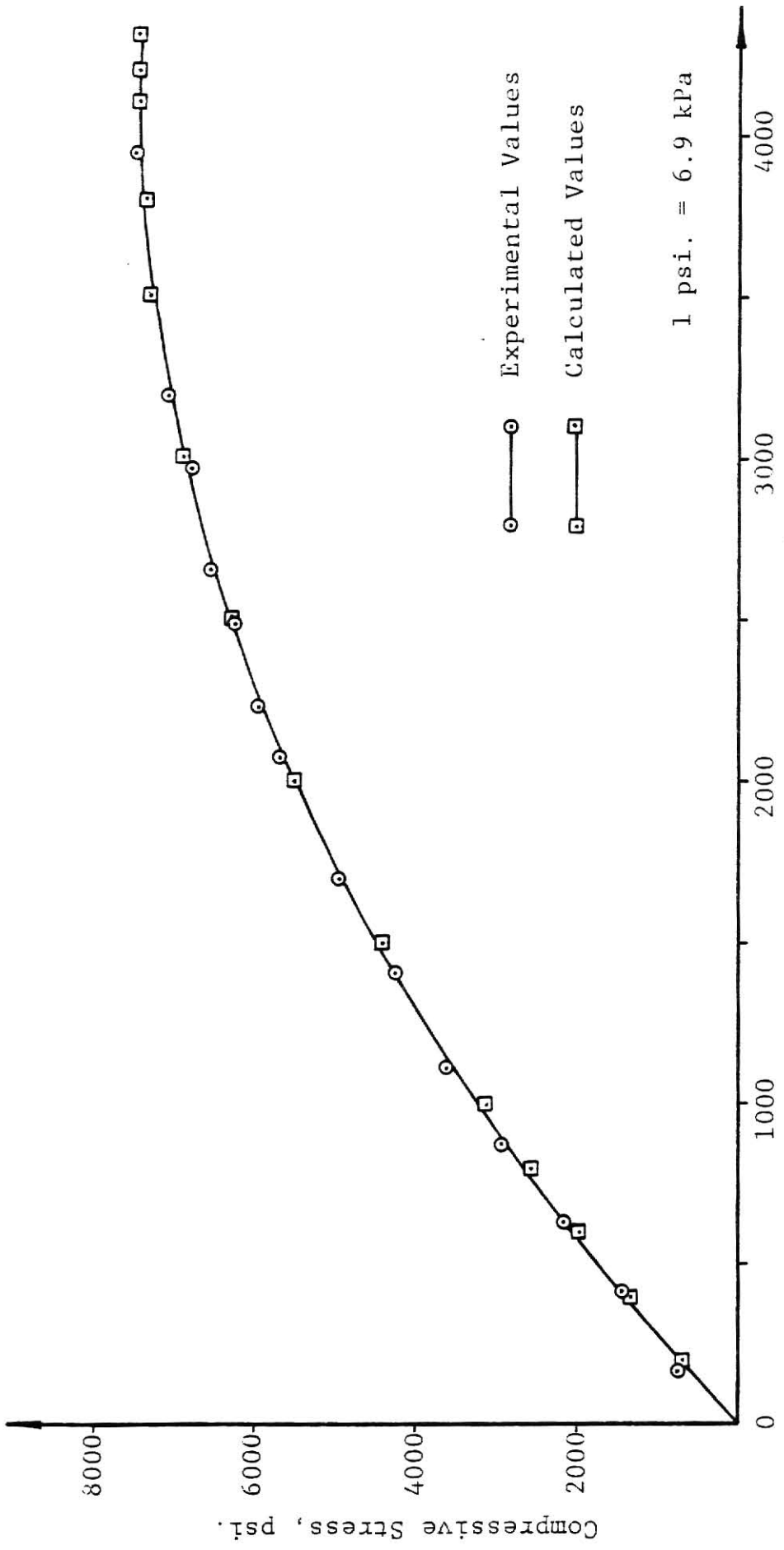

Figure 4.24 Stress-Strain Curve for Panel 9,10

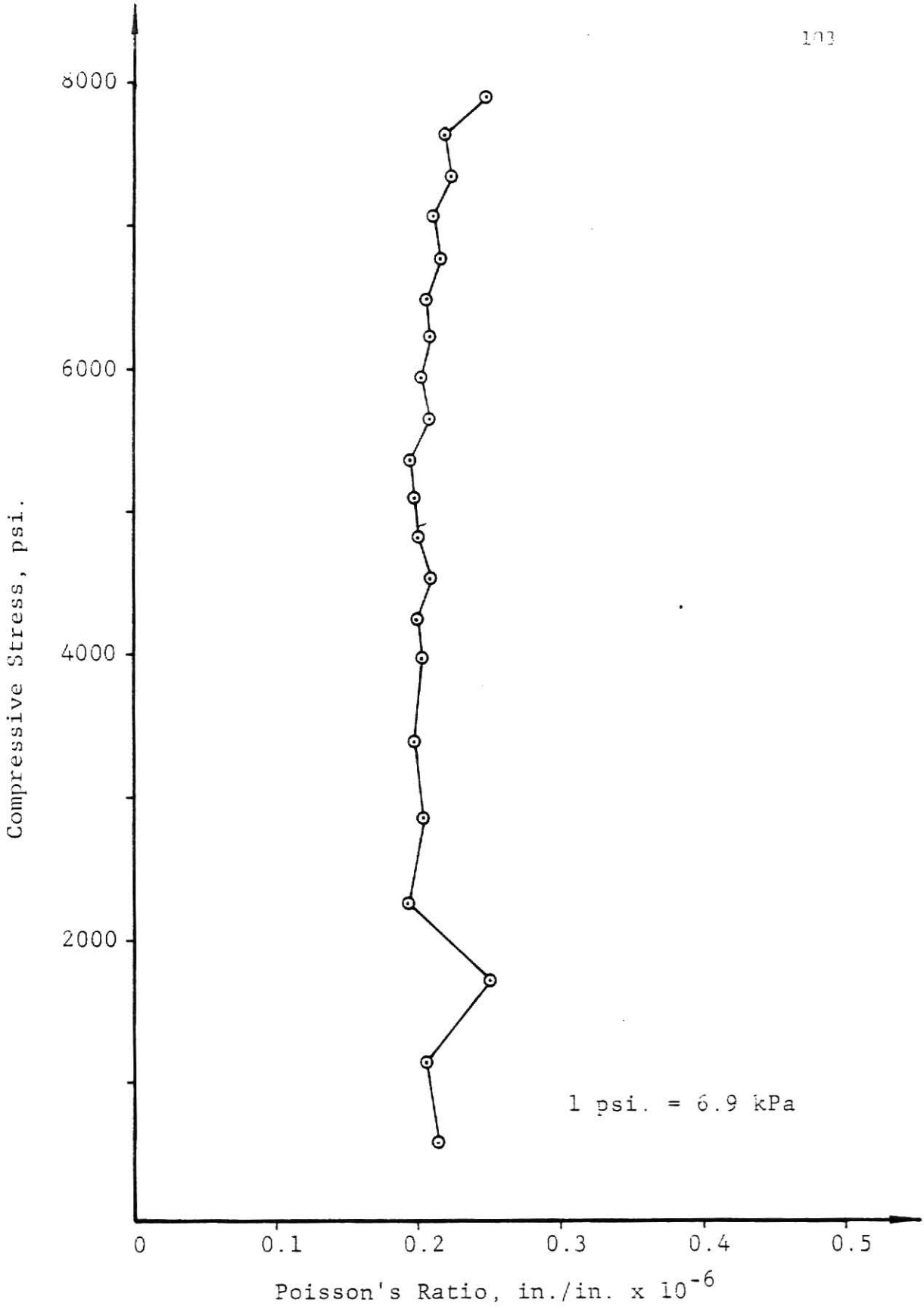

Figure 4.25 Stress vs. Poisson's Ratio for Panel 1,2,3,4

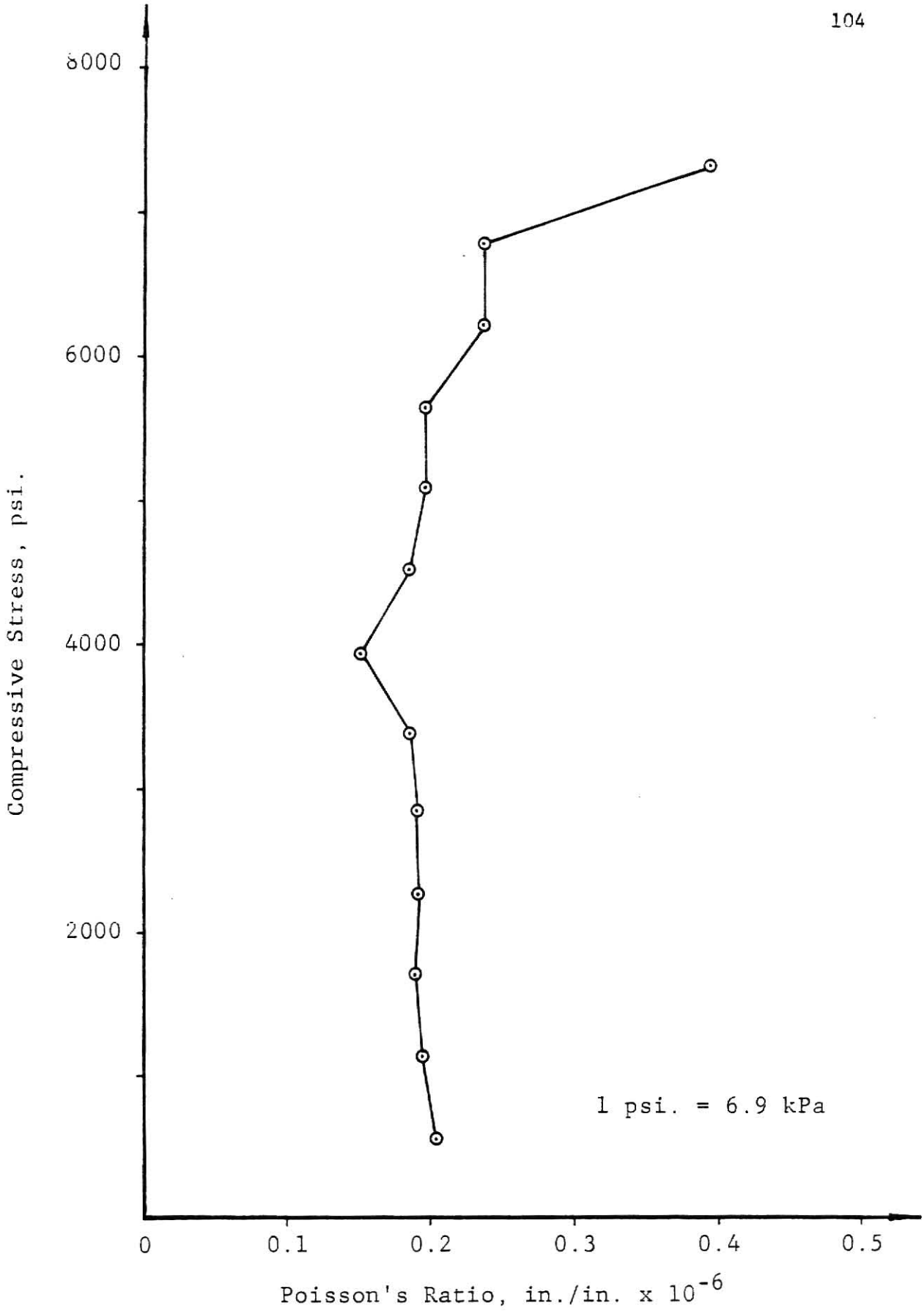

Figure 4.26 Stress vs. Poisson's Ratio for Panel 5,6

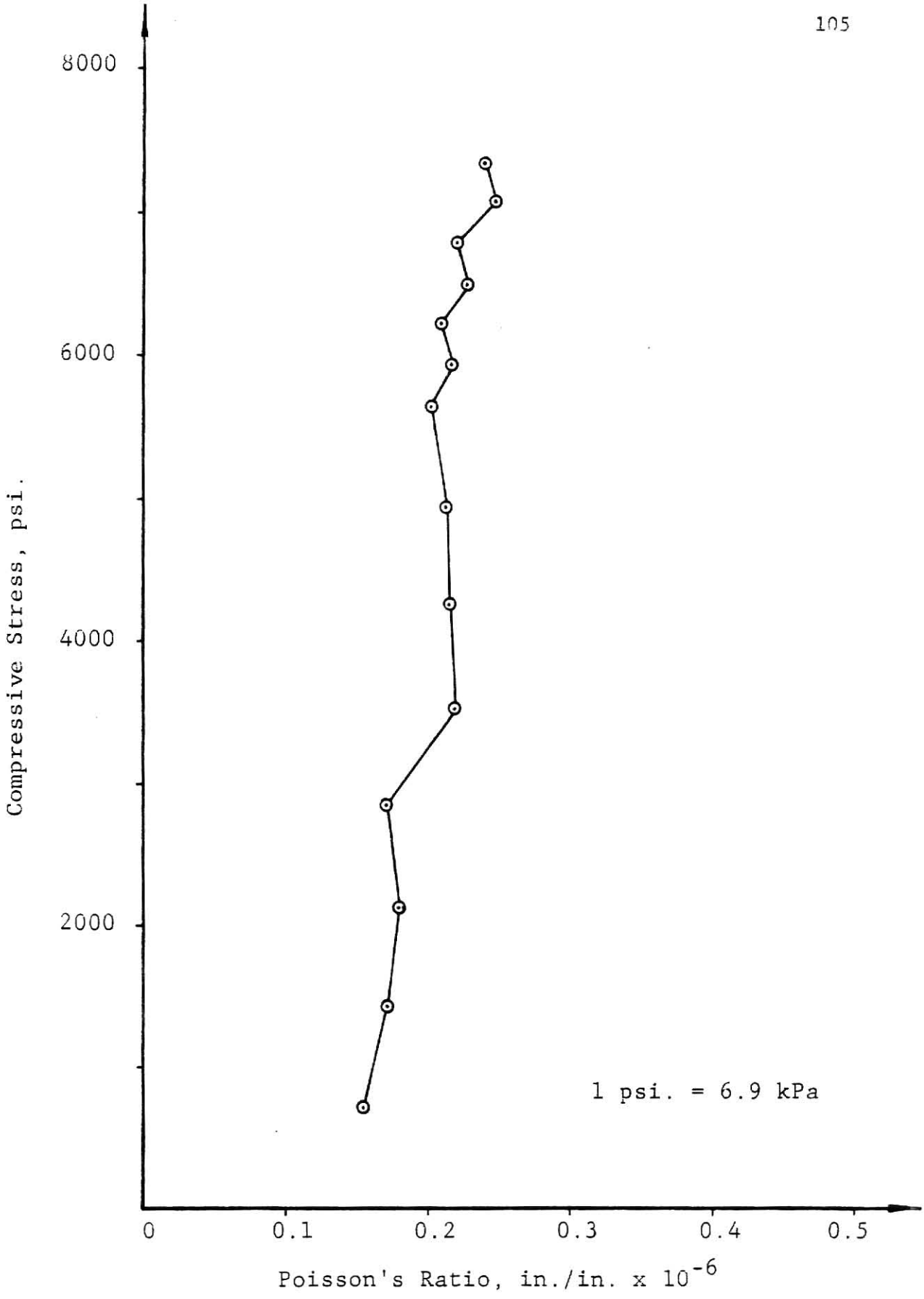

Figure 4.27 Stress vs. Poisson's Ratio for Panel 7,8

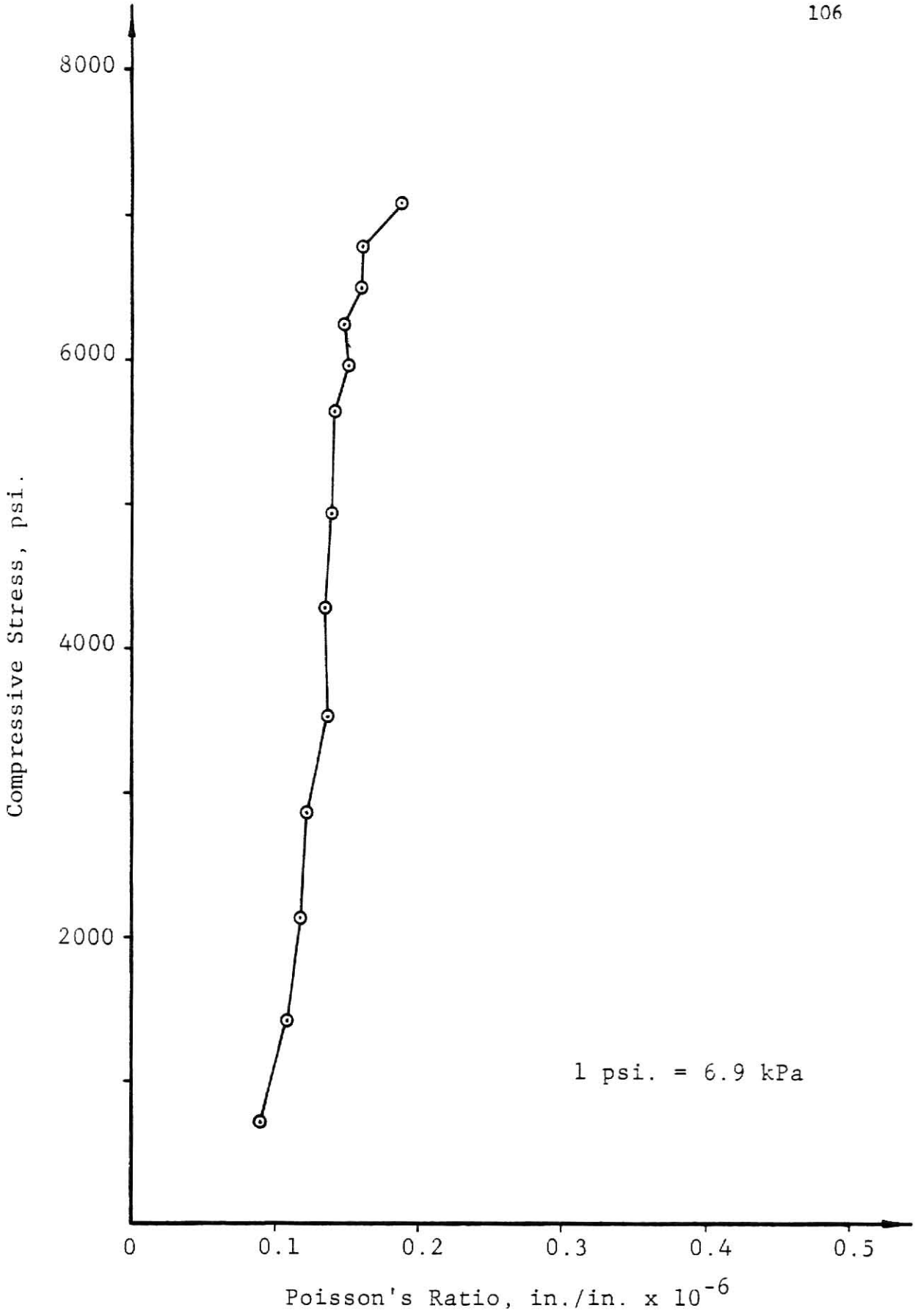

Figure 4.28 Stress vs. Poisson's Ratio for Panel 9,10

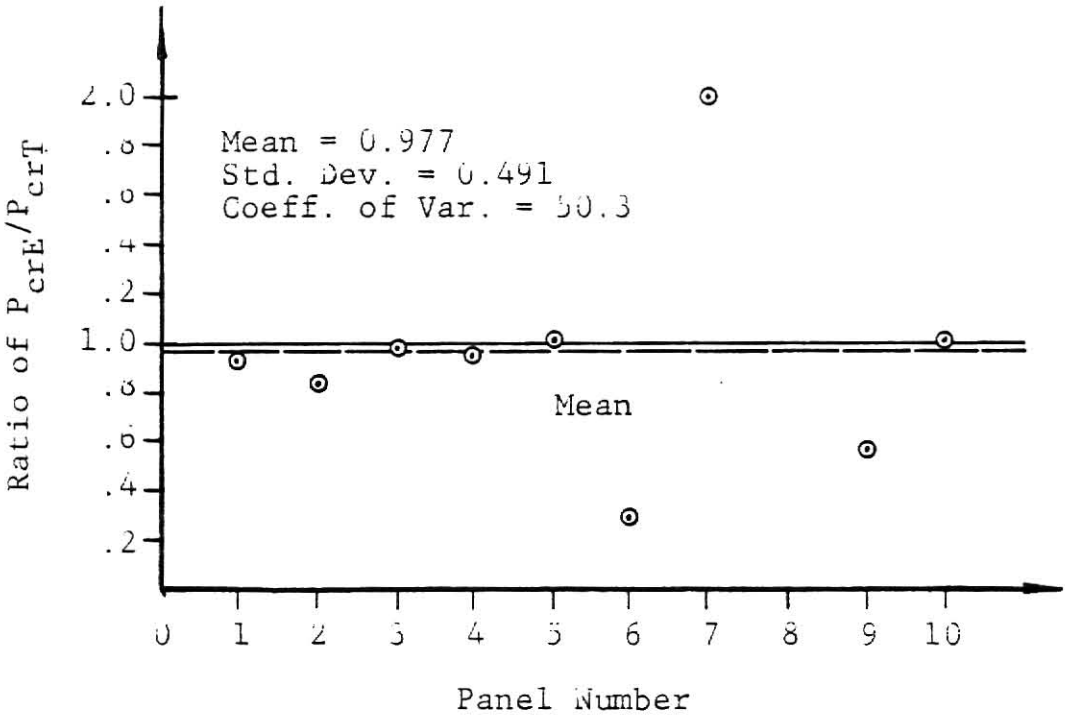

Figure 4.29 P_{crE}/P_{crT} vs. Panel Number, Using Theoretical Thickness

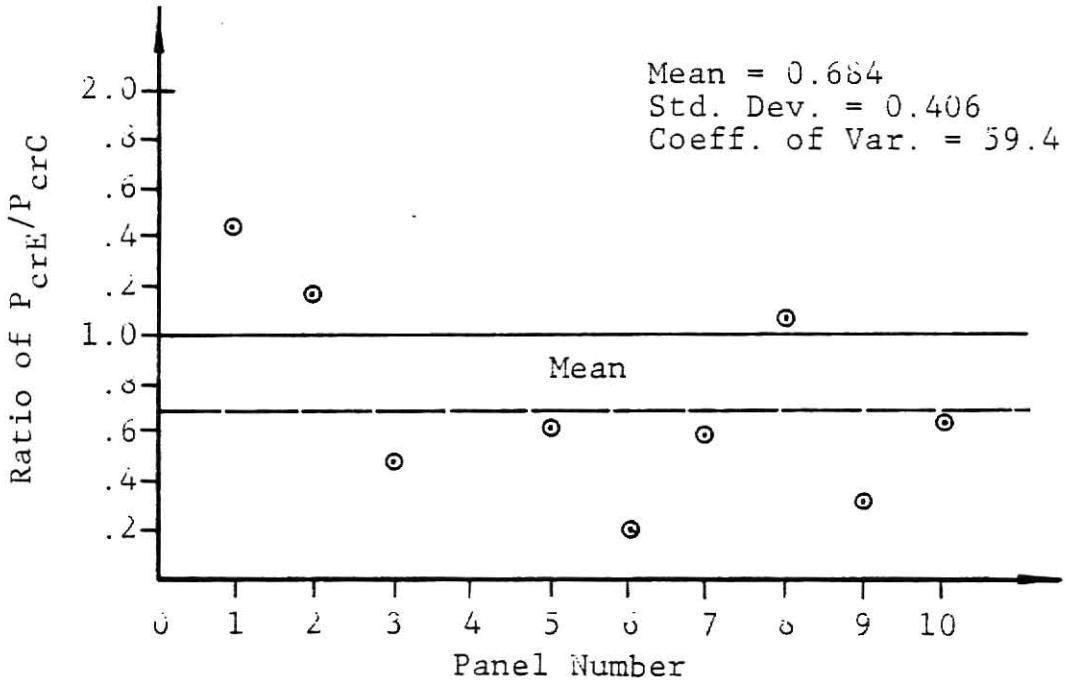

Figure 4.30 P_{crE}/P_{crC} vs. Panel Number, Using Actual Thickness

Table 4-1 Average Cylinder Compressive Strengths

Cylinder		Average Cylinder Strength f'_c, psi.	Poisson's Ratio μ
A	1,2	8,340	0.208
B	3,4	7,770	0.208
C	5,6	7,180	0.210
D	7,8	6,970	0.204
E	9,10	6,580	0.137

1 psi. = 6.9 kPa

Table 4-2 Values of P_{crT} using Theoretical Panel Thickness
t = 0.25 in. (6.4 mm)

Panel Number	Support per Long Side[2]	n[1]	ε_{cr}, με	f_{cr}, psi.	P_{crT}, lb.
1	S.S.	-	1150	4720	15,200
2	S.S.	-	1150	4720	15,200
3	2A	1	82.4	400	1,280
4	2A	1	82.4	400	1,280
5	3A	1	82.5	430	1,370
6	3A	2	314	1570	5,000
9	3A	2	312	1076	3,550
7	5A	1	81.8	354	1,150
8	5A	1	81.8	354	1,150
10	5A	1	80.6	286	940

[1] n = number of waves panel deflects.

[2] S.S. = Simply Supported; A = Angle Support

1 psi. = 6.9 kPa

1 lb. = 4.5 N

Table 4-3 Values of P_a using Theoretical Panel Thickness,
t = 0.25 in. (6.4 mm)

Plate	f'_c, psi.	ε_o, με	F_a, psi.	P_a, lb.
1 thru 4	8,500	3,460	337	1,010
5 & 6	7,360	2,790	314	941
9 & 10	7,430	4,150	315	945
7 & 8	7,780	3,560	323	968

1 psi. = 6.9 kPa

1 lb. = 4.5 N

Table 4-4 Comparison of P_{crE} and P_{crT}

Plate No.	Plate Behavior	Column Behavior	Theoretical Buckling Load (P_{crT}), lbs.	Experimental Buckling Load (P_{crE}), lbs.	$\frac{P_{crE}}{P_{crT}}$
1	2 waves		15,200	14,000	0.922
2	1 wave		15,200	12,600	0.827
3		1 wave	1,280	1,250	0.975
4		1 wave	1,280	1,230	0.956
5		1 wave	1,370	1,500	1.093
6		2 waves	5,020	1,500	0.299
9		2 waves	3,550	2,000	0.564
7		1 wave	1,150	2,400	2.096
8		1 wave	1,150	5,170	4.50
10		1 wave	940	1,000	1.064

1 lb. = 4.5 N

1 psi. = 6.9 kPa

Table 4-5 Values of P_{crC}, Using Actual Panel Thickness

Plate	Behavior P = Plate C = Column	Thickness t (in.)	I ($in.^4 \times 10^{-3}$)	ε_o ($\mu\varepsilon$)	f'_c, psi.	ε_{cr} ($\mu\varepsilon$)	f_{cr}, psi.	P_{crC}, lb.
1	P, 2 waves	0.299	53.5	3,460	8,490	490	910	9,900
2	P, 1 wave	0.308	58.4	3,460	8,490	517	957	10,700
3	C, 1 wave	0.254	32.8	3,460	8,490	170	815	2,620
4	C, 1 wave	0.280	43.9	3,460	8,490	226	1,070	3,450
5	C, 1 wave	0.244	29.1	2,790	7,360	151	777	2,490
6	C, 2 waves	0.231	24.7	2,790	7,360	477	2,300	7,400
9	C, 2 waves	0.251	31.6	4,150	7,430	604	2,000	6,630
7	C, 1 wave	0.309	59.0	3,560	7,780	298	1,250	4,060
8	C, 1 wave	0.327	69.9	3,560	7,780	350	1,460	4,730
10	C, 1 wave	0.238	27.0	4,150	7,430	138	486	1,600

1 in. = 25.4 mm

1 $in.^4$ = 416,000 mm^4

1 psi. = 6.9 kPa

1 lb. = 4.5 N

Table 4-6 Values of P_a, Using Actual Panel Thickness

Plate	f'_c, psi.	t, in.	F_a, psi.	P_a, lb.
1	8490	0.299	482	1450
2	8490	0.308	511	1530
3	8490	0.254	348	1040
4	8490	0.280	423	1270
5	7360	0.244	299	896
6	7360	0.231	268	803
9	7430	0.251	318	953
7	7781	0.309	492	1480
8	7781	0.327	552	1660
10	7430	0.238	286	857

1 in. = 25.4 mm

1 lb. = 4.5 N

1 psi. = 6.9 kPa

Table 4-7 Comparison of P_{crE} and P_{crC}; P_F and P_{crE}

Plate	Behavior P = Plate C = Column	Calculated Buckling Load, P_{crC} (lb.)	Experimental Buckling Load, P_{crE} (lb.)	$\frac{P_{crE}}{P_{crC}}$	Failure Load P_F (lb.)	$\frac{P_F}{P_{crE}}$
1	P, 2 waves	9,900	14,000	1.415	16,000	1.143
2	P, 1 wave	10,700	12,600	1.170	15,200	1.206
3	C, 1 wave	2,620	1,250	0.477	2,600	2.080
4	C, 1 wave	3,450	1,230	0.355	1,750	1.423
5	C, 1 wave	2,490	1,500	0.603	2,780	1.854
6	C, 2 waves	7,400	1,500	0.203	1,750	1.167
9	C, 2 waves	6,630	2,000	0.302	2,600	1.300
7	C, 1 wave	4,060	2,400	0.592	3,900	1.625
8	C, 1 wave	4,730	5,170	1.093	5,330	1.031
10	C, 1 wave	1,600	1,000	0.625	2,550	2.550

1 lb. = 4.5 N

Table 4-8 Summary of Critical Loads (lb.)

	Using Theoretical Plate Thickness				Using Actual Plate Thickness				
Plate	Euler's Formula	Plate Buckling Formula	ACI 318-77 Eq. (14-1)	ACI Journal	Euler's Formula	Plate Buckling Formula	ACI 318-77 Eq. (14-1)	ACI Journal	Experimental Results
1		15,200	0	1,010		9,900	0	1,450	14,000.0
2		15,200	0	1,010		10,700	0	1,530	12,560.0
3	1,280		0	1,010	2,620		0	1,040	1,250.0
4	1,280		0	1,010	3,450		0	1,270	1,225.0
5	1,370		0	940	2,490		0	896	1,500.0
6	5,020		0	940	7,400		0	803	1,500.0
9	3,550		0	945	6,630		0	953	2,000.0
7	1,150		0	967	4,060		0	1,480	2,400.0
8	1,150		0	967	4,730		0	1,660	5,170.0
10	940		0	945	1,600		0	857	1,000.0

1 lb. = 4.5 N

Chapter 5

CONCLUSIONS AND RECOMMENDATIONS

The ten model panels tested were fabricated from a model concrete or microconcrete which was designed to have strength characteristics similar to a prototype concrete. This was achieved as can be seen by viewing Figure 4.21 thru Figure 4.24, and noting the close agreement of the two curves. However, the microconcrete used here has the characteristic of being a "softer" concrete. This is shown by the value of the maximum strain at the ultimate stress. This is somewhat higher than prototype concrete.

The model panels were fabricated by pumping the concrete into molds. This was accomplished successfully after overcoming a number of difficulties as previously described. The panel thickness varied from the design thickness by -4.8% to +23.2%. Tighter quality control of the form probably can reduce the thickness variation. This can be accomplished by using spacers at various points within the mold to ensure the proper design thickness.

The ten panels were tested in basically three support systems. Plates 1 and 2 had simple supports on all edges. Plate 1 buckled in a 2-wave fashion. Although the panel buckled in plate-type behavior it failed due to an unsupported length near the top of the panel. Figure 3.17 shows how the panel fractured at the top. The failure was very explosive due to the large amount of energy absorbed. The support condition was modified prior to testing panel 2. Figure 5.1 shows that this panel buckled by plate action. This plate also failed in an explosive manner. Good agreement with the theoretical buckling strength of these two panels was obtained.

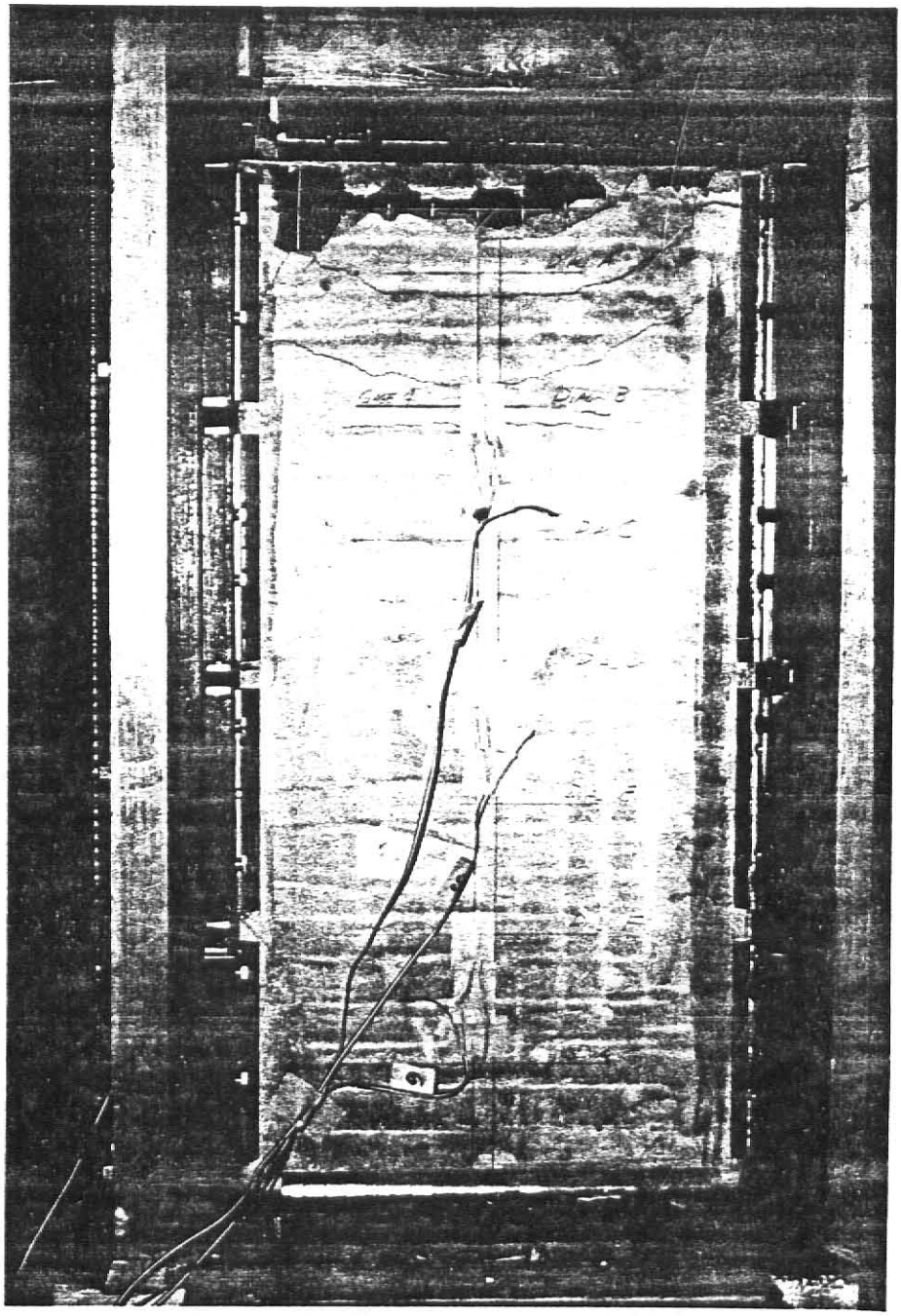

Figure 5.1 Photo of Panel 2 after Testing

Panels 3 and 4 buckled in column-type action. These two panels were simply-supported at the top and bottom edges. Also near each corner on the sides were small angles. These angles simulate the type of connections possible for tilt-up wall panels.[1] Their buckling strength was calculated by methods currently used in practice. For panels 5, 6, 9 and panels 7, 8, 10 the number of angles per side was increased to three and five, respectively. The increase in angle density did not change the buckling behavior of the panels. Figure 4.17 shows the two wave deflection profiles of panel 9. Figure 5.2 shows the same panel in the test frame. Panels 7, 8, 10 buckled in a single wave. Panel 8 is also shown in Figure 5.3. Note how the angles pulled out from the panel. This type of action is also expected to occur in a prototype panel.

The buckling capacity of the panels were predicted by using the methods currently used for column type buckling. These predictions did not agree well with experimental results. The failure loads for these panels were much lower than for those which had plate buckling behavior. The panels exhibited some post-buckling strength. However, this should not be counted upon in design.

Increasing the density of angles did not ensure plate-type action.

Recommendations

For pumping microconcrete an aggregate with a flat particle distribution curve is recommended. This will supply the needed fine particles required to lubricate the pumping system to allow a plug flow

---

[1] Personal communication with Prof. Thorson, Architectural Engineering and Construction Science Department, Kansas State University.

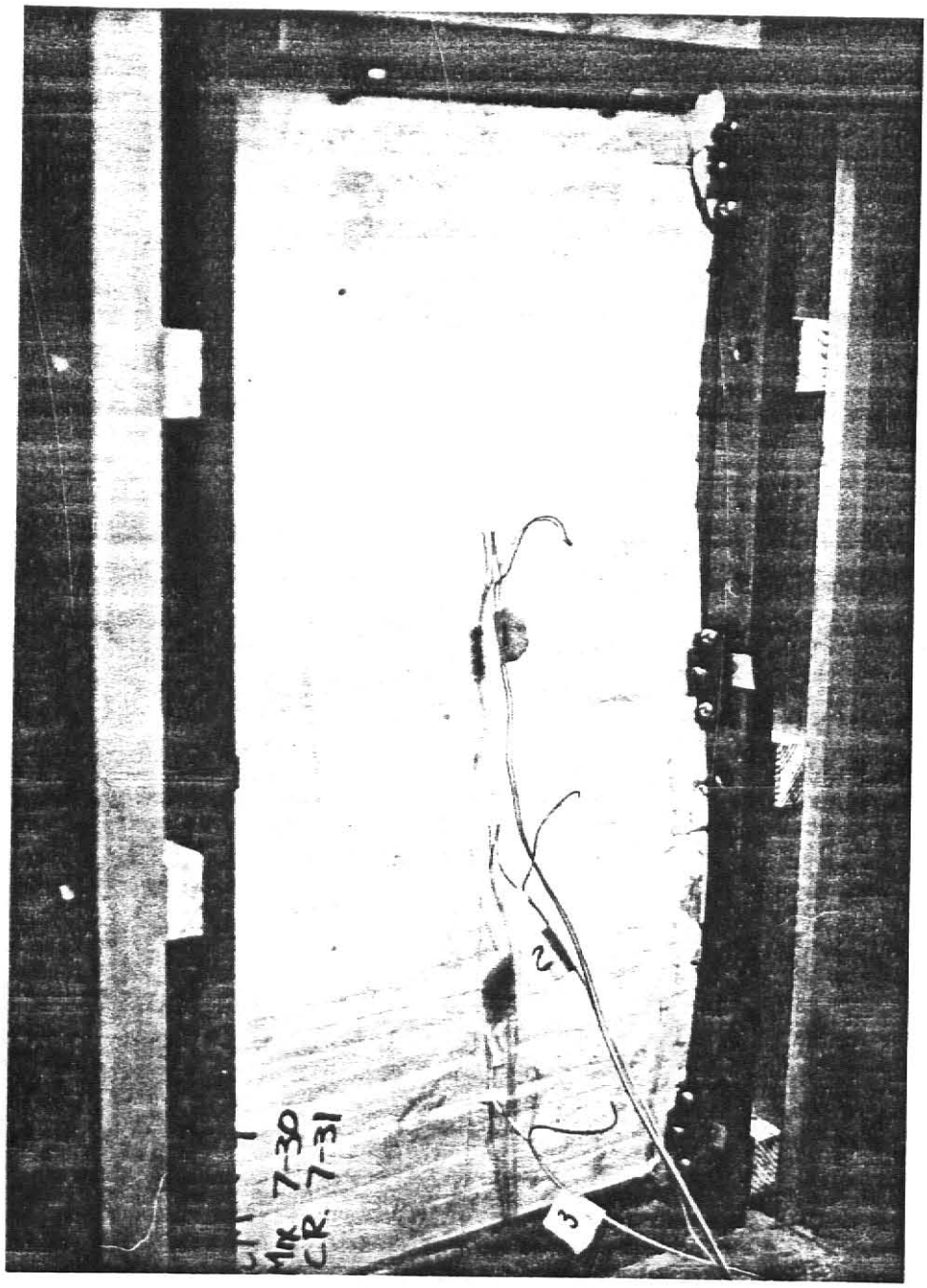

Figure 5.2 Photo of Panel 9 after Testing

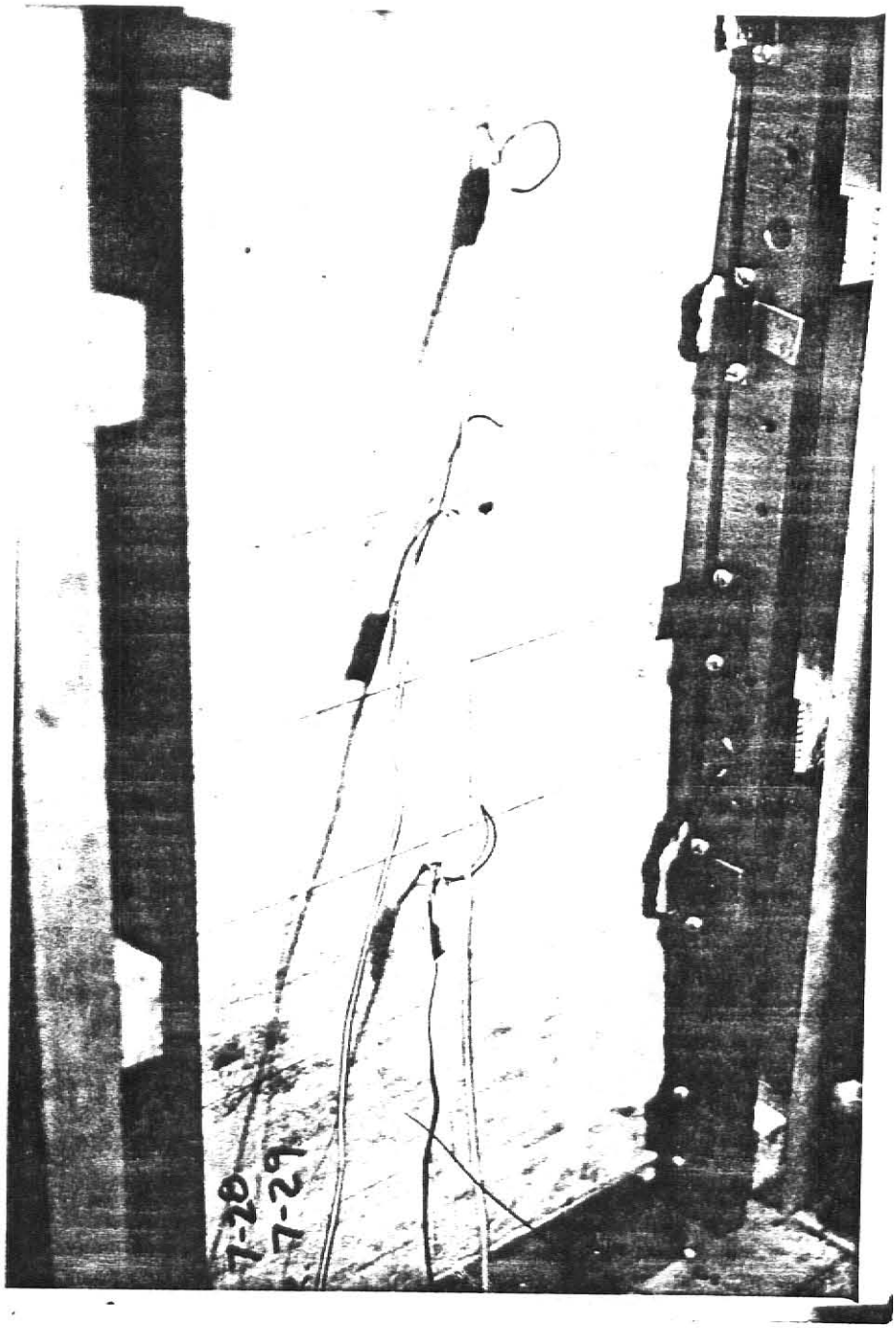

Figure 5.3 Photo of Panel 8 after Testing

mechanism. The system described herein is recommended for pumping these small forms. Tighter form accuracy for design thickness is recommended as previously stated. The selection of a ductile steel is also recommended for future studies. Harris, et al. ([8]) describe a method for deforming and annealing a straight wire. The support conditions could be changed to try to ensure plate buckling. Possibly this may be accomplished by attaching the angles on opposite surfaces along an edge. This will have a tendency to increase the resistance of deflection on both sides of the panel.

BIBLIOGRAPHY

1. Aldridge, Weldon W., Breen, John E., "Useful Techniques in Direct Modeling of Reinforced Concrete Structures," Paper SP 24-5, ACI Publications, pp. 125-140.

2. Anderson, Wayne G., "Analyzing Concrete Mixtures for Pumpability," Title No. 74-42, ACI Journal, September 1977, pp. 447-451.

3. Best, J. F., Lane, O. R., "Testing for Optimum Pumpability of Concrete," Concrete International, October 1980, pp. 9-17.

4. Browne, Roger D., Bamforth, Phillip B., "Tests to Establish Concrete Pumpability," Title No. 74-19, ACI Journal, May 1977, pp. 193-203.

5. Carpenter, James E., Roll, Fredric, Zelman, Maier I., "Techniques and Materials for Structural Models," Paper SP 24-3, ACI Publications, pp. 41-63.

6. Committee 318, ACI, "Building Code Requirements for Reinforced Concrete (ACI 318-77)," October 1978, pp. 63-64.

7. Committee 533, ACI, "Design of Precast Concrete Wall Panels," ACI Journal, July 1971, pp. 504-513.

8. Harris, Harry G., Sabnis, Gajanan M., White, Richard N., "Reinforcement for Small Scale Direct Models of Concrete Structures," Paper SP 24-6, ACI Publications, pp. 141-158.

9. Houghton, Donald L., Committee 304, "Placing Concrete by Pumping Methods," Title No. 68-33, ACI Journal, May 1971, pp. 327-345.

10. Litle, W. A., Cohen, E., Somerville, G., "Accuracy of Structural Models," Paper SP 24-4, ACI Publications, pp. 65-84.

11. Sabnis, Gajanan M., Mirza, Saeed M., "Size Effects in Model Concrete?" Journal of the Structural Division, ST6, June 1979, pp. 1007-1020.

12. Swartz, S., Rosebraugh, V., "Buckling of Reinforced Concrete Plates," Journal of the Structural Division, ASCE, January 1974, pp. 195-208.

13. Swartz, S., Rosebraugh, V., Berman, M., "Buckling Tests on Rectangular Concrete Panels," Title No. 71-5, ACI Journal, January 1974, pp. 33-39.

14. Zia, Paul, White, Richard N., Vanhorn, David A., "Principles of Model Analysis," Paper SP 24-2, ACI Publications, pp. 19-37.

APPENDIX A

Notation

NOTATION

A_c, A_g = Gross cross-sectional area of concrete panel, sq. in.

A_s = Area of steel reinforcement, sq. in.

B = Parameter for buckling stress-strain calculations

C_s = Factor of safety

E = Modulus of elasticity for concrete, psi.

E_s = Modulus of elasticity for steel reinforcement, psi.

E_T = Tangent modulus for concrete, psi.

e = ratio of ε_c to ε_o

e_{cr} = ratio of ε_{cr} to ε_o

F_a = Compressive stress, psi.

f_c = Compressive concrete stress, psi.

f'_c = Specified compressive strength of concrete, psi.

f_{cr} = Critical stress of concrete, psi.

f_y = Yield strength of reinforcement, psi.

I = Moment of inertia about bending axis of panel, $in.^4$

L = Unsupported length of panel, in.

ℓ = Ratio of length to width of panel

n = Number of waves panel deflects

P_a, P_{cr}, P_{nw} = Critical axial load on panel, lbs., computed by various methods

P_{crC} = Calculated critical panel load using actual thickness

P_{crT} = Calculated critical panel load using theoretical thickness

P_{crE} = Experimentally-obtained panel buckling load

t = Thickness of panel, in.

w = Width of panel, in.

w_c = Unit weight of concrete, pcf.

ε_c = Concrete strain, in. per in.

ε_{cr} = Critical strain, buckling strain, in. per in.

ε_o = Maximum concrete strain, in. per in.

ε_y = Yield strain of reinforcing steel, in. per in.

μ = Poisson's ratio

ρ = Ratio of reinforcing steel

ϕ = Strength reduction factor, 0.7 for buckling

BUCKLING BEHAVIOR OF REINFORCED CONCRETE WALL PANEL MODELS

by

Arturo C. Muñoz

B.S., Kansas State University, 1977

AN ABSTRACT OF A MASTER'S THESIS

submitted in partial fulfillment of the

requirements for the degree

MASTER OF SCIENCE

Department of Civil Engineering

KANSAS STATE UNIVERSITY

Manhattan, Kansas

1981

ABSTRACT

Rectangular reinforced concrete panels are commonly used as tilt-up walls. These wall panels are used extensively in high-rise building construction. The panels may be cast in place or tilt-up precast panels. They are utilized as shear walls, bearing walls or as shear and bearing walls.

It is becoming more feasible and economical to fabricate thinner panel sections by precasting methods. These thinner panels help reduce the dead load of a structure substantially. However, thinner wall panels are not currently used due to the lack of knowledge of the ultimate strength and buckling capacity of these panels.

This report contains test results conducted on thin reinforced concrete panel models. It contains background information on modelling concrete as well as a discussion on buckling of concrete plates. Difficulties encountered during fabrication of the panel models are discussed as well as recommendations for future studies in this area.